

NASA TECHNICAL
MEMORANDUM

NASA TM X 62,231

NASA TM X-62,231

**LOW SPEED WIND TUNNEL INVESTIGATION OF A LARGE
SCALE LIFT FAN STOL TRANSPORT MODEL.**

Adolph Atencio, Jr., Leo P. Hall, and Jerry V. Kirk

**Ames Research Center
and
U.S. Army Air Mobility R&D Laboratory
Moffett Field, Calif. 94035**

1973
**(NASA-TM-X-62231) LOW SPEED WIND TUNNEL
INVESTIGATION OF A LARGE SCALE LIFT FAN
STOL TRANSPORT MODEL (NASA) 123 p HC
\$8.50**

N73-20014



L 01B

G3/02 Unclassified
 66667

NOTATION

A	fan exit area, m^2 (sq ft), or wing aspect ratio
b	wing span, m (ft)
c	wing chord parallel to the plane of symmetry, m (ft)
\bar{c}	mean aerodynamic chord, $\frac{2}{S} \int_0^{b/2} c^2 dy$, m (ft)
C_D	drag coefficient, $\frac{D}{qS}$
C_l	rolling moment coefficient, $\frac{l}{qSb}$
C_L	lift coefficient, $\frac{L}{qS}$
C_m	pitching moment coefficient, $\frac{M}{qSc}$
C_n	yawing moment coefficient, $\frac{N}{qSb}$
C_y	side force coefficient, $\frac{Y}{qS}$
D	drag, N (lb)
i_t	horizontal tail incidence angle, deg
l	rolling moment, N-m (ft lb), or length, m (ft)
L	total lift on the model, N (lb)
M	pitching moment, N-m (ft lb)
N	yawing moment, N-m (ft lb)
P_o	standard atmospheric pressure, N/m^2 (lb/sq ft)
P_s	free stream static pressure, N/m^2 (lb/sq ft)
q	free stream dynamic pressure; N/m^2 (lb/sq ft)
RPM	corrected fan rotational speed, $\frac{\text{fan speed}}{\sqrt{\theta}}$
S	wing area, m^2 (sq ft)

T	fan thrust, $\rho A V_j^2$, N (lb)
v	air velocity, m/sec (ft/sec)
V	free stream air velocity, knots or m/sec (ft/sec)
\bar{v}	tail volume coefficient, $\frac{S_{t\ell} t}{Sc}$
Y	side force, N (lb)
α	angle of attack of the wing chord plane, deg
β	angle of sideslip, deg
δ_v	lift fan exit louver deflection angle; 0° in the direction to produce maximum thrust in the lift direction with $\alpha = 0^\circ$, $\sigma_v = 0^\circ$, deg
σ_v	lift fan exit louver cascade rotation angle; 0° in the direction to produce maximum thrust in the lift direction
δ	relative static pressure, $\frac{P_s}{P_o}$
δ_{cn}	lift-cruise fan exhaust duct angle; 0° in the cruise direction, deg
δ_f	trailing edge flap deflection measured normal to the hinge line, deg
θ	ratio of ambient temperature to standard temperature (519° rankine)
μ	tip speed ratio, $\frac{V}{\omega R}$
ρ	density, Kg/m^3 ($\text{lb-sec}^2/\text{ft}^4$)
ω	fan rotational speed, radians/sec

Subscripts

c	corrected
j	fan exit
s	static conditions
w	wing
t	tail

LOW SPEED WIND TUNNEL INVESTIGATION OF A LARGE SCALE
LIFT FAN STOL TRANSPORT MODEL

Adolph Atencio Jr., Leo P. Hall, and Jerry V. Kirk

Ames Research Center
and
U.S. Army Air Mobility R&D Laboratory

INTRODUCTION

Ames Research Center is studying the low-speed aerodynamic characteristics of large scale V/STOL transport models with lift fan and lift-cruise fan propulsion systems. Previous large scale studies conducted in the 40- by 80-Foot Wind Tunnel have investigated the aerodynamic characteristics and propulsion system performance of fan-in-fuselage, fan-in-wing, and podded fan configurations. References 1 through 13 summarize these results.

Lift fan configurations for the most part have had shallow fan inlets (i.e., XV-5A/B), which may give poor inlet performance. The model of this investigation had two fans mounted side by side in the nose section of the fuselage. This permitted a reasonably deep inlet on the inboard side of each fan while the outboard side had a fairly shallow inlet. Lift-cruise fans were installed on the aft section of the fuselage. Hood-type deflection ducts were used to turn the fan flow from the cruise direction to the lift direction for STOL performance.

Fan performance is shown for all four fans both statically and with crossflow. Longitudinal force and moment results are shown for a representative tip speed (forward speed) range through wing supported flight. Lateral-directional characteristics are also presented.

The results included herein are presented without analysis.

MODEL DESCRIPTION

Photographs of the model mounted in the Ames 40- by 80-Foot Wind Tunnel are shown in figure 1. Figure 2 is a drawing of the model giving pertinent dimensions and geometric details.

Fuselage

The fuselage was circular in cross section with a maximum diameter of 1.75 m (69 in). Overall fuselage length was 14.48 m (570 in). The forward or nose section of the fuselage housed two thirty-six-inch diameter lift fans necessitating the bulbous fairing that extended aft to the vicinity of the wing leading edge. Mounted at the sides of the aft fuselage were two thirty-six-inch diameter lift-cruise fans with axes parallel to the free stream direction. The gas generators used to propel the four fans were housed on top of the fuselage (figure 2(a)).

Wing

The wing was mounted low on the fuselage with 3° of dihedral and 0° incidence with respect to the fuselage reference line. Aspect ratio was 8.14, taper ratio 0.233, and sweep along the quarter chord line was 23.5° . An NACA 65-412 airfoil section was basic for the wing. A 22% chord single-slotted trailing-edge flap extended from the fuselage to 63% semi-span. A flap deflection of 30° was used for the entire investigation. A 7% chord leading-edge slat extended full span and was deflected 20° for the entire investigation (figure 2(f)).

Tail

The tail geometry and location are given in figure 2. The all-moveable horizontal tail was an NACA 64-009 airfoil. It was pivoted about the quarter chord and had a range of -10° to $+20^{\circ}$ incidence. For tests with the tail off, only the horizontal tail was removed.

Propulsion System

The propulsion system consisted of 4 lift fans driven by 4 gas generators. The lift fans were General Electric X-376 lift fans with a design pressure ratio of 1.1. The gas generators were modified T58-8B engines. The location and arrangement of each engine and fan are shown in figure 2(a). All 4 lift fans rotated in a clockwise direction looking into the inlet.

Forward lift fans.- The two forward lift fans were installed as shown in figures 2(b) and 2(c). The fans were mounted with the thrust axis canted 10° with respect to the horizontal plane. The fan exit ducting was designed to direct the fan exhaust flow in a plane 40° from the vertical. A cascade of fourteen 0.114 m (4.50 in) chord highly cambered exit vanes was mounted at the duct exit of each forward lift fan (vane ordinates are given in figure 2(d)). The vanes spanned the exit ducts and were used both for thrust vectoring and as a lower surface closure during power-off testing. The exit cascade was manually rotatable in the 40° canted plane. With the ring oriented to align the vane spans parallel to the aircraft centerline, maximum lift was provided; this position defined $\sigma_v = 0^{\circ}$. Rotation of the ring in the direction giving positive thrust vectoring was defined as positive σ_v . σ_v values used ranged from -40° to 110° . The exit vanes were remotely operated and varied from -16° to $+16^{\circ}$ about the maximum lift position. $\beta_v = 0^{\circ}$ was established at $\alpha = 0^{\circ}$, $\psi = 0^{\circ}$, $\sigma_v = 0^{\circ}$, RPM = 3600 by trimming side force to zero. The forward lift fan inlets were bellmouth-shaped and contoured to fit within boundaries dictated by space available. After initial testing the forward inlets were modified by providing a more generous lip radius in an effort to improve fan performance at forward speed. Data in the report is for the modified inlets except figure 7(a).

Lift-cruise fans.- The two aft fans were mounted in cruise pods as shown in figure 2(e). The fan exhaust was deflected through ducts for thrust vectoring. The ducts were adjustable from 0° to 138.5° with

0° in a direction to provide maximum horizontal thrust. The exhaust nozzle area was sized to accommodate fan and turbine flow.

TESTING AND PROCEDURE

Longitudinal force and moment data were obtained for an angle of attack range from -4° to 22° . Lateral-directional results were obtained for a range of sideslip angles from -16° to $+8^{\circ}$ at 0° and 10° angle of attack.

At zero angle of attack, fan RPM and wind tunnel speed were varied independently. Data were obtained at several exit vane deflection angles, cascade rotation angles, and lift-cruise fan exit-nozzle deflection angles; with the horizontal tail both on and off; and with the trailing edge flaps deflected 30° for all tests.

When angle of attack or angle of sideslip was varied, fan RPM and wind tunnel speed were held constant. With all four fans operating, various combinations of β_v , σ_v , and δ_{cn} were held constant throughout the angle of attack or angle of sideslip range. With the horizontal tail installed, the deflection angle was varied at 0° and 10° angle of attack to obtain tail effectiveness.

CORRECTIONS

Force and moment data obtained without the lift fans operating (power off) have been corrected for the effects of wind-tunnel wall interference in the following manner.

$$\alpha = \alpha_u + 0.484 C_{L_u}$$

$$C_D = C_{D_u} + 0.0084 C_{L_u}^2$$

$$C_m = C_{m_u} + 0.0240 C_{L_u} \quad (\text{tail on only})$$

Appropriate tares have been applied to the results to account for exposed strut tips.

Reference 14 defines model to wind-tunnel sizing ratios that give small wind-tunnel wall corrections when airplane drag is trimmed. The subject model, according to these guide lines, should produce only small wall effects; therefore, no wind-tunnel wall corrections have been applied to the results with the fans operating.

RESULTS

Table 1 presents an index to the figures. Fan performance, both statically and with forward speed, are shown in figures 3 through 6. Figure 3 presents the zero forward speed characteristics (lift and thrust) for the forward lift fans, the aft lift-cruise fans, and all four fans operating. Figure 4 shows the variation in lift with exit louver deflection (β_v) for the left forward fan while figure 5 presents the

turning effectiveness of the lift-cruise fan hooded deflector. The relationship between velocity ratio and tip-speed ratio is shown in figure 6. The variation in fan thrust with forward speed for the forward lift fans and the lift-cruise fans is given in figure 7. Fan thrust variation with angle of attack is shown in figure 8 for both the front and rear fans at various tip-speed ratios.

The variation in longitudinal characteristics with tip-speed ratio at zero angle of attack is shown in figures 9 through 13. Figure 9 is with the forward fans operating at various exit louver deflections (β_v) and cascade rotation angles (σ_v) over the tip-speed ratio range examined. Lift-cruise fan results are given in figure 10 for selected hooded deflection angles (δ_{cn}). Figures 11 through 13 are for four fan operation with the lift-cruise fan hooded deflectors at 23° , 56° , and 90° , respectively. The variation of power-off (fans not operating) longitudinal characteristics with angle of attack is presented in figure 14 with the horizontal tail on and off. Figures 15 through 20 give the power-on variation of longitudinal characteristics with angle of attack. Lift-cruise fan exhaust-hood deflector angles were held constant while σ_v and tip-speed ratio were varied to give the results shown. δ_{cn} values of 23° , 56° , 90° , and 138.5° are presented. The effect of differentially varying lift fan RPM between the front and rear fans is shown for a $\delta_{cn} = 56^\circ$ on figure 17 and $\delta_{cn} = 90^\circ$ on figure 19.

Horizontal tail effectiveness is presented in figure 21 for both the power off and power on conditions. These results are shown for angles of attack of 0° and 10° .

Figures 22 and 23 show the variation in lateral-directional characteristics with sideslip angle. Figure 22 is for the power off condition while figure 23 presents the power on results.

REFERENCES

1. Aoyagi, Kiyoshi; Hickey, David H.; and deSavigny, Richard A.: Aerodynamic Characteristics of a Large-Scale Model with a High Disk-Loading Lifting Fan Mounted in the Fuselage. NASA TN D-775, 1961.
2. deSavigny, Richard A.; and Hickey, David H.: Aerodynamic Characteristics in Ground Effect of a Large-Scale Model with a High Disk-Loading Lifting Fan Mounted in the Fuselage. NASA TN D-1557, 1962.
3. Hickey, David H.; and Hall, Leo P.: Aerodynamic Characteristics of a Large-Scale Model with Two High Disk-Loading Fans Mounted in the Wing. NASA TN D-1650, 1963.
4. Kirk, Jerry V.; Hickey, David H.; and Hall, Leo P.: Aerodynamic Characteristics of a Full-Scale Fan-in-Wing Model Including Results in Ground Effect with Nose-Fan Pitch Control. NASA TN D-2368, 1964.
5. Hall, Leo P.; Hickey, David H.; and Kirk, Jerry V.: Aerodynamic Characteristics of a Large-Scale V/STOL Transport Model with Lift and Lift-Cruise Fans. NASA TN D-4092, 1967.
6. Hickey, David H.; Kirk, Jerry V.; and Hall, Leo P.: Aerodynamic Characteristics of a V/STOL Transport Model with Lift and Lift-Cruise Fan Power Plants. NASA SP-116, Paper 15, 1966.
7. Hickey, David H.; and Cook, Woodrow L.: Aerodynamics of V/STOL Aircraft Powered by Lift Fans. AGARD CP 22, Paper 15, 1967.
8. Kirk, Jerry V.; Hodder, Brent K.; and Hall, Leo P.: Large-Scale Wind-Tunnel Investigation of a V/STOL Transport Model with Wing-Mounted Lift Fans and Fuselage-Mounted Lift-Cruise Engines for Propulsion. NASA TN D-4233, 1967.

9. Hodder, Brent K.; Kirk, Jerry V.; and Hall, Leo P.: Aerodynamic Characteristics of a Large-Scale Model with a Lift Fan Mounted in a 5-percent Thick Triangular Wing, Including the Effects of BLC on the Lift-Fan Inlet. NASA TN D-7031, 1970.
10. Dickinson, Stanley O.; Hall, Leo P.; and Hodder, Brent K.: Aerodynamic Characteristics of a Large-Scale V/STOL Transport Model with Tandem Lift Fans Mounted at Mid-Semispan of the Wing. NASA TN D-6234, 1971.
11. Kirk, Jerry V.; Hall, Leo P.; and Hodder, Brent K.: Aerodynamics of Lift Fan V/STOL Aircraft. NASA TM X-52,086, 1971.
12. Hall, Leo P.; and Kirk, Jerry V.: Large-Scale Wind-Tunnel Investigation of a V/STOL Transport Model with Podded Lift Fans Forward and Aft of a Low Mounted Wing. NASA TM X-62, 102, 1971.
13. Kirk, Jerry V.; Dickinson, Stanley O.; Hall, Leo P.; and Coffman, Mary G.: Aerodynamic Characteristics of a Large Scale Lift Fan Transport Model with Podded Fans Forward and Lift Cruise Fans Mounted Above the Wing. NASA TM X-62,151, 1972.
14. Cook, Woodrow L.; and Hickey, David H.: Comparison of Wind-Tunnel and Flight-Test Aerodynamic Data in the Transition Flight Speed Range for Five V/STOL Aircraft. Paper 26, NASA SP-116, 1966.

TABLE 1 LIST OF FIGURES

FIGURE	α , DEG.	β , DEG.	FANS	μ	β_V , DEG.	σ_V , DEG.	δ_{cn} , DEG.	i_t , DEG.	REMARKS
3(a)(b)	0	0	LIFT	-	0	0	90	0	STATIC PERFORMANCE
3(c)(d)			LIFT-CR	-	90	0	VAR.		
3(e)(f)			ALL	-	0	VAR.	VAR.		
4			LIFT	-	VAR.	VAR.	90		TURNING ↓
5			LIFT-CR	-	VAR.	-	VAR.		
6			ALL	VAR.	0	0	90		μ VERSUS V_o/V_j
7(a)			LIFT	VAR.	0	0	90		ORIGINAL INLET
7(b)			LIFT	VAR.	0	0	90		REVISED INLET
7(c)			LIFT-CR	VAR.	-	-	90		
8(a)			LIFT	.12	0	0	40		VARIATION IN FAN
8(b)			LIFT	.18	0	0	40		THRUST WITH α
8(c)			LIFT-CR	.12	0	0	56		
8(d)			LIFT-CR	.17	0	0	23		
8(e)			LIFT-CR	.26	0	0			
8(f)			LIFT-CR	.26	0	0			
LONGITUDINAL DATA AT ZERO ANGLE OF ATTACK									
9(a)(b)	0	0	LIFT	VAR.	0	VAR.	90	0	OFF
9(c)(d)					-8				OFF
9(e)(f)					+8				OFF
9(g)(h)					+16				OFF
9(i)(j)					90				OFF
10(a)			LIFT-CR						ALL
10(b)									
10(c)									
11(a)(b)									

TABLE 1 CONTINUED

-12-

FIGURE	α , DEG.	β , DEG.	FANS	μ	σ_v , DEG.	δ_{cn} , DEG.	δ_t , DEG.	REMARKS
11 (ctd)	0	0	ALL	VAR.	-8	23	0	
11 (exf)	0	0			-16			
11 (gm)	0	0			+8			
11 (iij)	0	0			+16			
12 (are)	0	0			0			
12 (ctd)	0	0			-8			
12 (ewf)	0	0			-16			
12 (gpm)	0	0			+8			
12 (ixj)	0	0			+16			
13 (cm)	0	0			0			
13 (cm)	0	0			VAR.	0		
14	VAR.	VAR.	ALL	ALL	-	90	90	POWER OFF
15 (a)	0	0	ALL	ALL	.12	0	0	
15 (b)	0	0	ALL	ALL	.18	23	0	
15 (c)	0	0	ALL	ALL	.26	56	0	
16 (a)	0	0	ALL	ALL	.08	20	0	
16 (b)	0	0	ALL	ALL	.08	-40	0	
16 (c)	0	0	ALL	ALL	.12	0	0	
16 (d)	0	0	ALL	ALL	.18	40	0	
16 (e)	0	0	ALL	ALL	.18	26	0	
16 (f)	0	0	ALL	ALL	.26	20	0	
16 (g)	0	0	ALL	ALL	.26	80	0	
16 (h)	0	0	ALL	ALL	.26	-40	0	
16 (i)	0	0	ALL	ALL	.08	56	0	
17 (a)	0	0	ALL	ALL	0	0		

TABLE 1 CONTINUED

-13-

FIGURE	α , DEG.	β , DEG.	FANS	μ	β_V , DEG.	σ_V , DEG.	Scn, DEG.	i_t , DEG.	REMARKS
17 (b)	VAR.	0	ALL	.07	0	56	0		
17 (c)	VAR.	0	ALL	.09	40	↓	0, OFF		
18 (a)	VAR.	0	ALL	.06	VAR.	90	0		
18 (b)	VAR.	0	ALL	.08	40	20	0, OFF		
18 (c)	VAR.	0	ALL	.06	40	40	0, OFF		
18 (d)	VAR.	0	ALL	.08	60	60	0, OFF		
18 (e)	VAR.	0	ALL	.12	40	40	0, OFF		
18 (f)	VAR.	0	ALL	.12	60	60	0, OFF		
18 (g)	VAR.	0	ALL	.17	40	40	0, OFF		
18 (h)	VAR.	0	ALL	.17	40	40	0, OFF		
18 (i)	VAR.	0	ALL	.03	0	0	0, OFF		
19	VAR.	0	ALL	.08	0	0	0, OFF		
20 (a)	VAR.	0	ALL	.12	0	0	0, OFF		
20 (b)	VAR.	0	ALL		138.5	138.5	OFF		
<hr/>									
HORIZONTAL TAIL EFFECTIVENESS									
21 (a)	0, 10	0	—	—	90	90	VAR.	2.3	POWER OFF
21 (b)	0	0	ALL	VAR.	0	-40	0	56	
21 (c)	0	0	ALL	VAR.	0	40	0	56	
21 (d)	0, 10	0	ALL	VAR.	0	80	0	56	
21 (e)	0, 10	0	ALL	VAR.	0	0	0	90	
21 (f)	0, 10	0	ALL	VAR.	0	40	0	90	
21 (g)	0	0	ALL	VAR.	0	0	0	90	
21 (h)	0, 10	0	ALL	VAR.	0	0	0	56	
<hr/>									
LATERAL-DIRECTIONAL CHARACTERISTICS									
22	0, 10	VAR.	—	—	90	90	0	0	POWER OFF
23 (a)	0, 10	VAR.	ALL	.13	0	0	56	0	

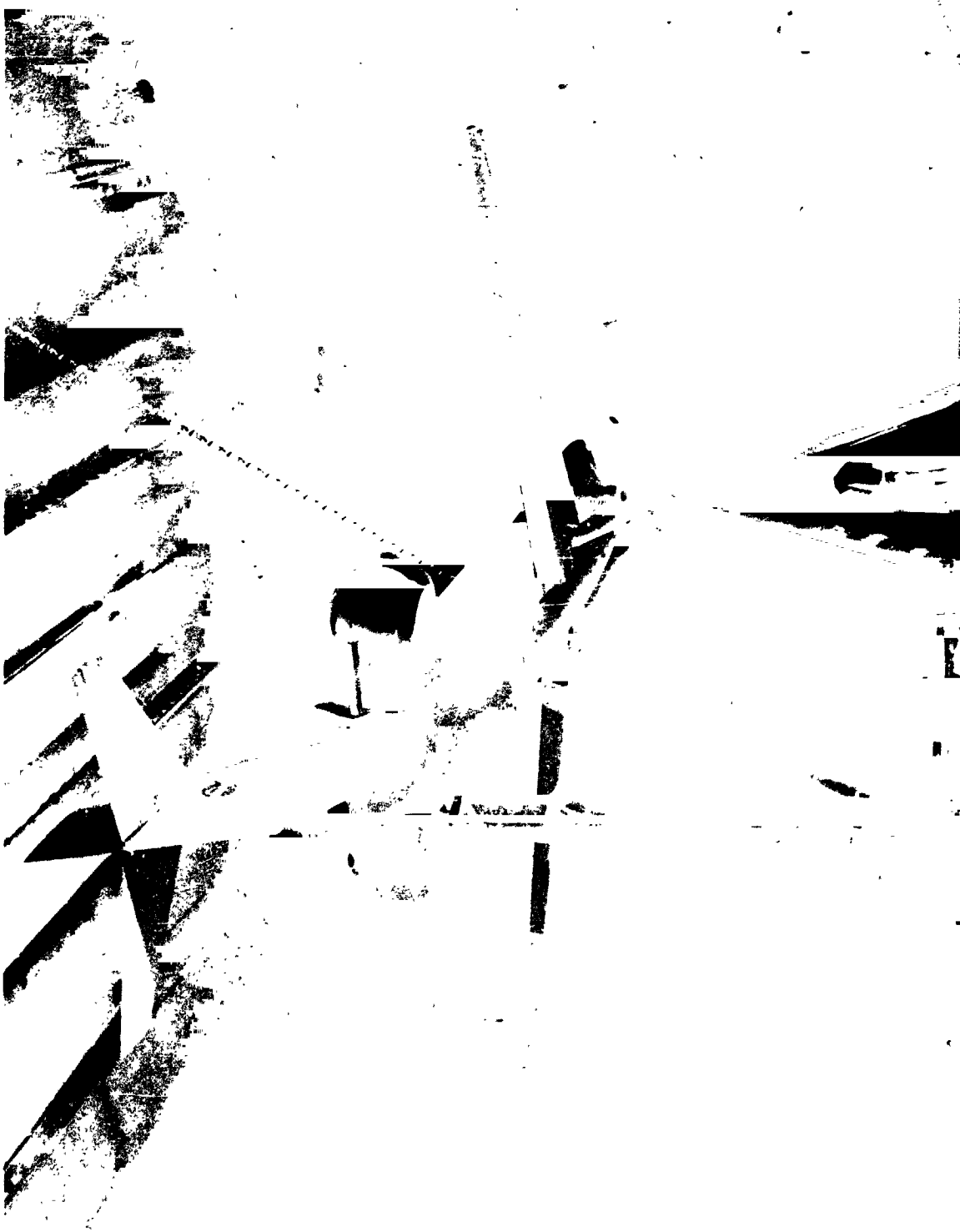
TABLE 1 CONCLUDED

FIGURE	α , DEG.	β , DEG.	FANS	μ	β_V , DEG.	σ_V , DEG.	σ_{en} , DEG.	δ , DEG.	REMARKS
23(b)	0, 10	VAR	ALL	.18	0	40	56	0	
23(c)				.25		80	56		
23(d)				.06		40	90		
23(e)				.08		40	90		
23(f)				.12		40	90		



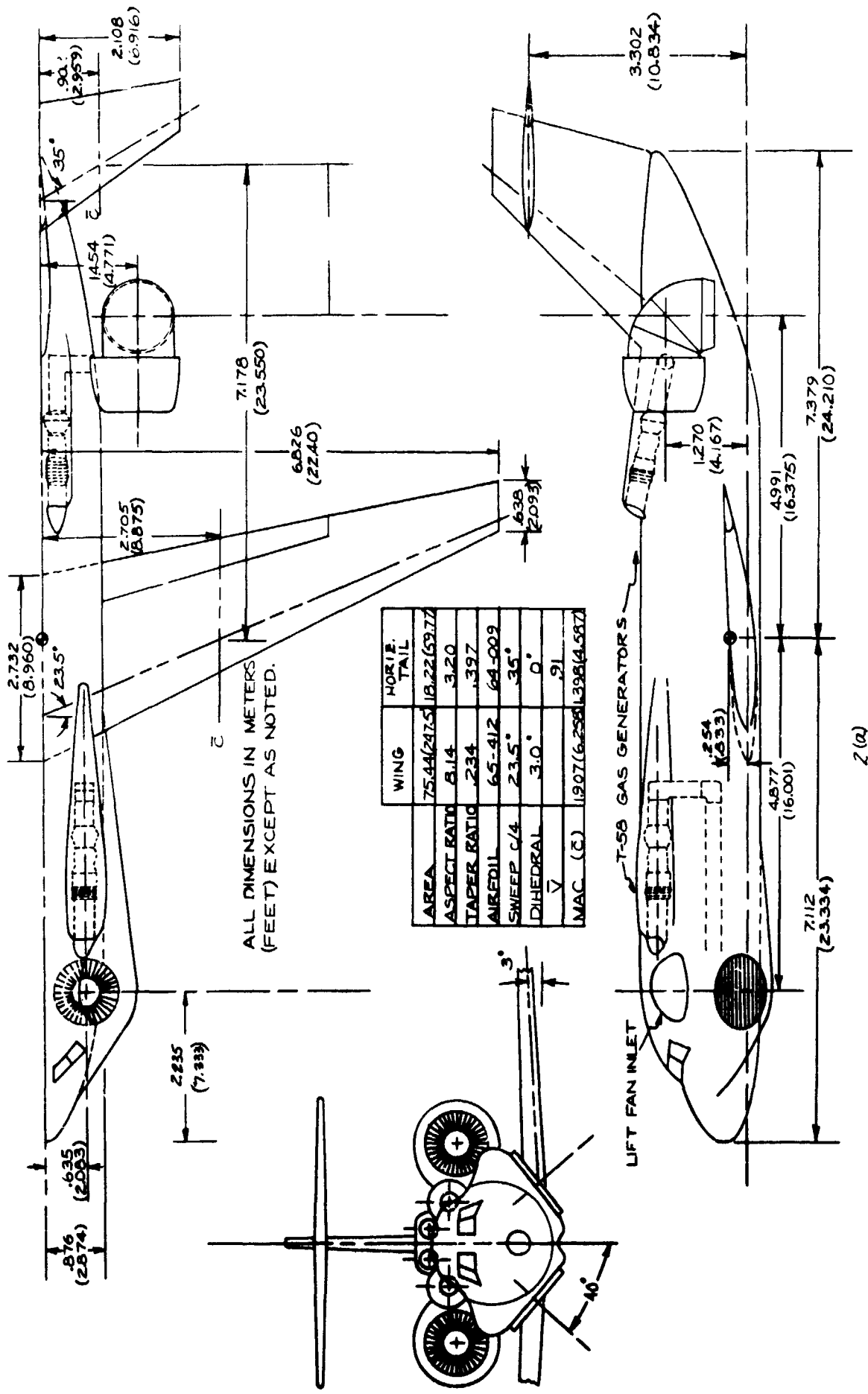
(a) 3/4 front view.

Figure 1.- Photographs of the model mounted in the Ames 40- by 80-foot wind tunnel.



(b) 3/4 rear view.

Figure 1.- Concluded.



(a) Overall dimensions and geometry.

Figure 2.— Model characteristics and details.

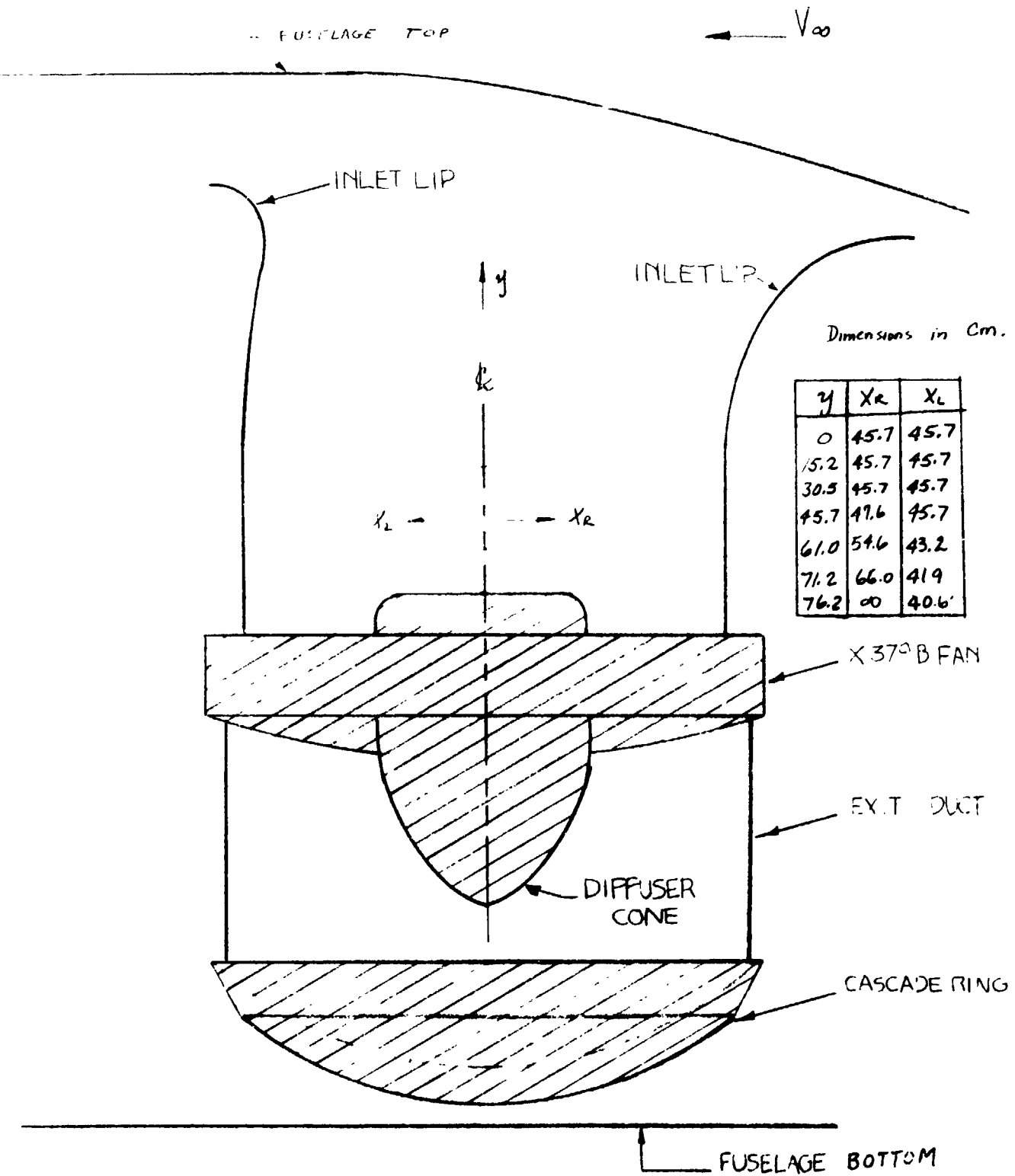


Figure 2.(b) Forward Lift Fan Inlet Cross Section Along Free Stream

(b) Forward lift fan inlet cross section along free stream.

Figure 2.- Continued.

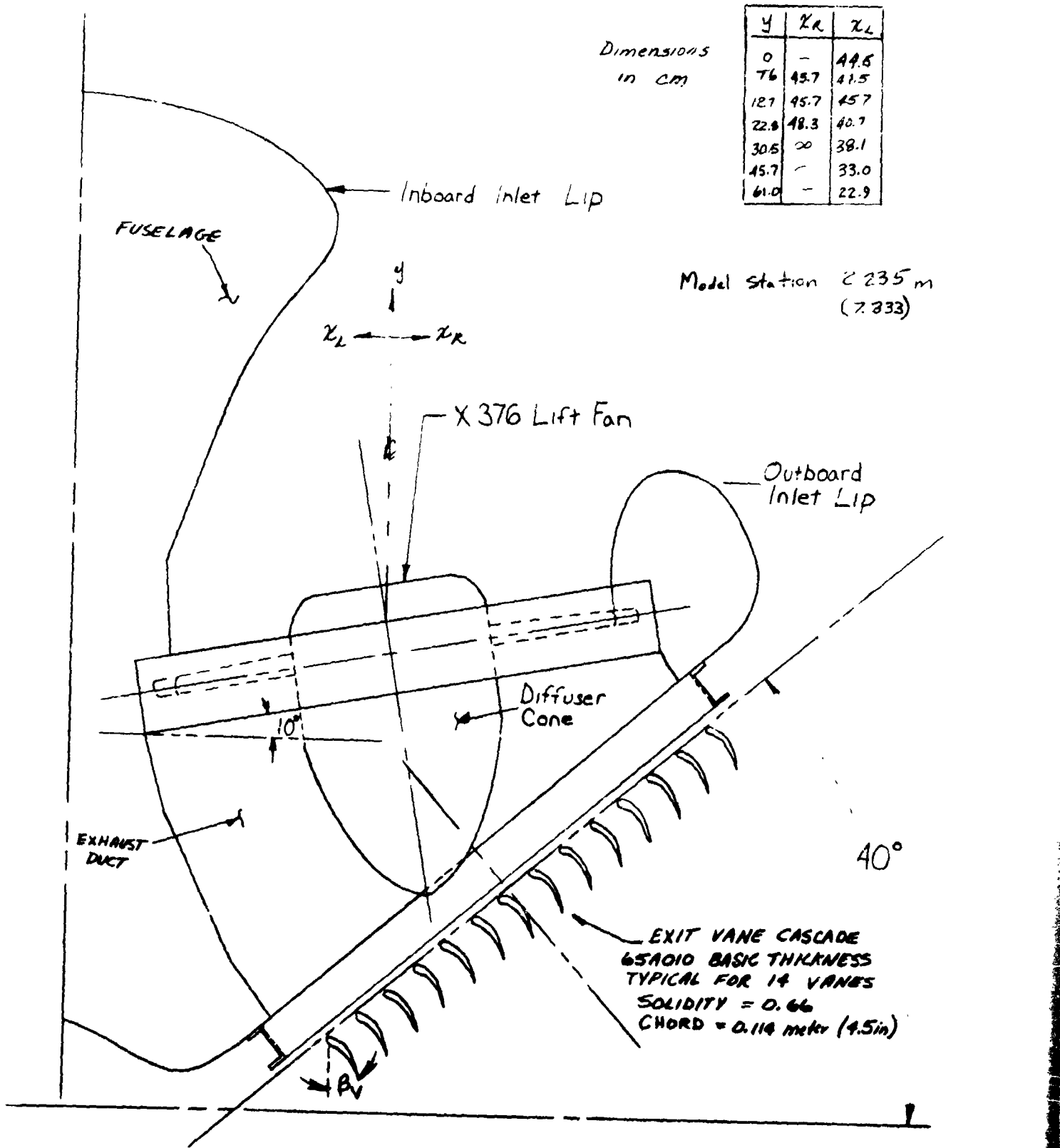
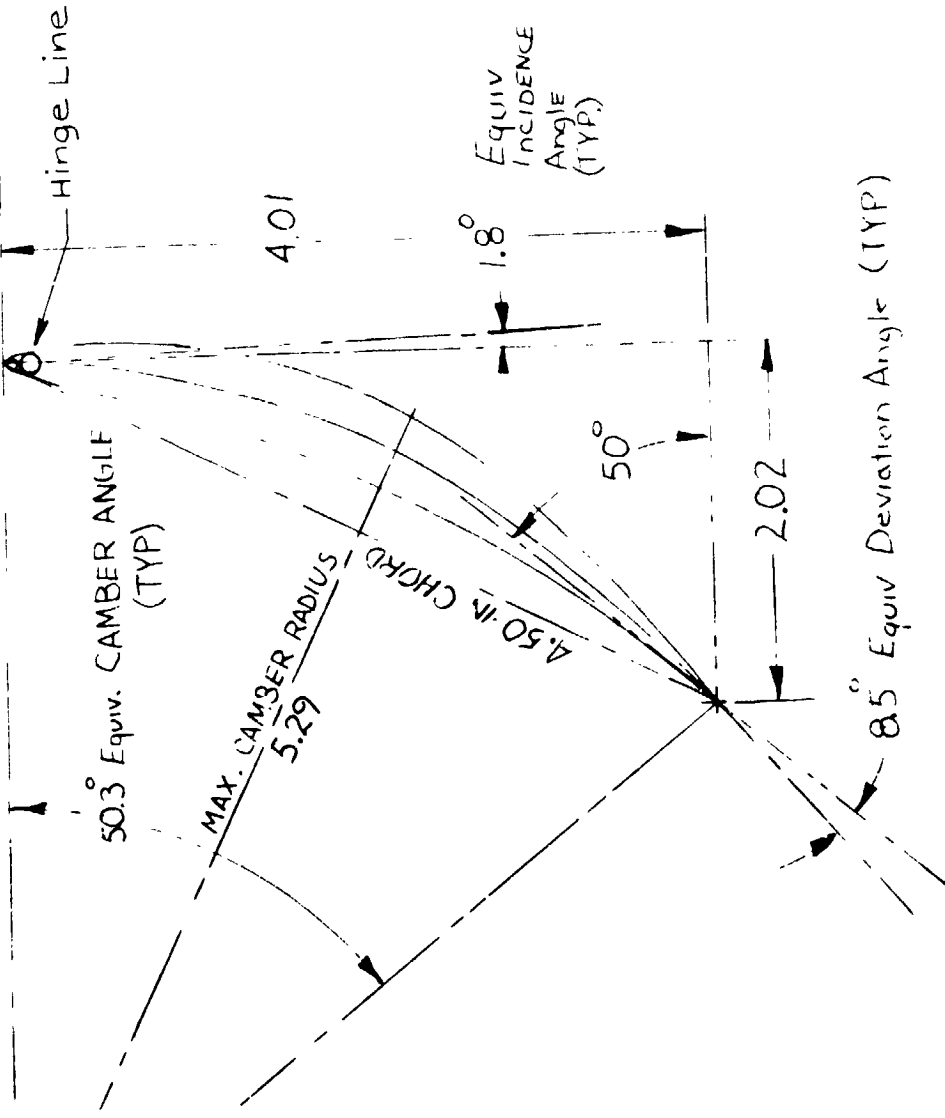


Figure 2.(c) TYPICAL LIFT FAN AND EXIT VANE INSTALLATION.

(c) Forward lift fan and exit lower installation.

Figure 2.- Continued.



X%	X-IN	Y-IN	Y%-IN
0	0	0	0
0.50	.0225	.765	.0344
0.75	.0338	.928	.0418
1.25	.0563	1.183	.0532
2.50	.1125	1.623	.0730
5.00	.2250	2.182	.0982
7.50	.3380	2.650	.1193
10	.4500	3.040	.1368
15	.6750	3.658	.1646
20	.9000	4.127	.1857
25	1.1250	4.483	.2017
30	1.3500	4.742	.2134
35	1.5750	4.912	.2210
40	1.8000	4.995	.2248
45	2.0250	4.983	.2242
50	2.2500	4.863	.2188
55	2.4750	4.632	.2084
60	2.7000	4.304	.1937
65	2.9250	3.899	.1755
70	3.1500	3.432	.1544
75	3.3750	2.912	.1310
80	3.6000	2.352	.1058
85	3.8250	1.771	.0797
90	4.0500	1.188	.0535
95	4.2750	0.604	.0272
100	4.5000	0.021	.0095

(d) Lift-fan exit louver details.

Figure 2.- Continued.

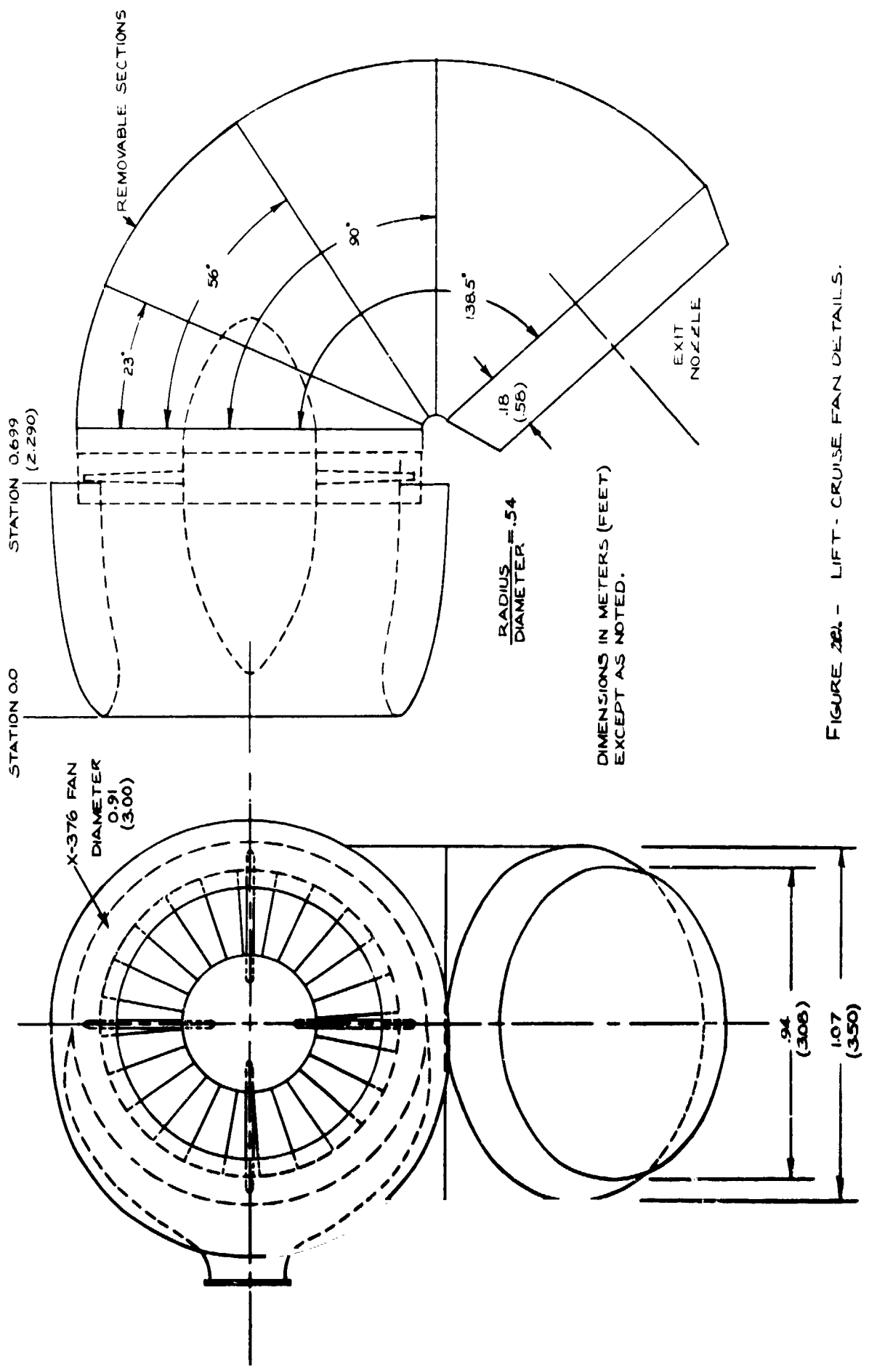
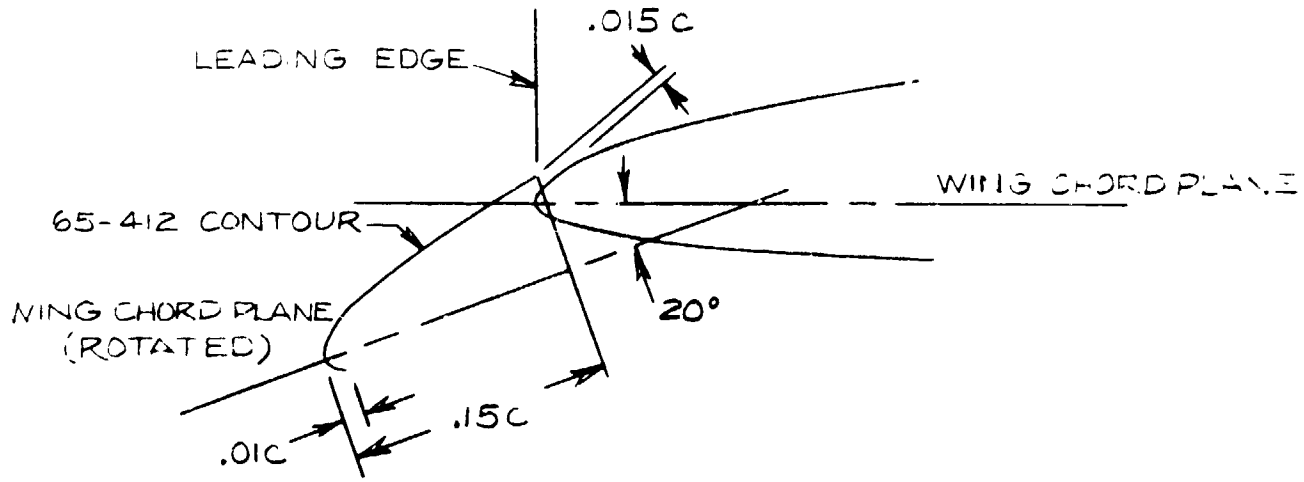


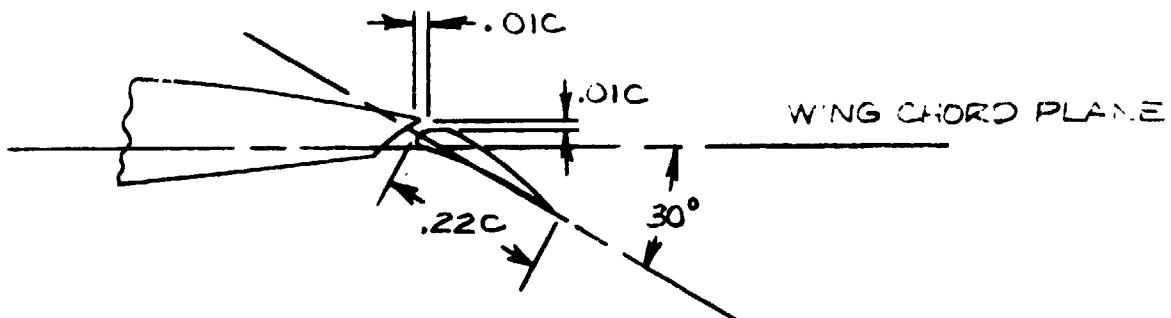
FIGURE 2(e) - LIFT-CRUISE FAN DETAILS.

(e) Lift-cruise fan details.

Figure 2. - Continued.



A - LEADING EDGE SLAT



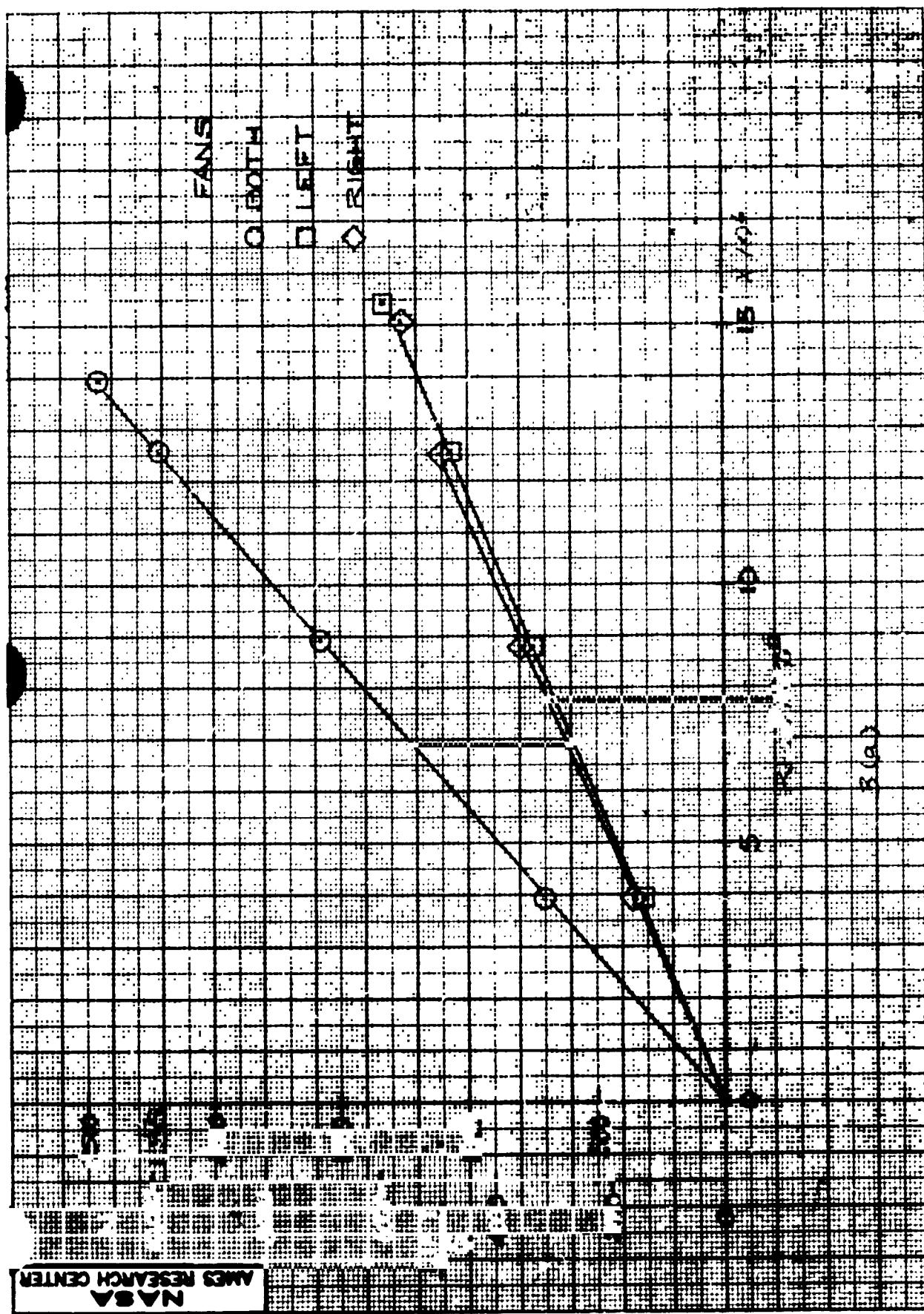
B - TRAILING EDGE FLAP

FIG 2(f).- LEADING AND TRAILING EDGE HIGH LIFT DEVICES.

(f) Leading- and trailing-edge high-lift devices.

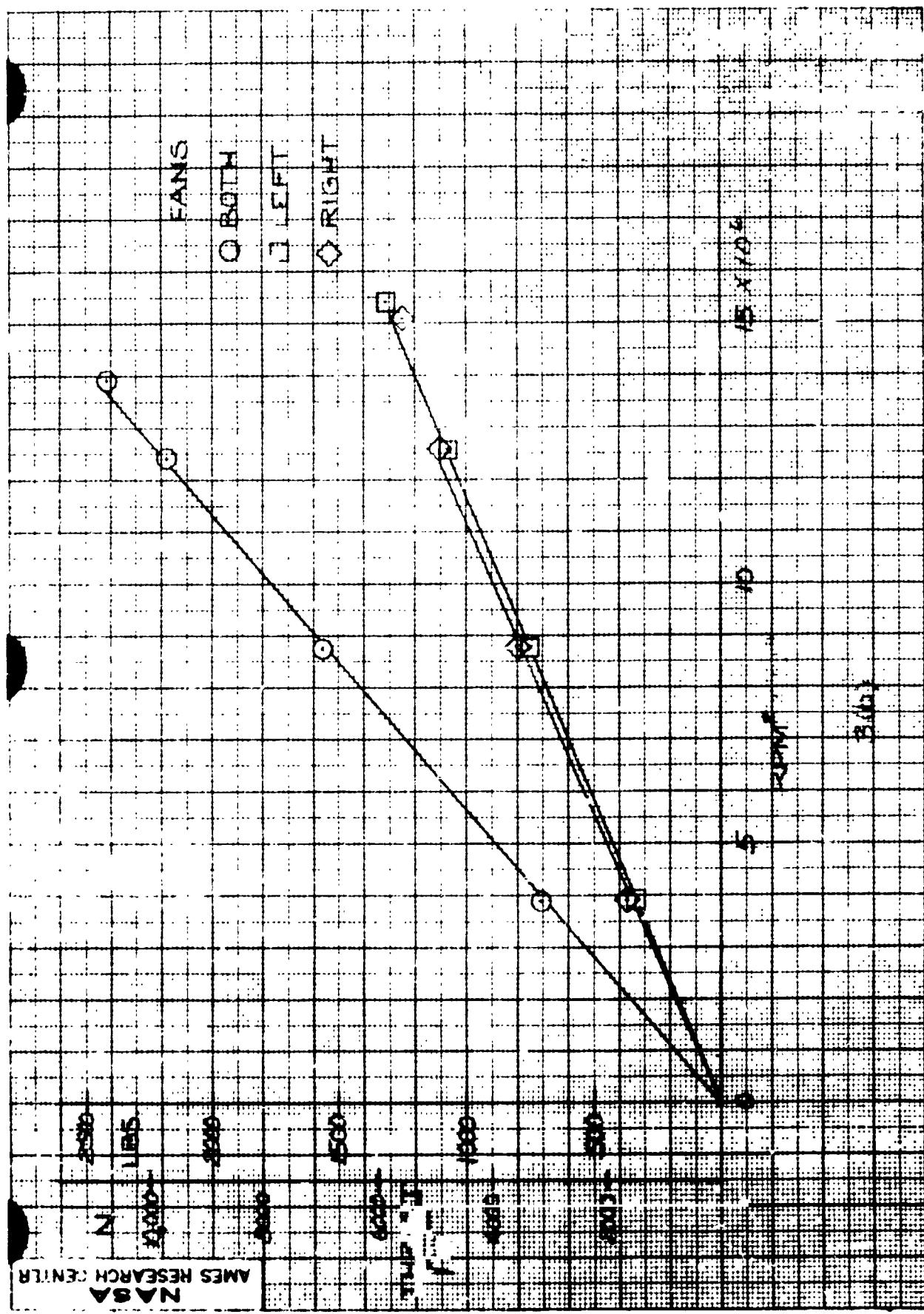
Figure 2.- Concluded.

REPRODUCIBILITY OF THE ORIGINAL PAGE IS POOR.



(a) $\frac{L}{c}$, forward fans, $v_v = 0$, $\omega_v = 0$.

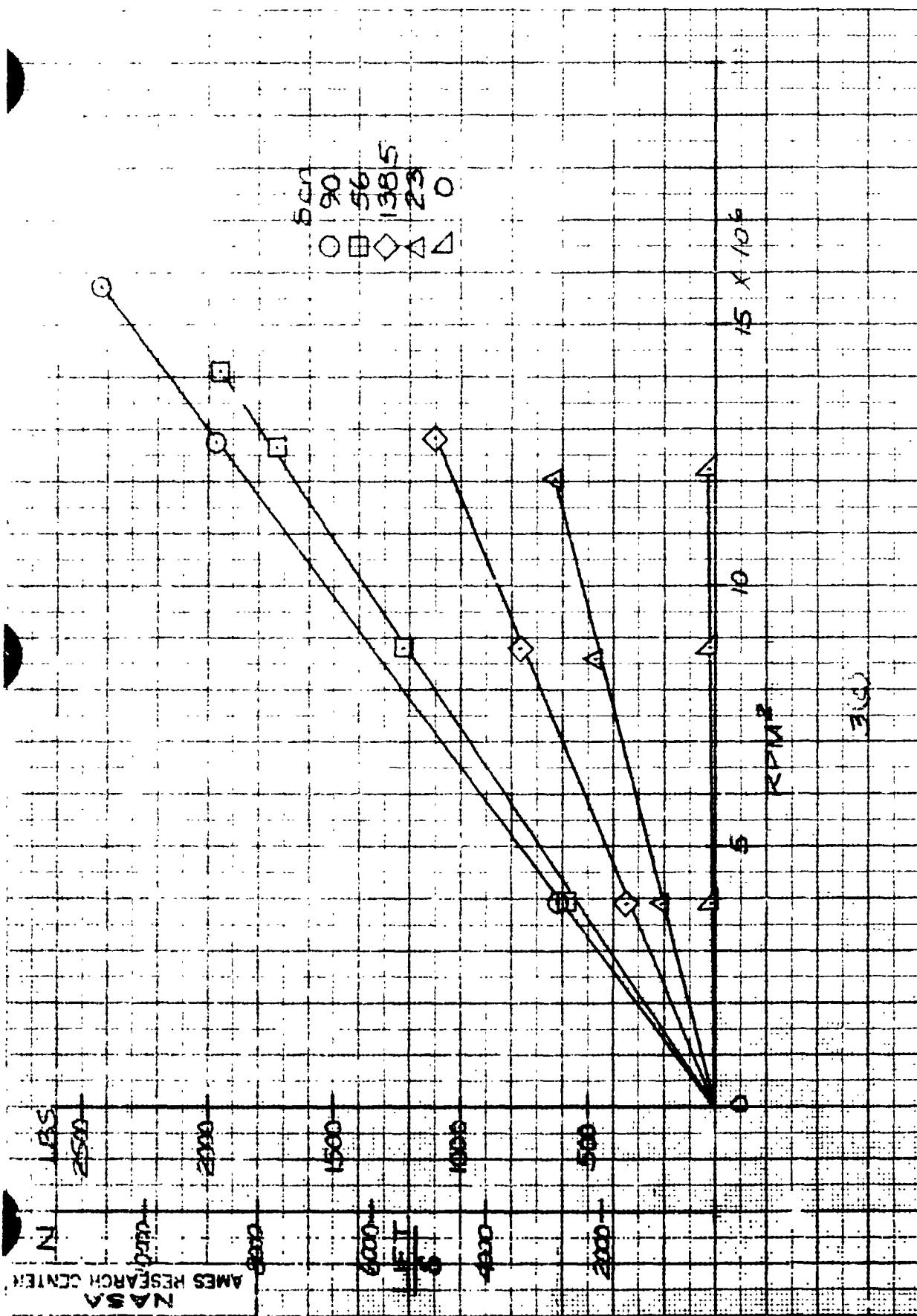
Figure 3.- Zero forward speed characteristics.



(b) $\frac{V_x}{V_w}$, forward fans, $V_z = 0$, $V_y = 0$, $V_w = 0$,

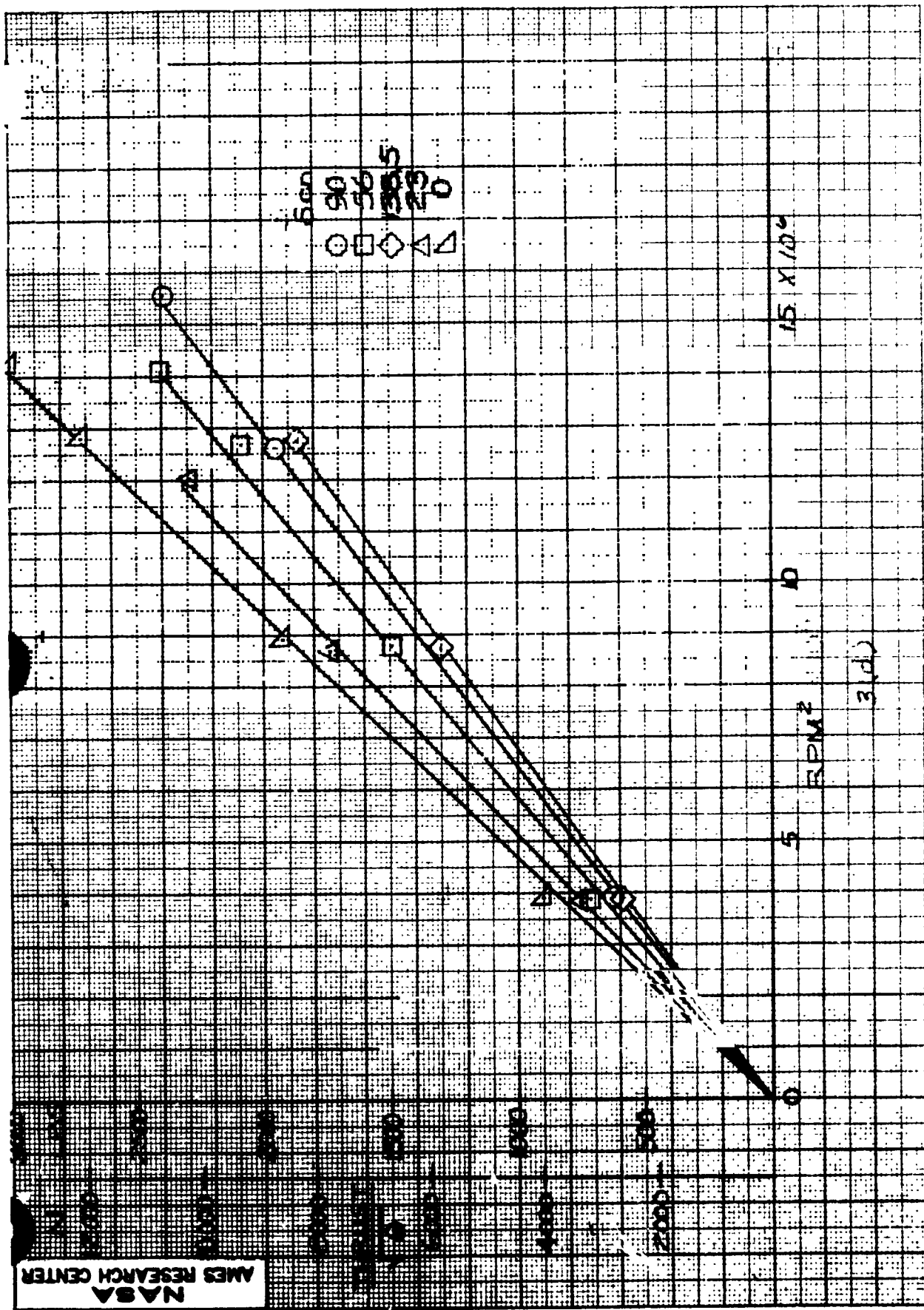
Figure 3. - Continued.

REPRODUCIBILITY OF THE ORIGINAL PAGE IS POOR.



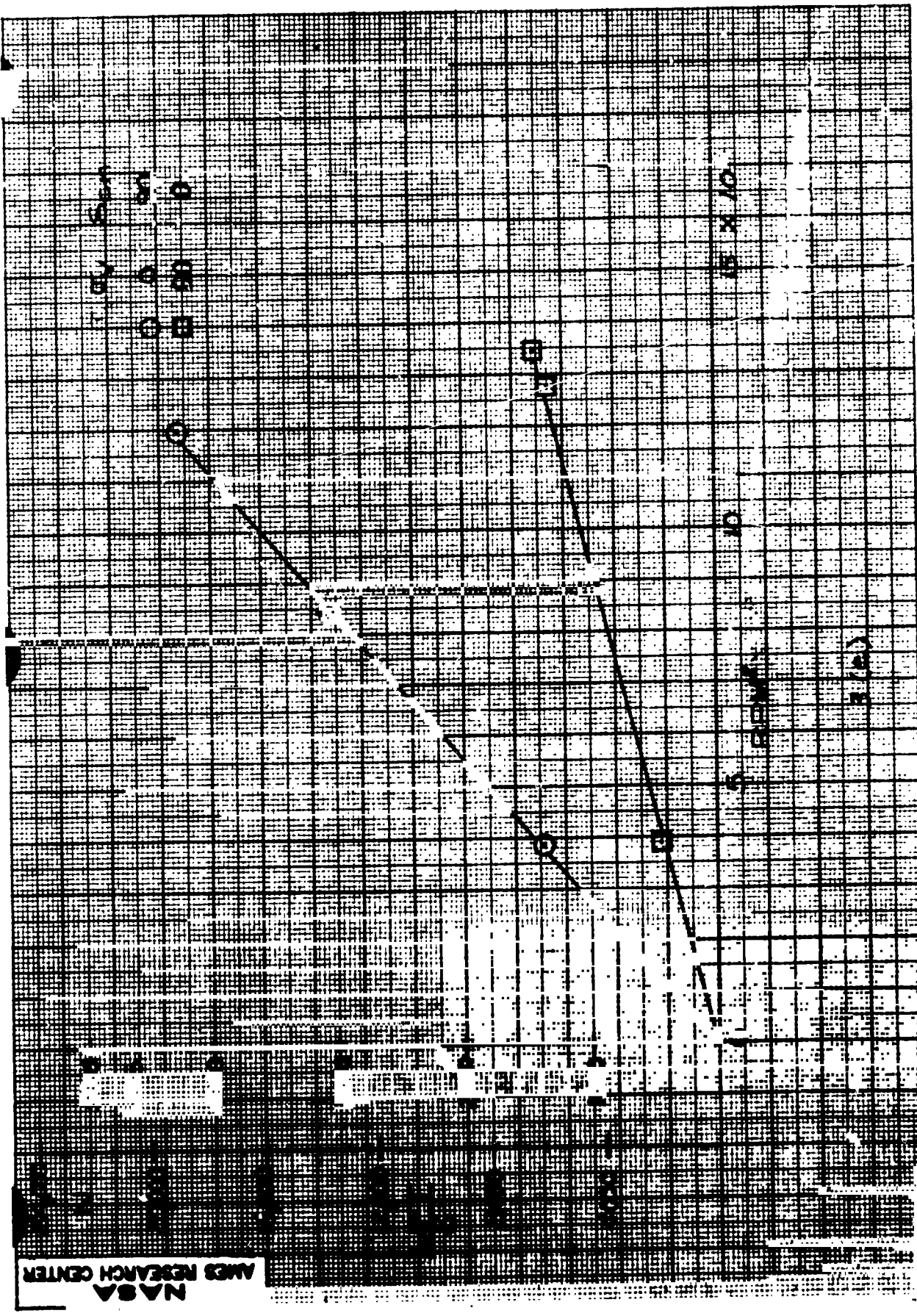
(c) $\frac{L}{S}$, lift-cruise fans, $\beta_v = 0$, $\beta_v = 90^\circ$.

Figure 3.- Continued.



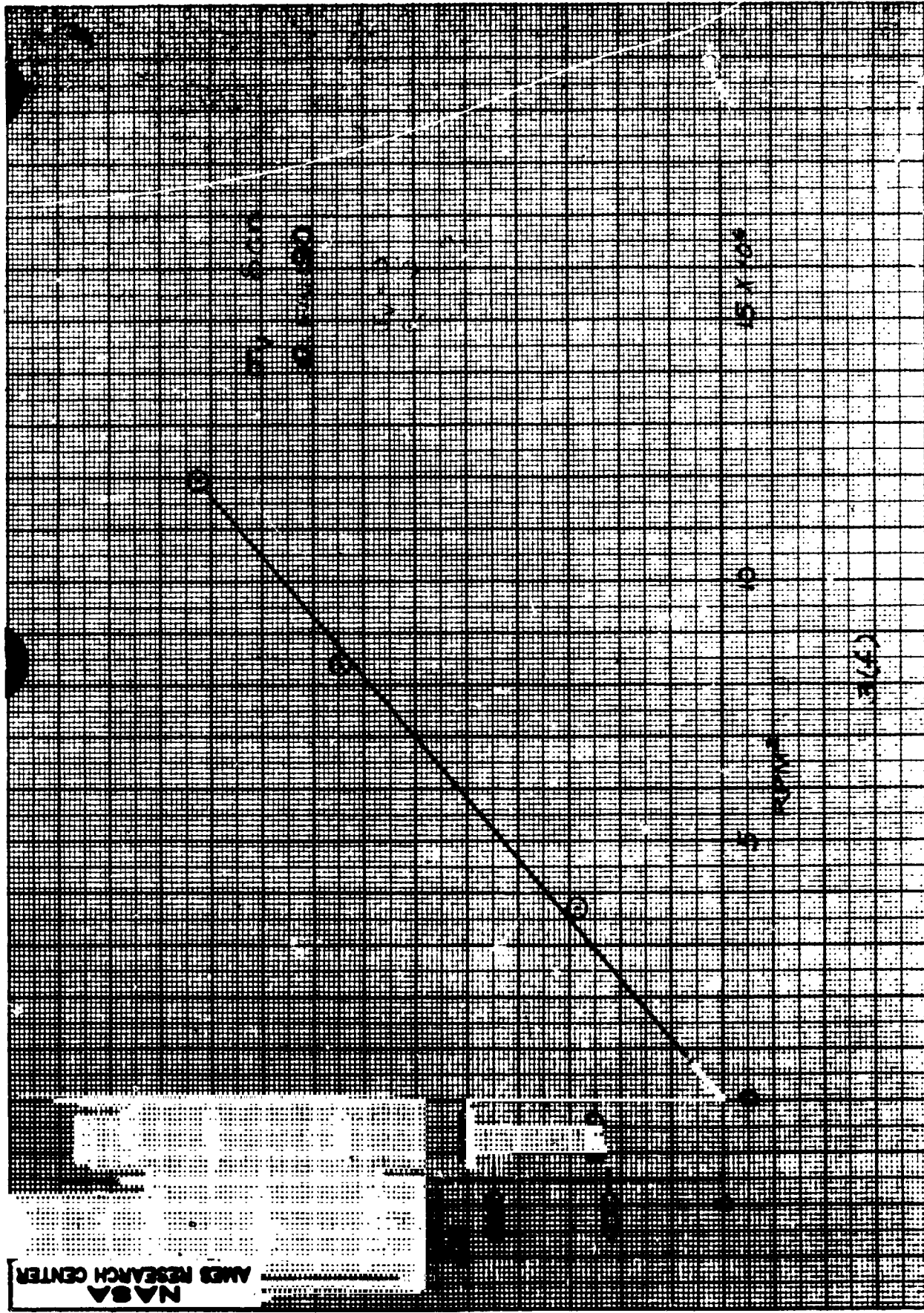
(d) $\frac{T}{\sqrt{6}}$, lift-cruise fans, $\gamma_v = 0$, $\delta_v = 90^\circ$.

Figure 3.- Continued.



(e) $\frac{L}{\delta}$, all four fans, $\beta_v = 0$.

Figure 3.- Continued.



(f) $\frac{T}{\sqrt{\theta}}$, all four fair, $\beta_v = 0$.

Figure 3.- Concluded.

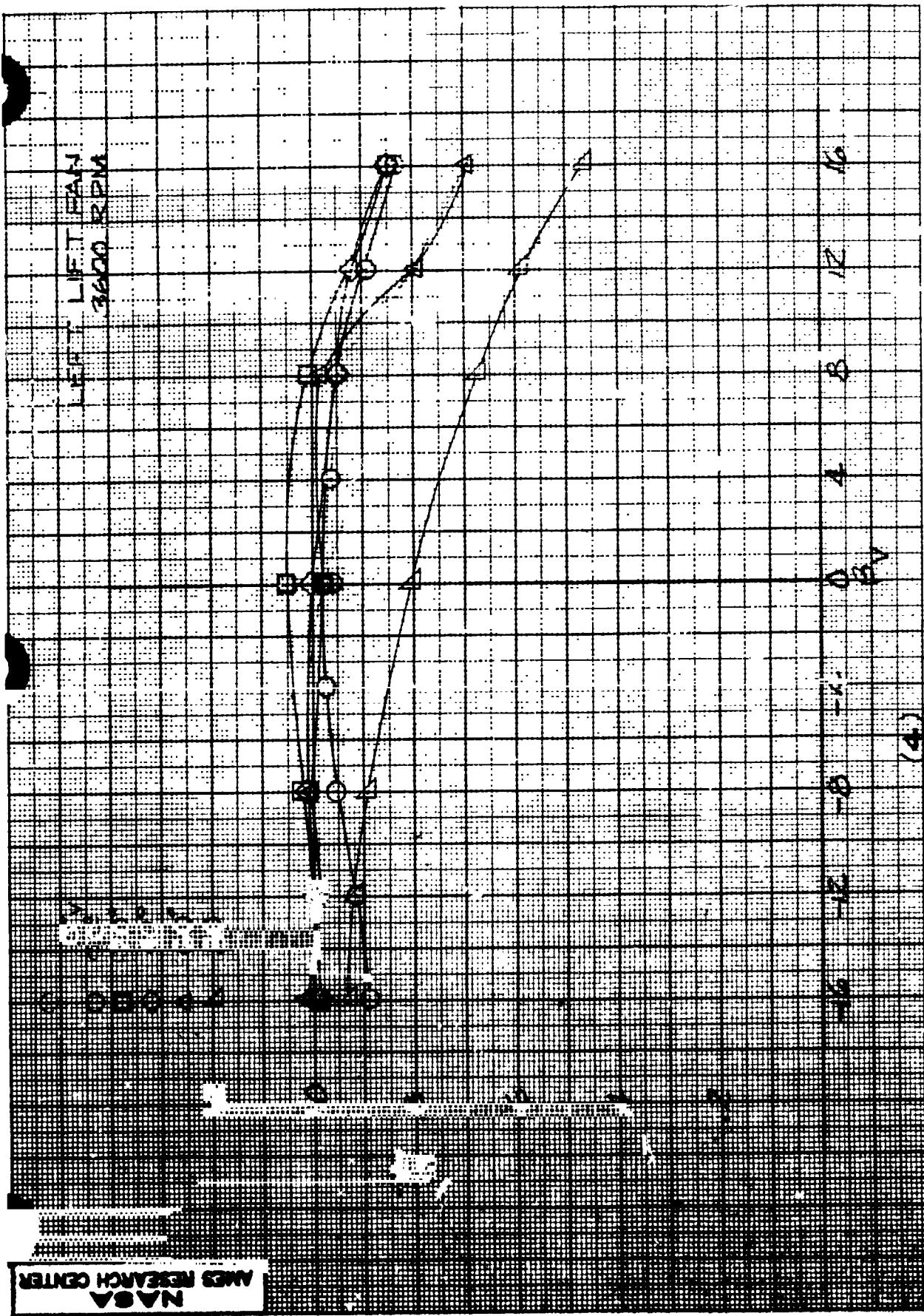


Figure 4.— The variation in lift with exit louver deflection; left forward fan, $\text{RPM} = 3600$, $V = 0$.

REPRODUCIBILITY OF THE ORIGINAL PAGE IS POOR.

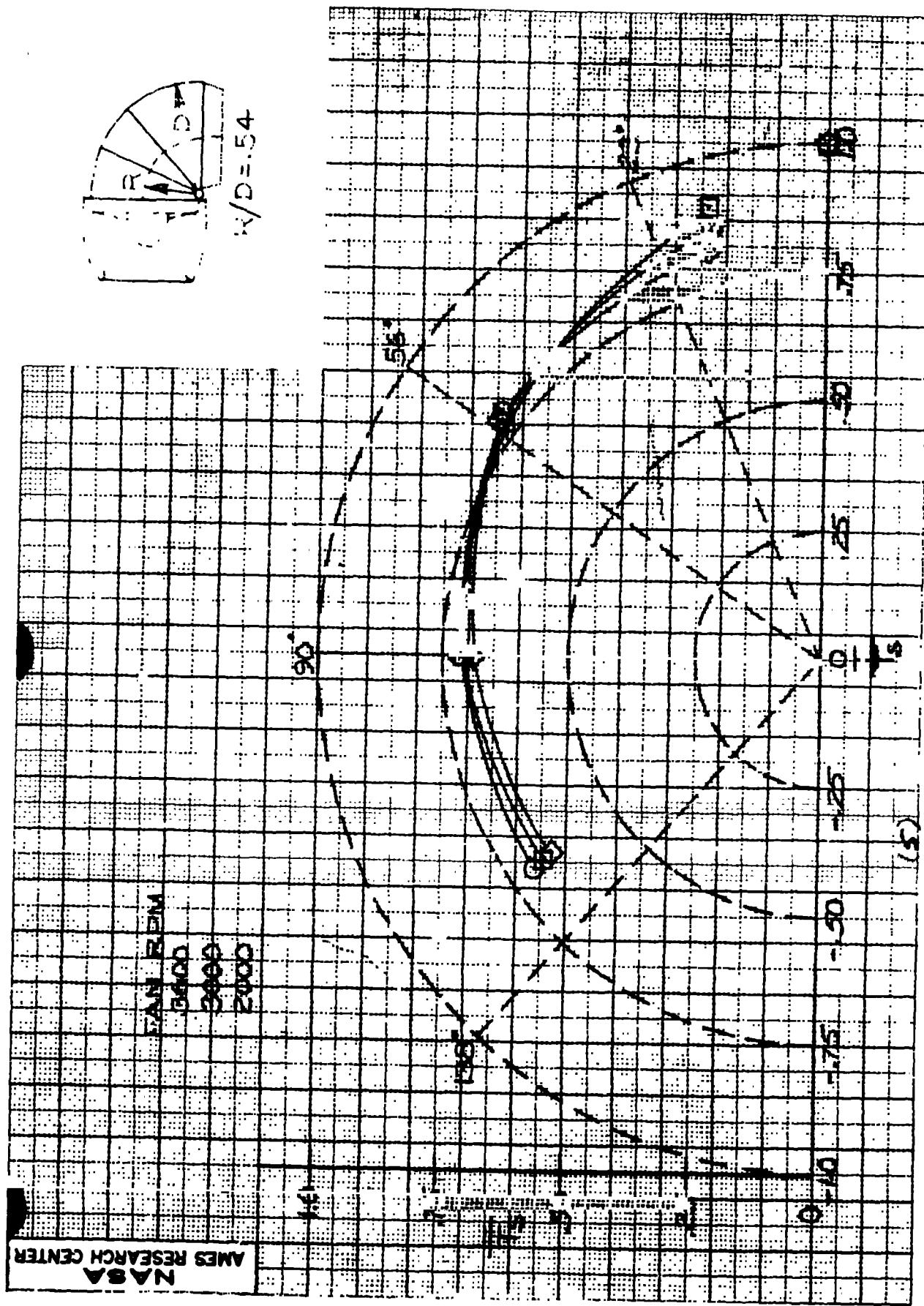


Figure 5.- Lift-cruise fan vectoring with the hooded exhaust deflector; $V = 0$.

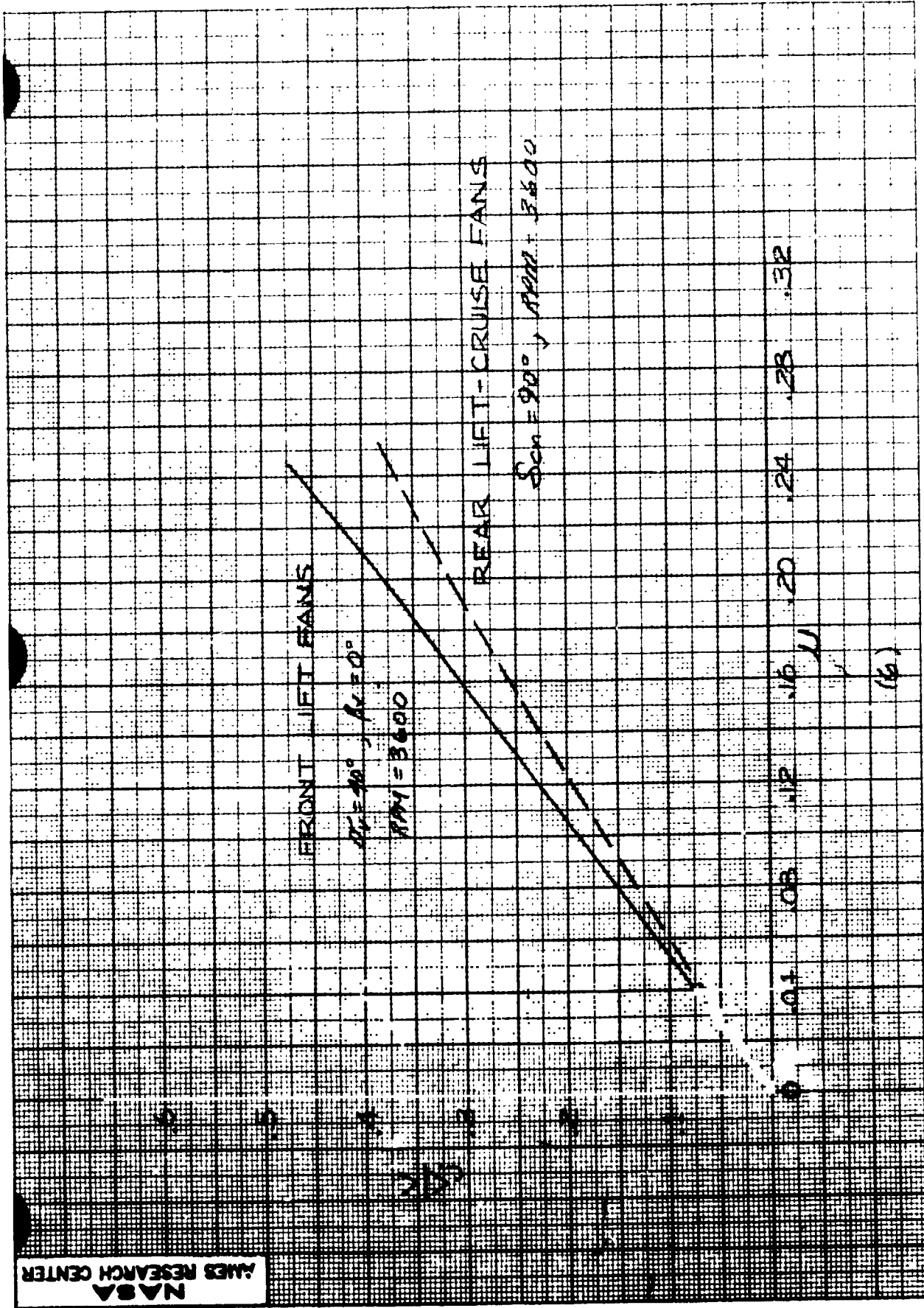
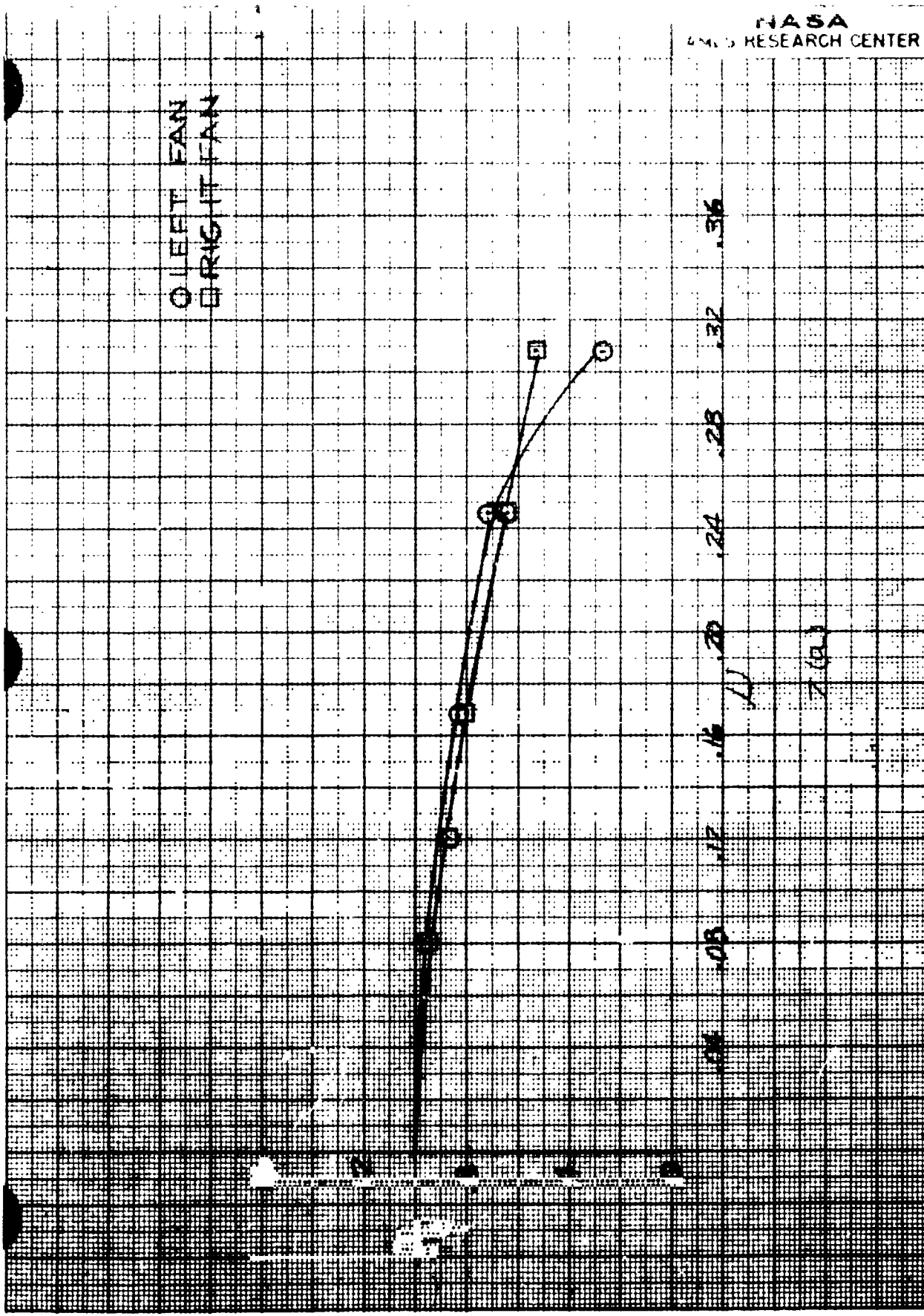


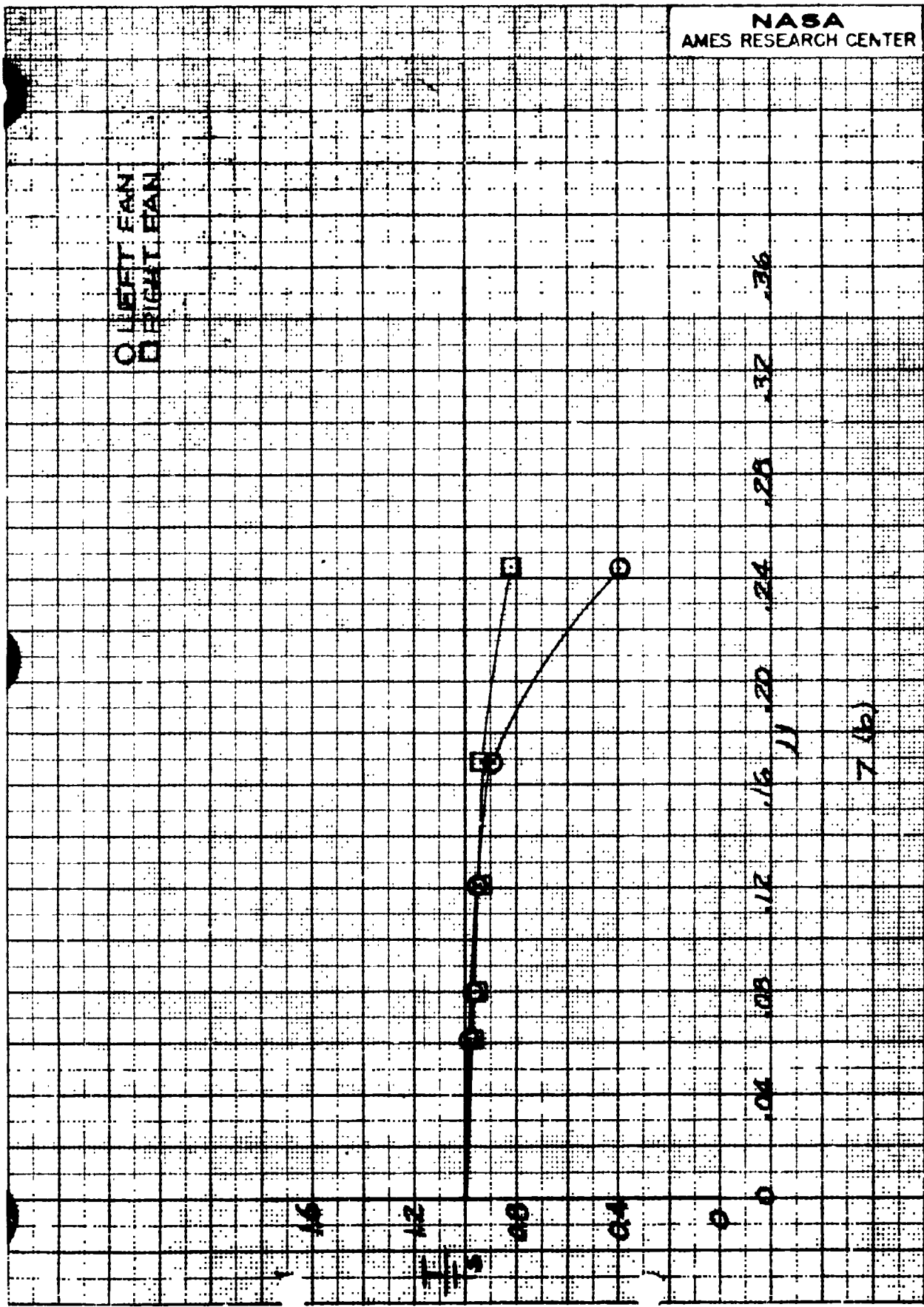
Figure 6.- The relationship between tip-speed ratio and velocity ratio; $\lambda = 0$.

REPRODUCIBILITY OF THE ORIGINAL PAGE IS POOR.



(a) Forward lift fans, original inlet, RPM = 3600, $V_{\infty} = 0$, $V_T = 0$.

Figure 7.- The variation in fan thrust with tip speed ratio.



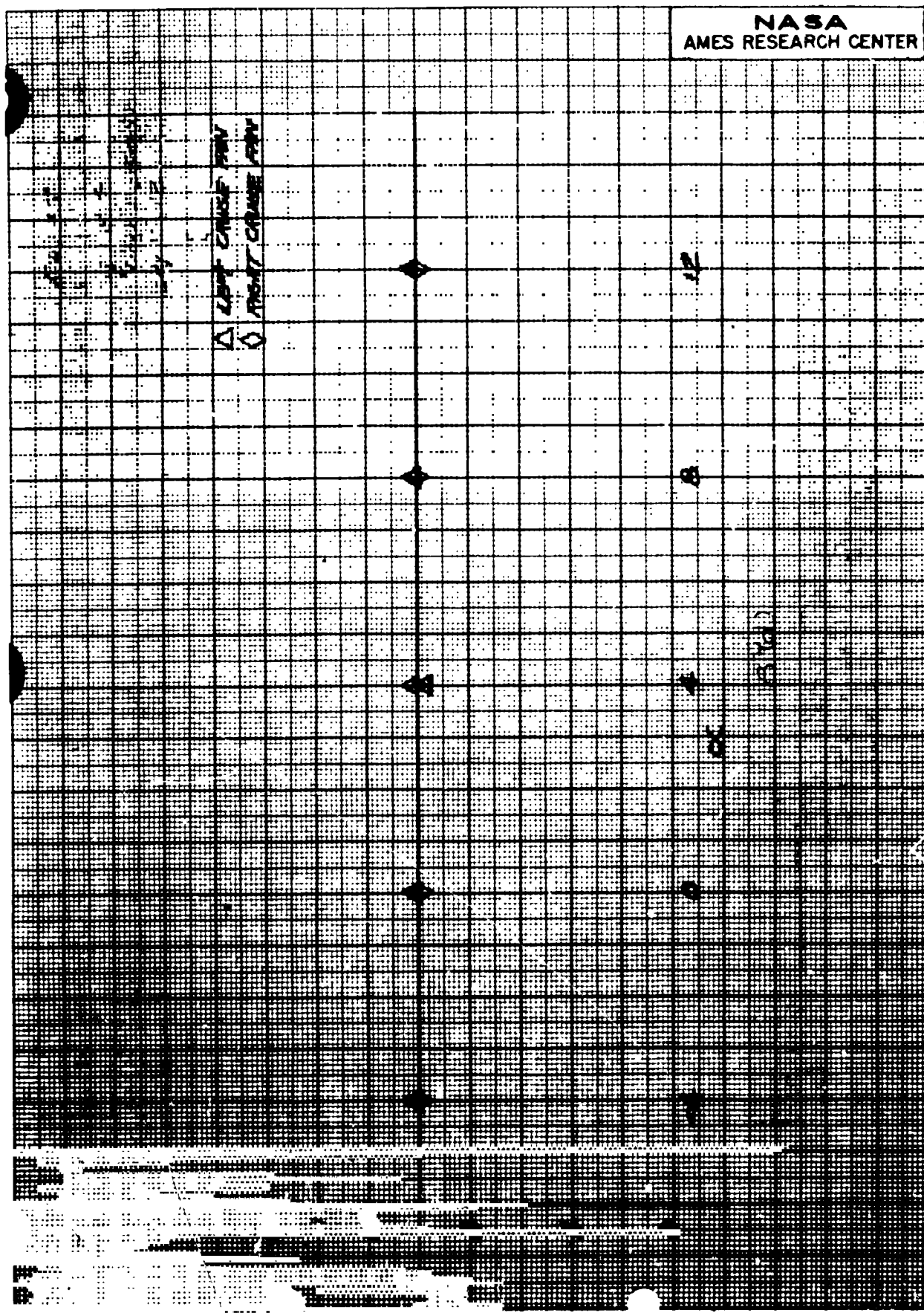
(b) Forward lift fans, revised inlet, RPM = 3600, $\nu = 0$, $\zeta_v = 0$.

Figure 7.- Continued.



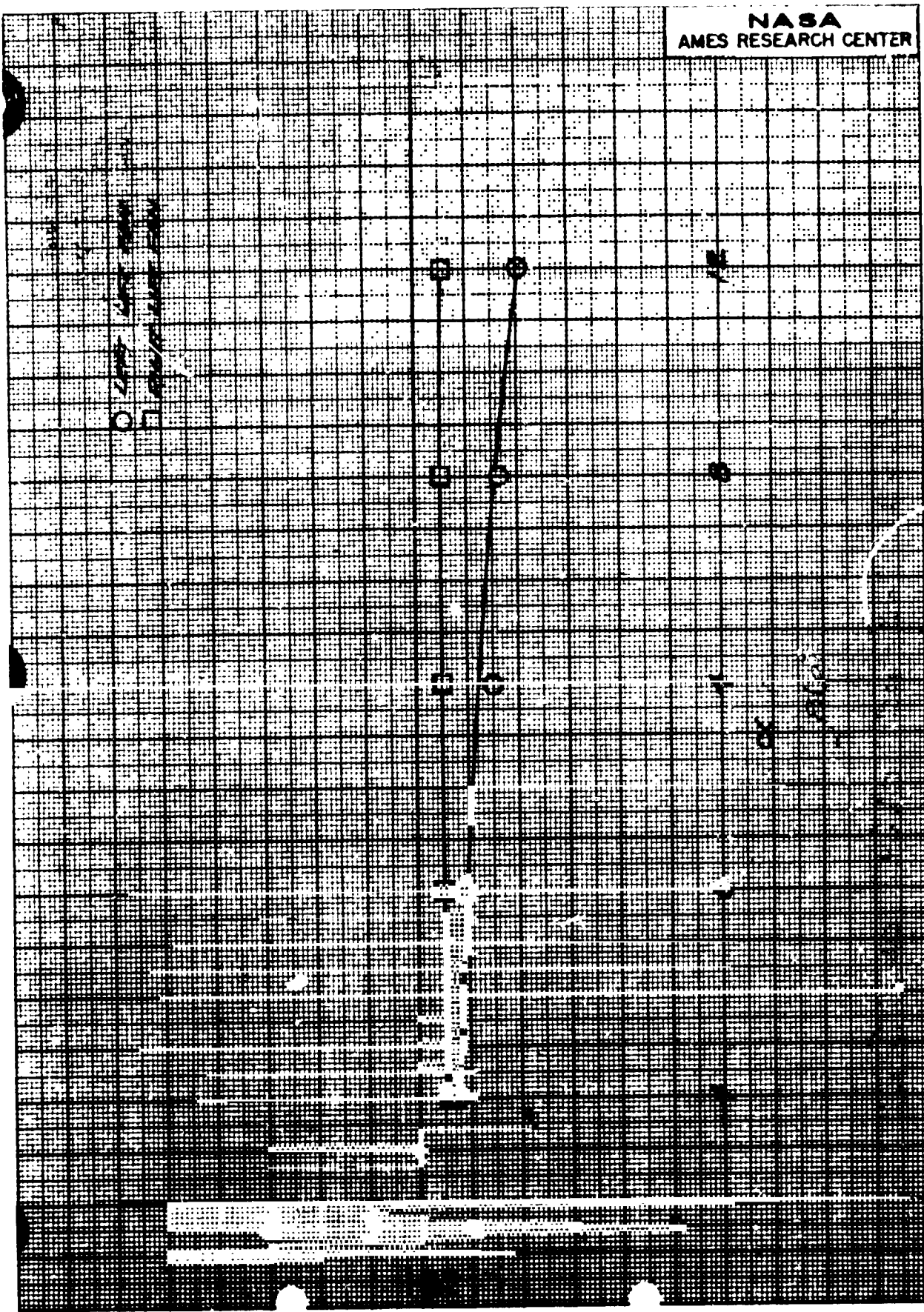
(c) Aft lift-cruise fans, RPM = 3600, $c_n = 90^\circ$.

Figure 7. - Concluded.



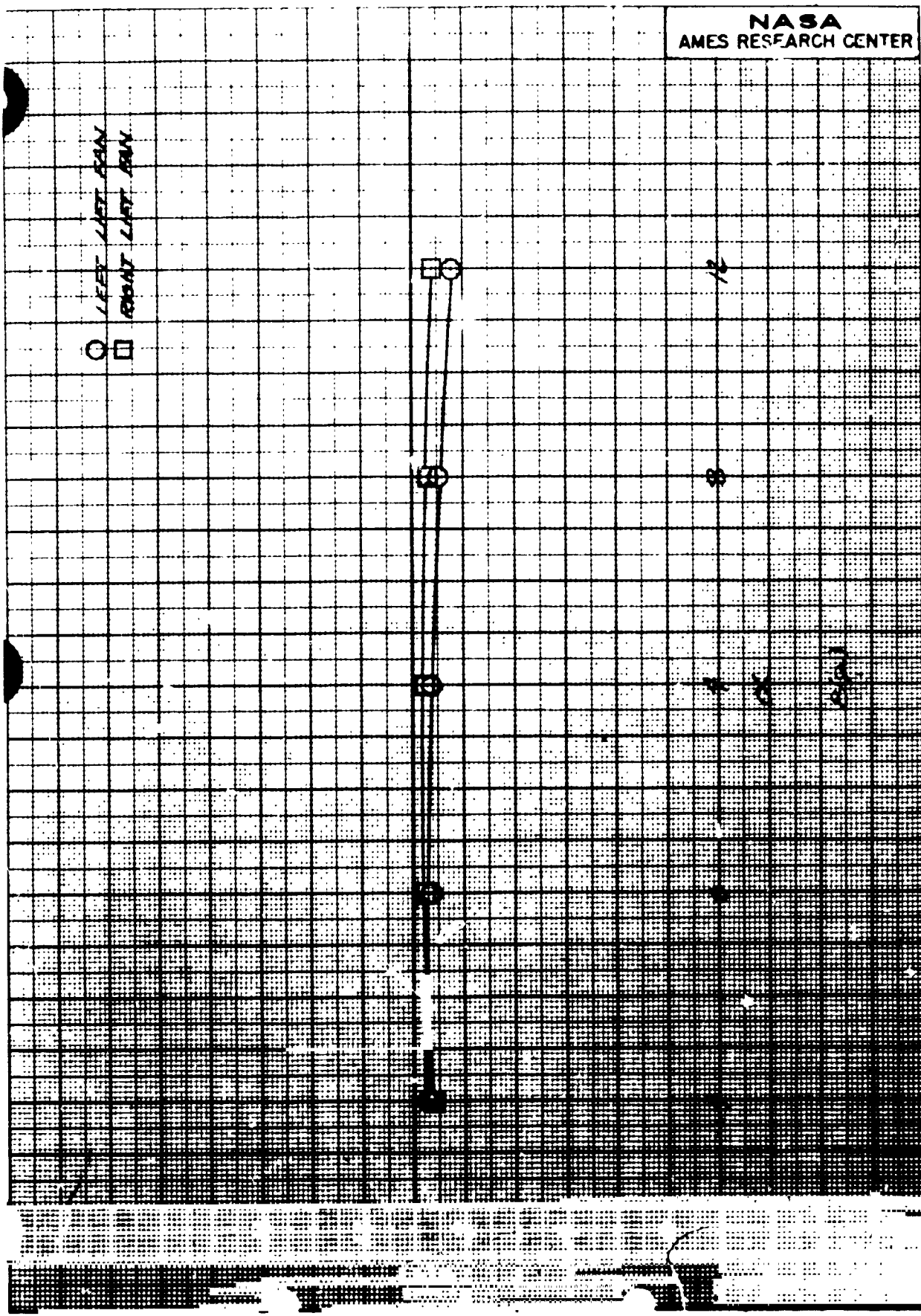
(a) Forward lift fans, $\sigma_v = 0$, $r_v = 0$, RPM = 3600, $\alpha = .12$.

Figure 8. - The variation in fan thrust with model angle of attack.



(b) Forward lift fans, $\alpha_v = 40$, $\beta_v = 0$, RPI = 3600, $\lambda = .18$.

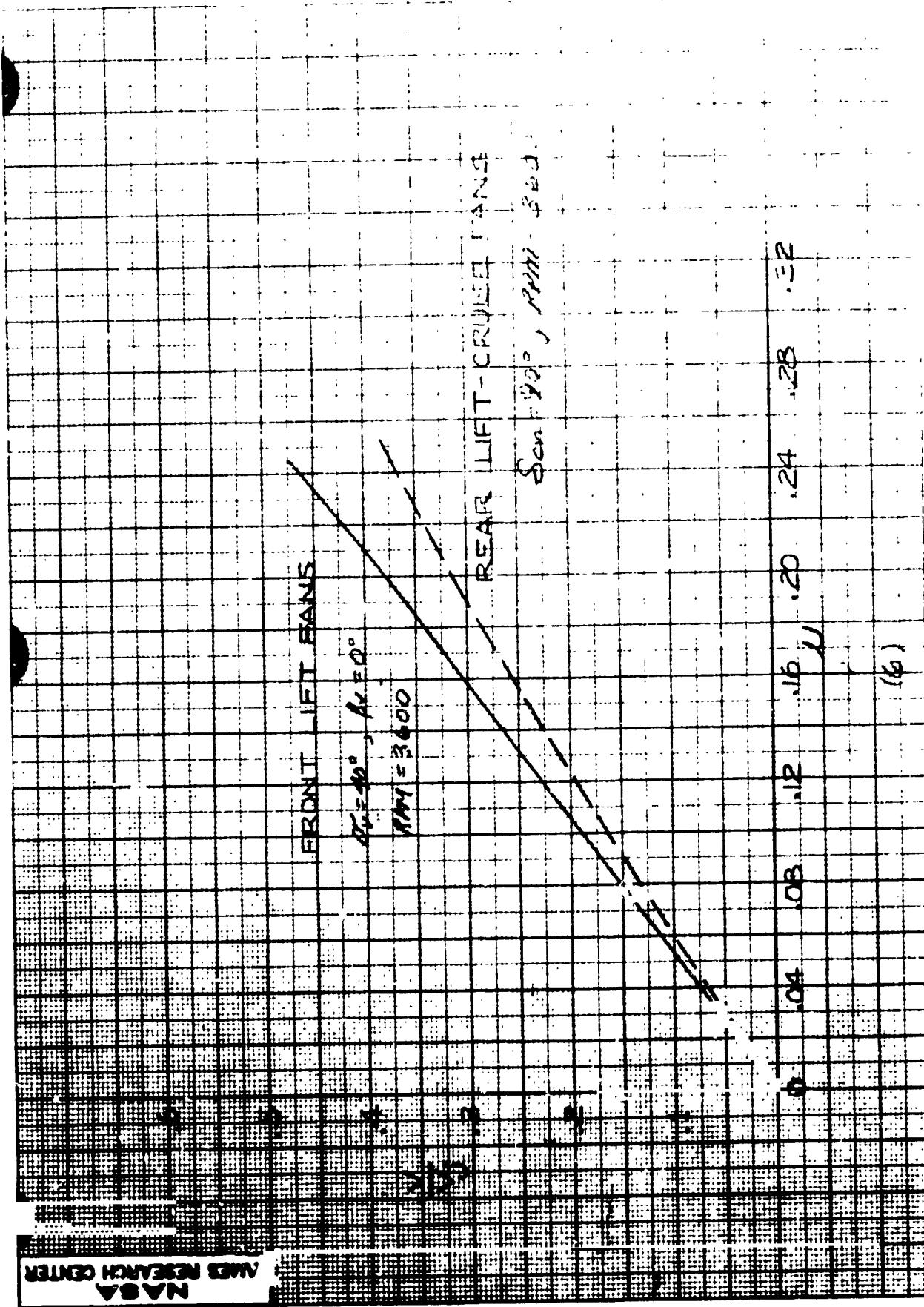
Figure 8.- Continued.



(c) Forward lift fans, $\alpha_V = 40^\circ$, $\beta_V = 0^\circ$, RPM = 3500, $\mu = .26$.

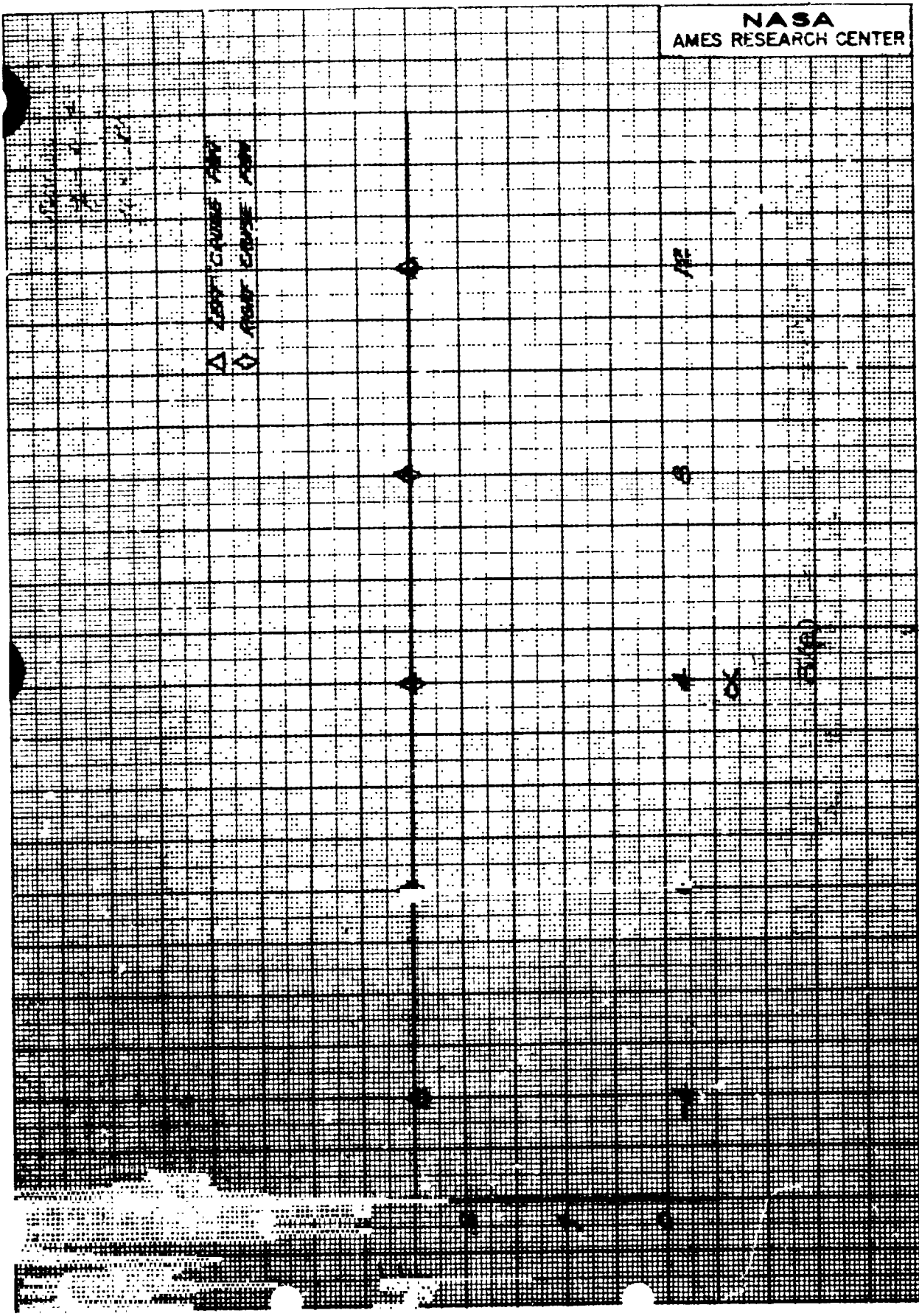
Figure 8.- Continued.

REPRODUCIBILITY OF THE ORIGINAL PAGE IS POOR.



(d) After lift-cruise fans, $\dot{m}_{in} = 56$, RPM = 3600, $\mu = .12$.

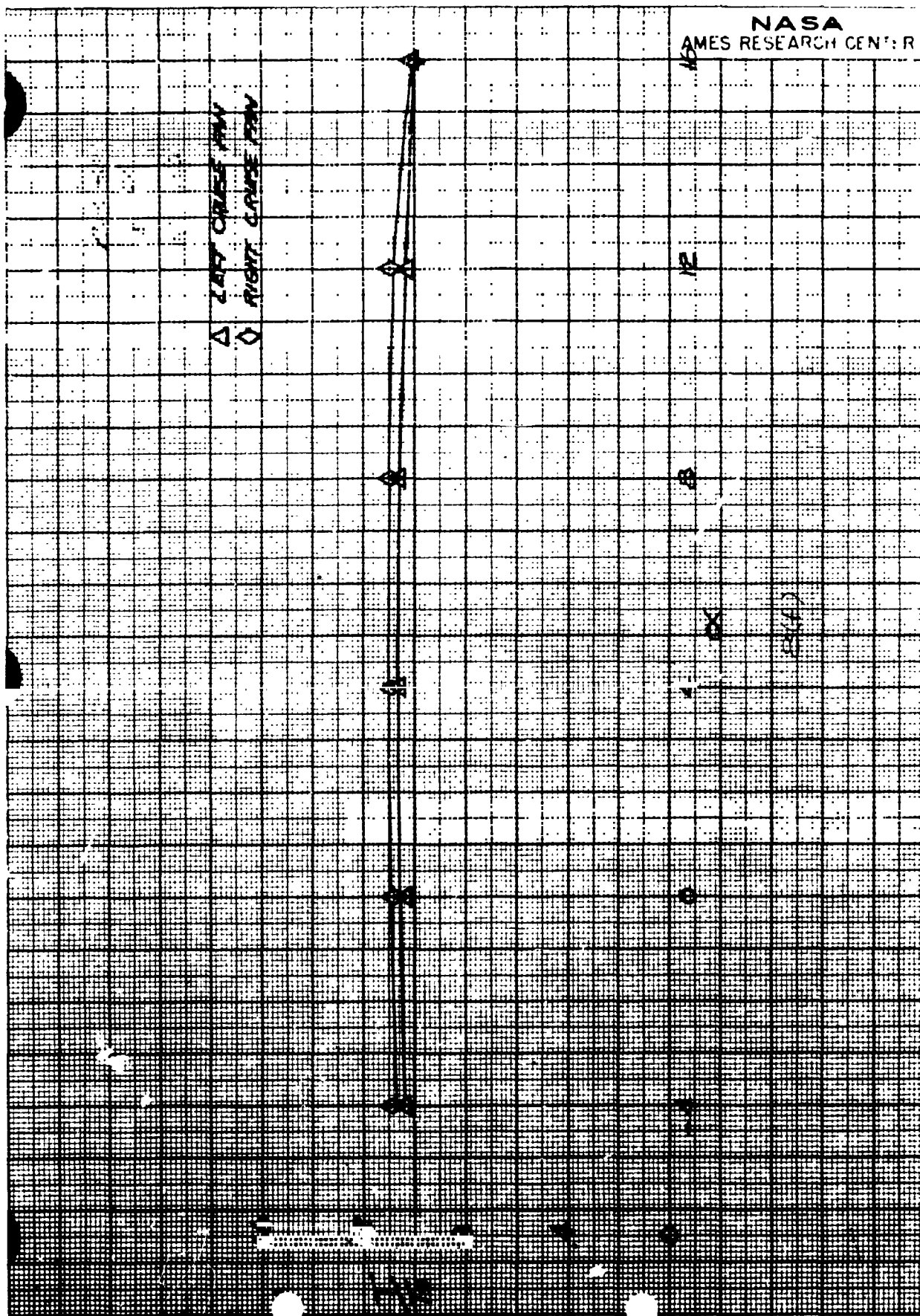
Figure 8.- Continued.



(e) Aft lift-cruise fans, $\delta_{cn} = 56$, RPM = 3600, $\mu = .17$.

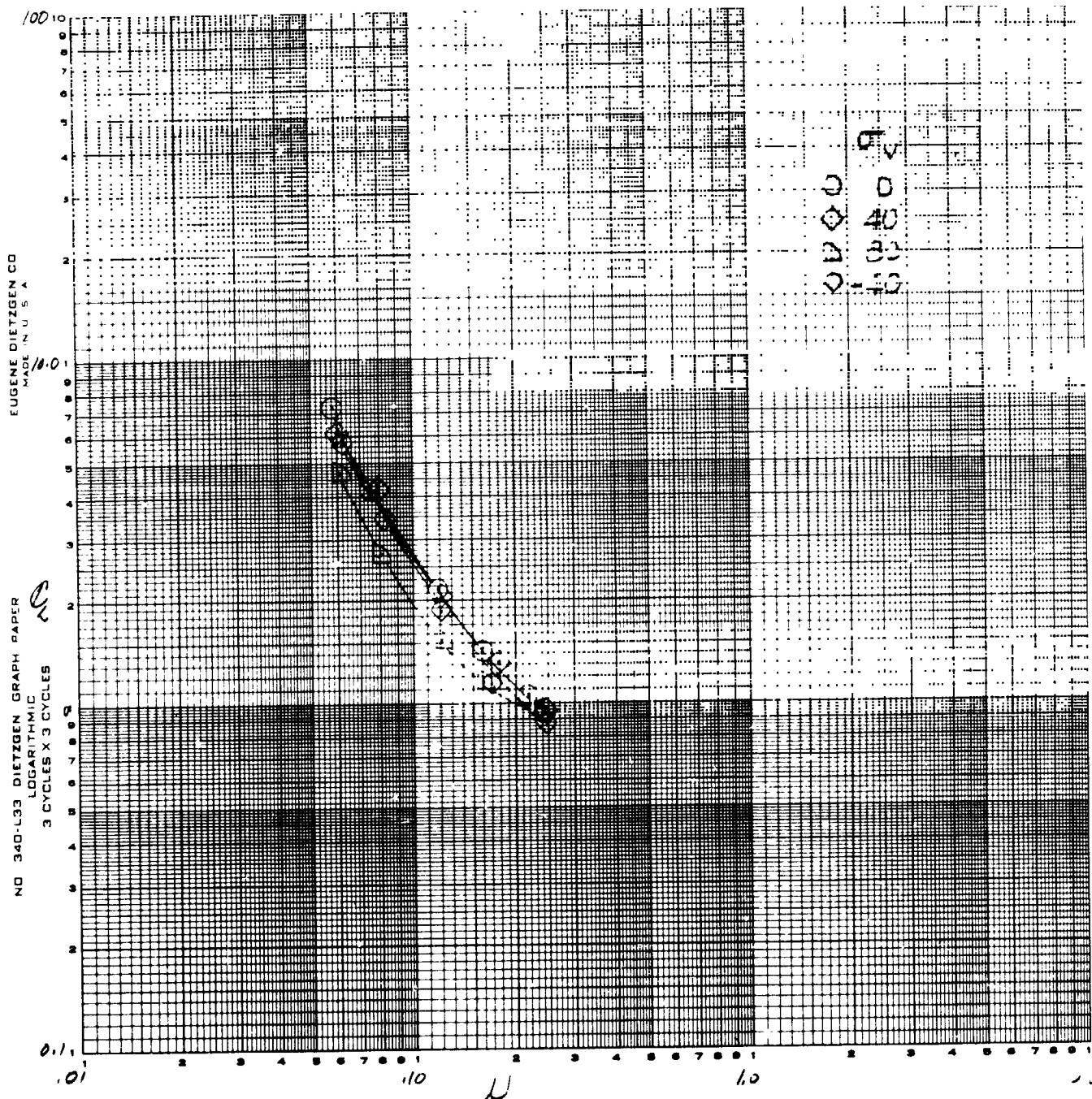
Figure 8.- Continued.

REPRODUCIBILITY OF THE ORIGINAL PAGE IS POOR.



(f) Aft lift-cruise fans, $\delta_{cn} = 23$, RPM = 3500, $\nu = .26$.

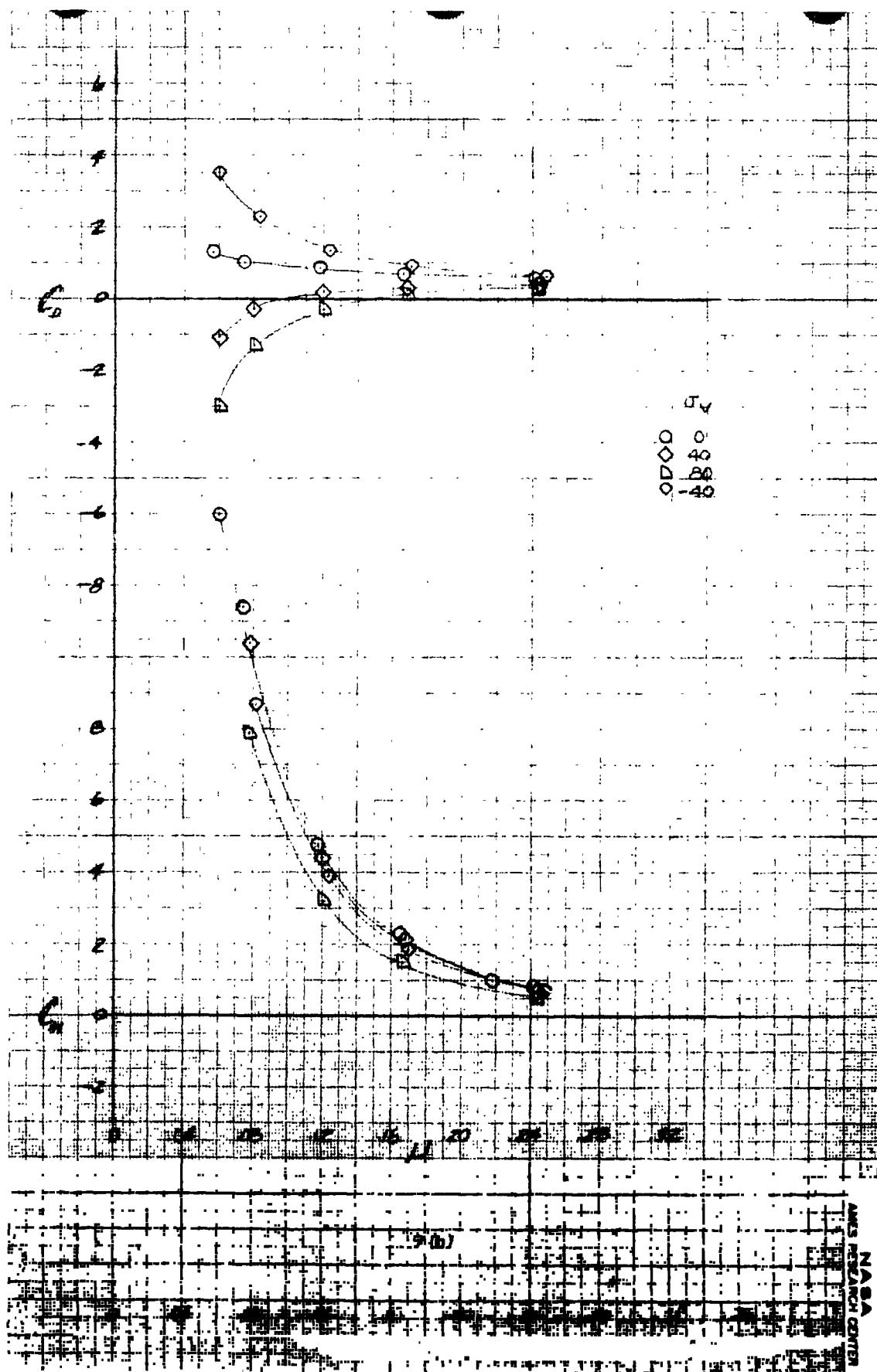
Figure 8.- Concluded.



(a) $\beta_v = 0$, C_L vs μ .

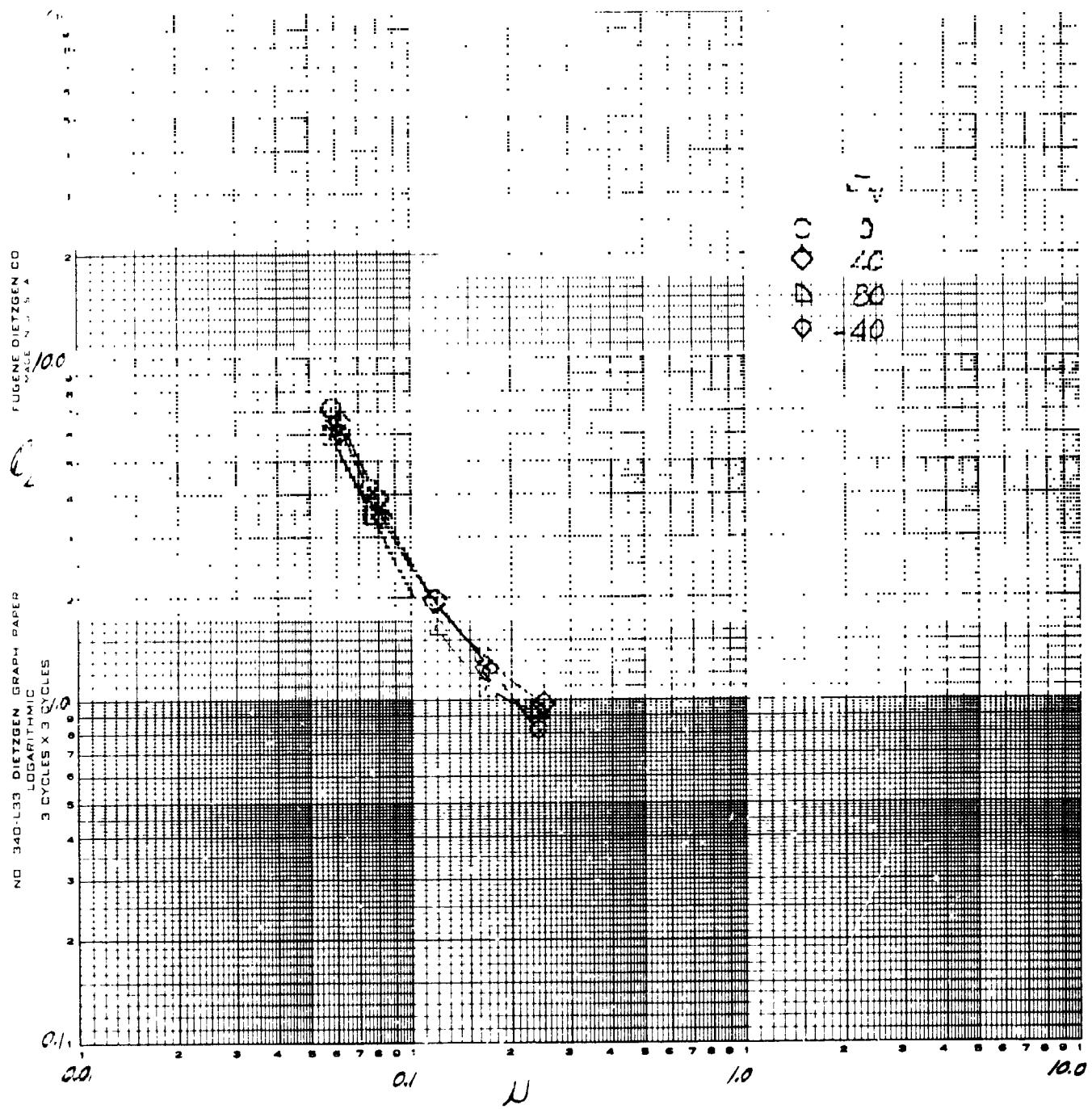
Figure 9.- The variation in longitudinal characteristics with tip-speed ratio; forward lift fans, RPM = 3600, $\delta_{cn} = 90$, tail on, $\delta_f = 30$.

REPRODUCIBILITY OF THE ORIGINAL PAGE IS POOR.



(b) $\beta_v = 0$, C_D and C_m vs μ .

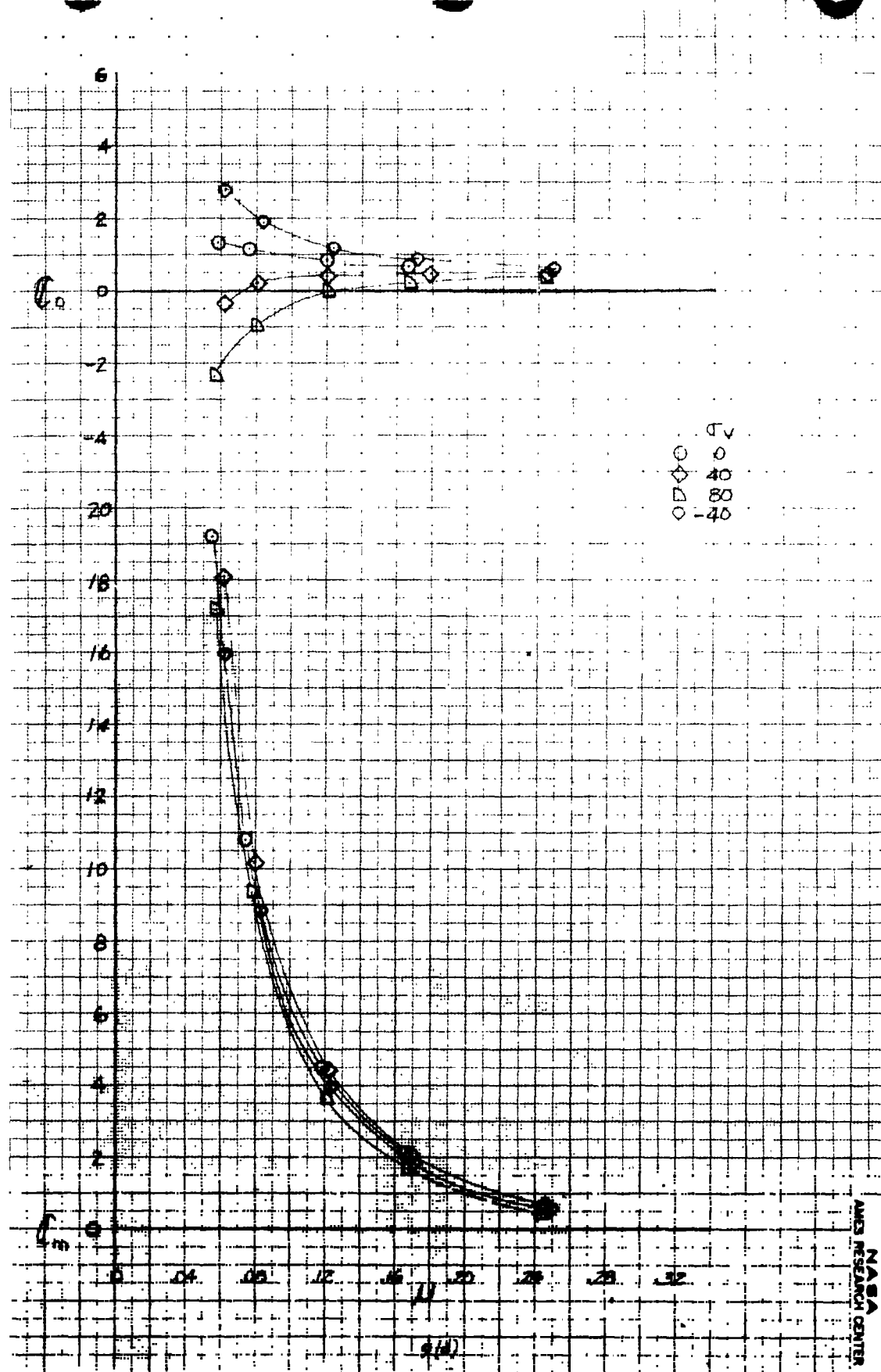
Figure 9.- Continued.



(c) $\beta_v = -8$, C_L vs μ .

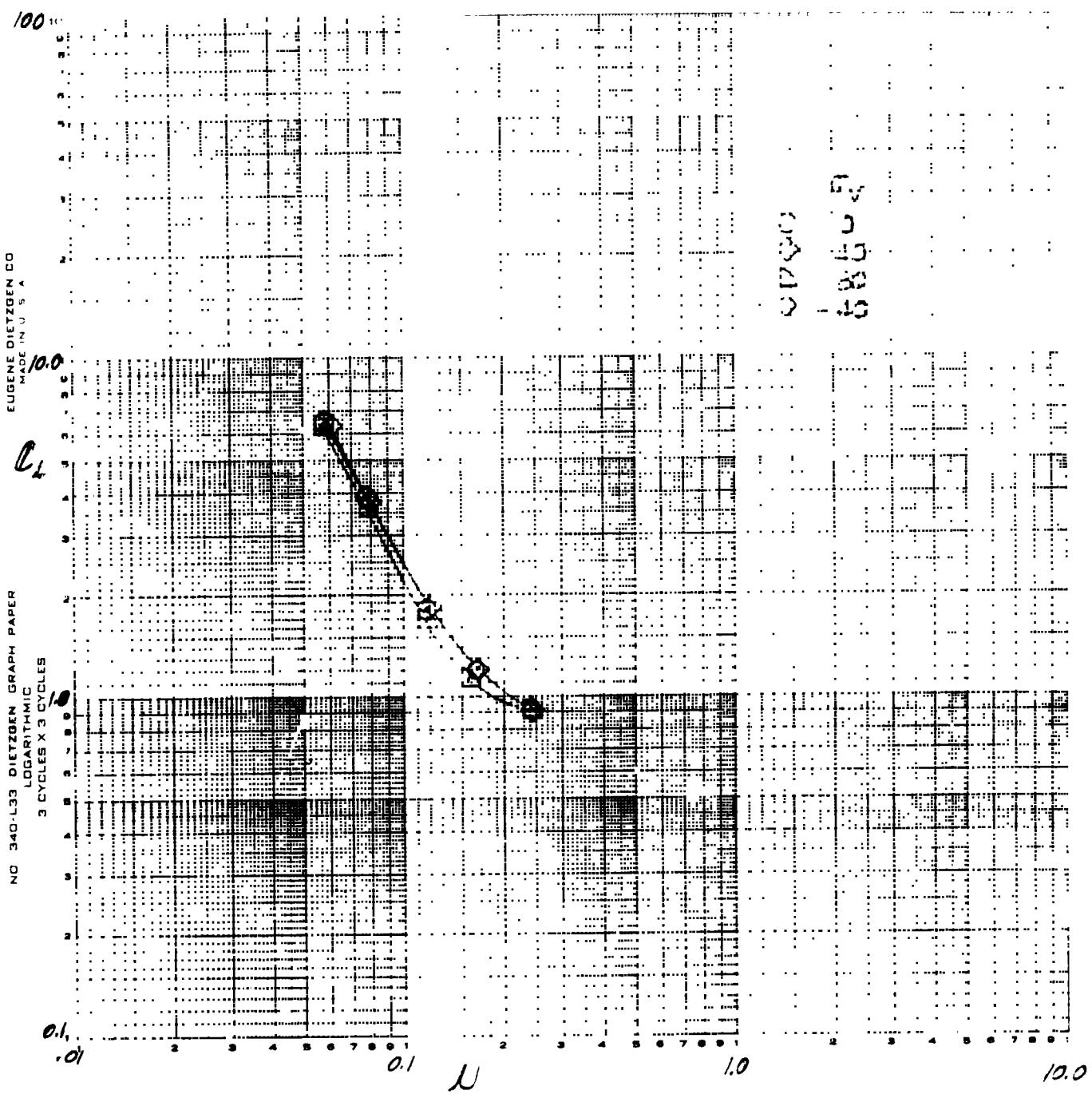
Figure 9.- Continued.

REPRODUCIBILITY OF THE ORIGINAL PAGE IS POOR.



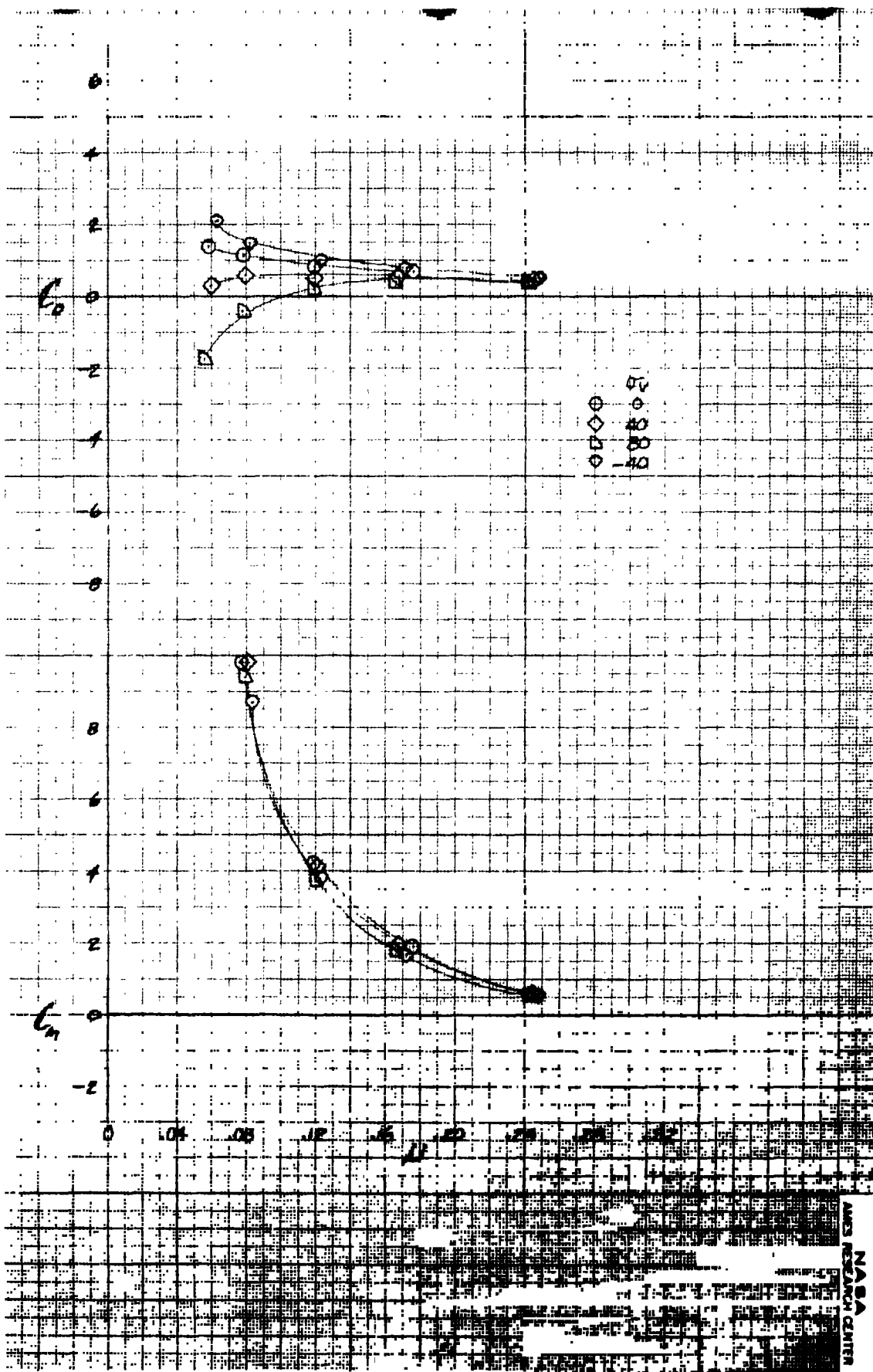
(d) $\beta_v = -8$, C_D and C_m vs μ .

Figure 9.- Continued.



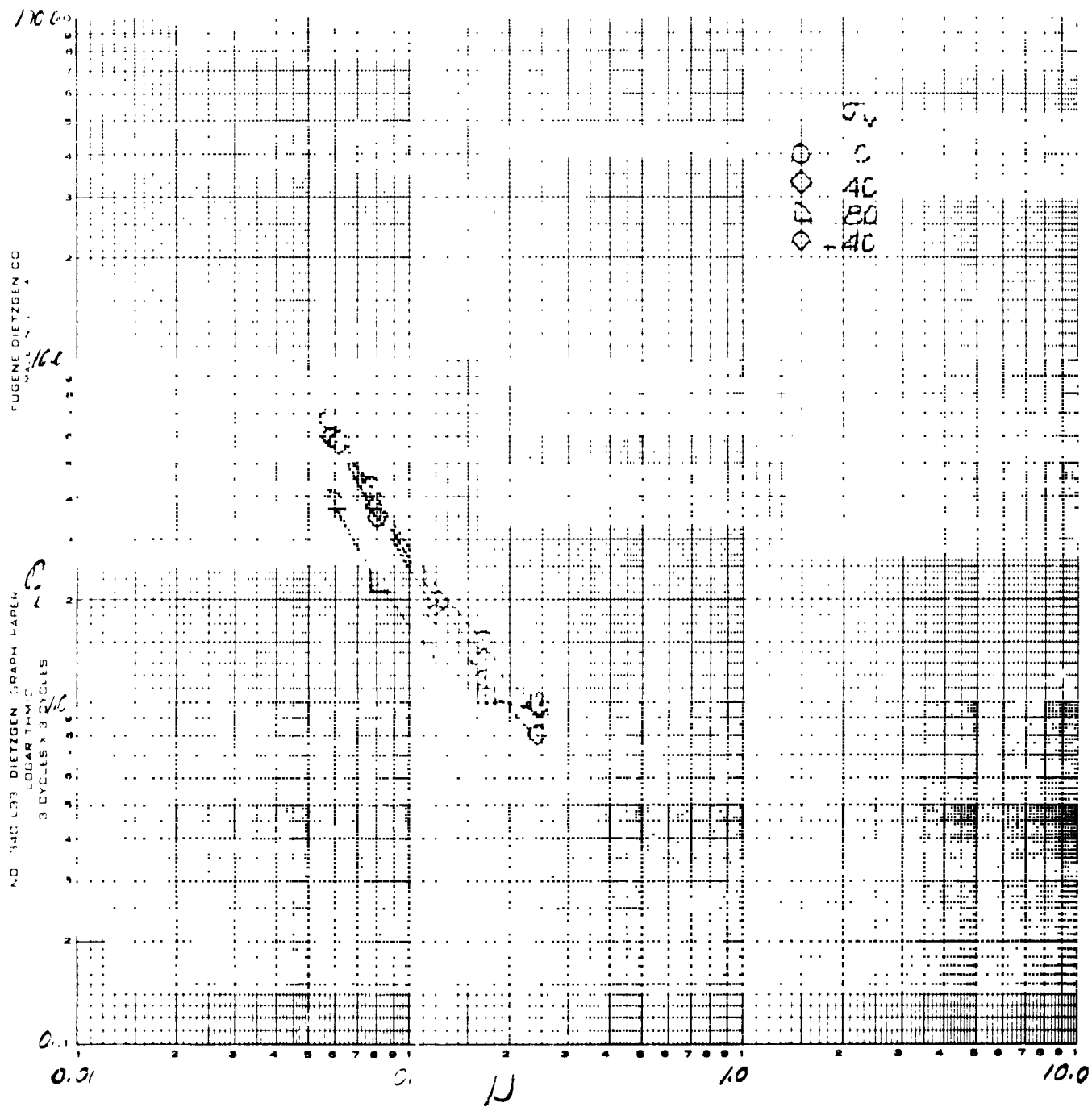
(e) $\beta_v = -16$, C_L vs μ .

Figure 9.- Continued.



(f) $\beta_v = -16$, C_D and C_m vs μ .

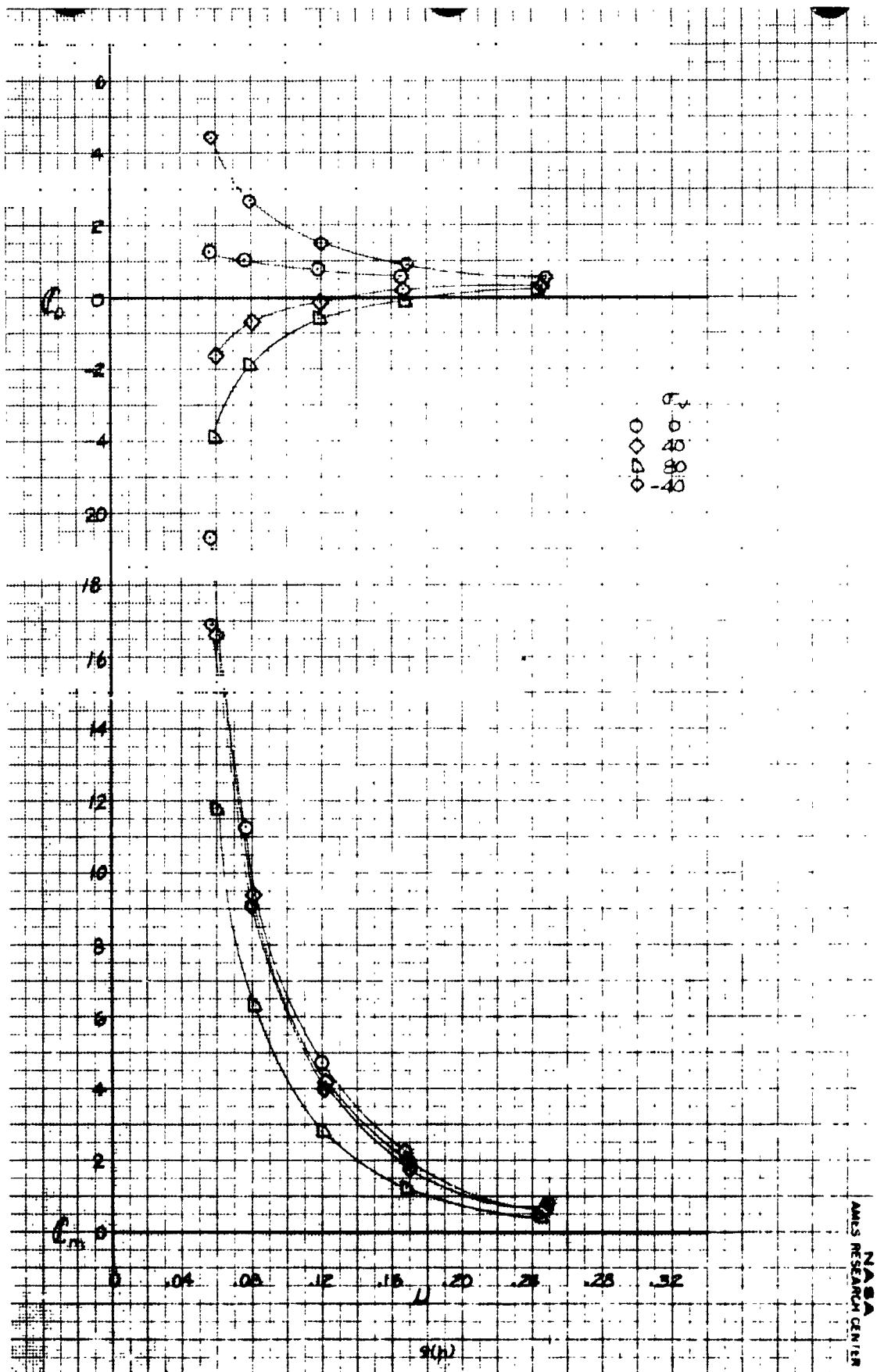
Figure 9.- Continued.



(g) $\beta_v = +8$, C_L vs μ .

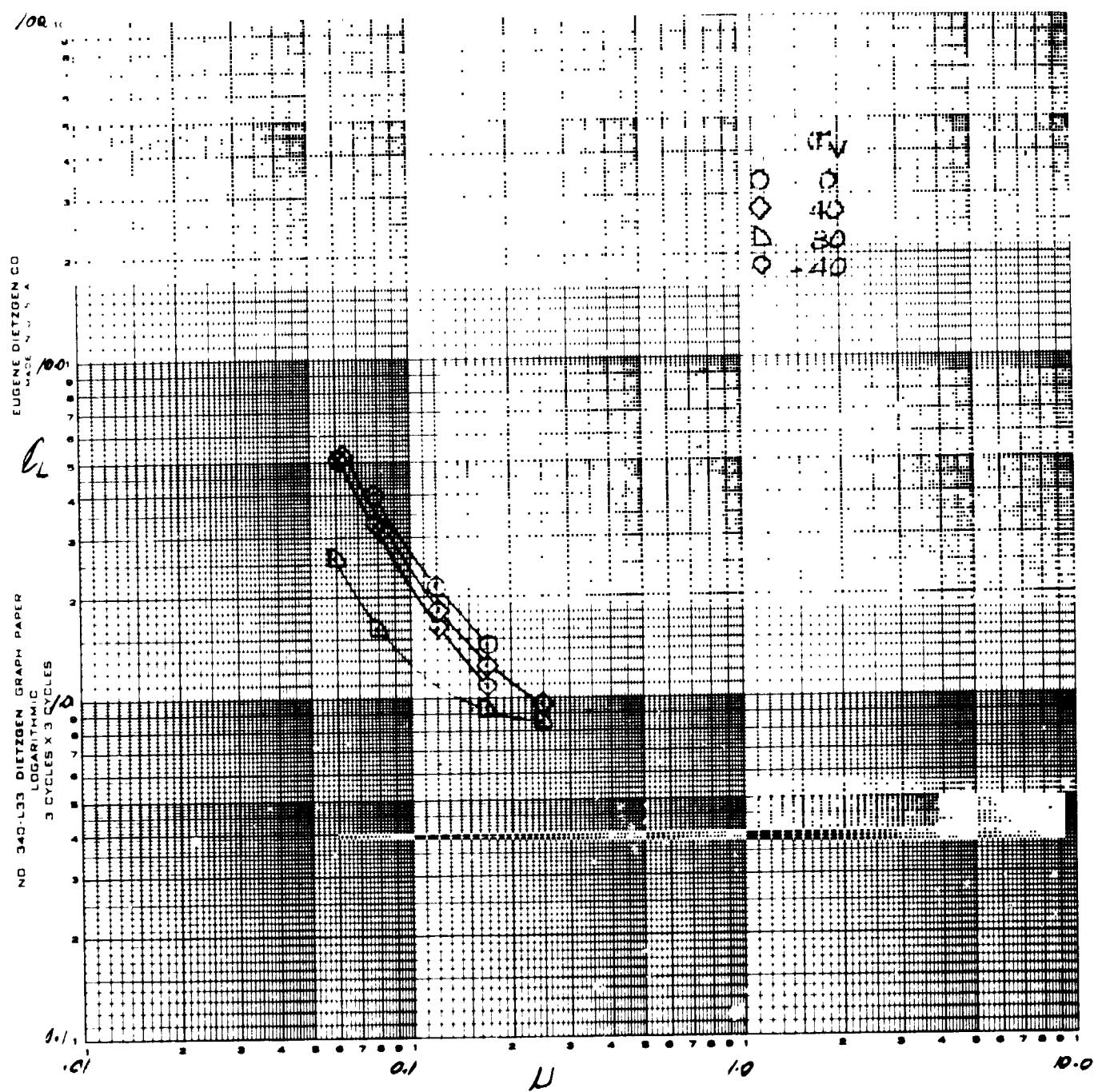
Figure 9.- Continued.

REPRODUCIBILITY OF THE ORIGINAL PAGE IS POOR.



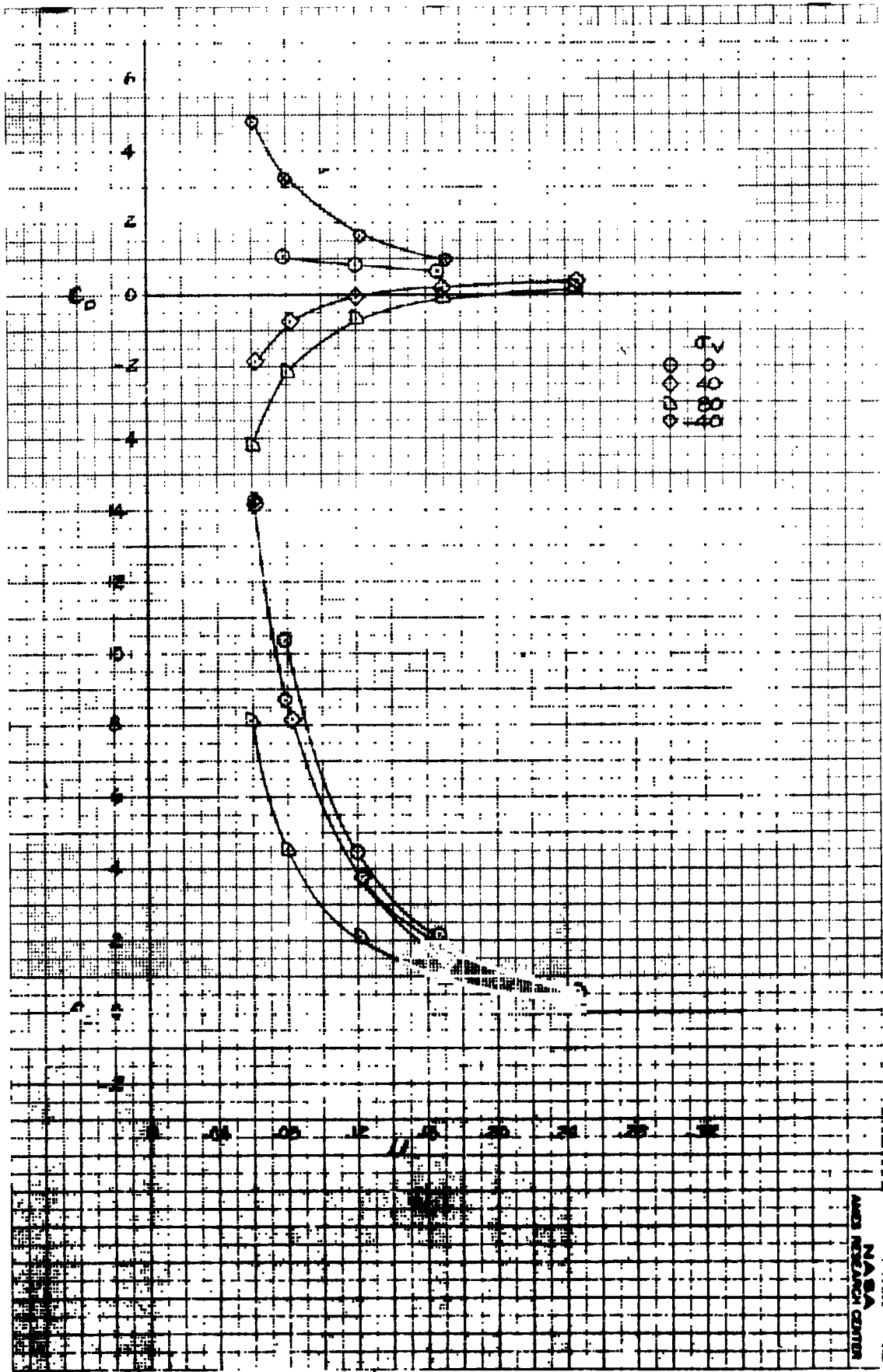
(h) $\beta_v = +8$, C_D and C_m vs μ .

Figure 9.- Continued.



(i) $\beta_v = +16$, C_L vs μ .

Figure 9.- Continued.



(j) $\beta_v = +16$, C_D and C_m vs μ .

Figure 9.- Concluded.

REPRODUCIBILITY OF THE ORIGINAL PAGE IS POOR.

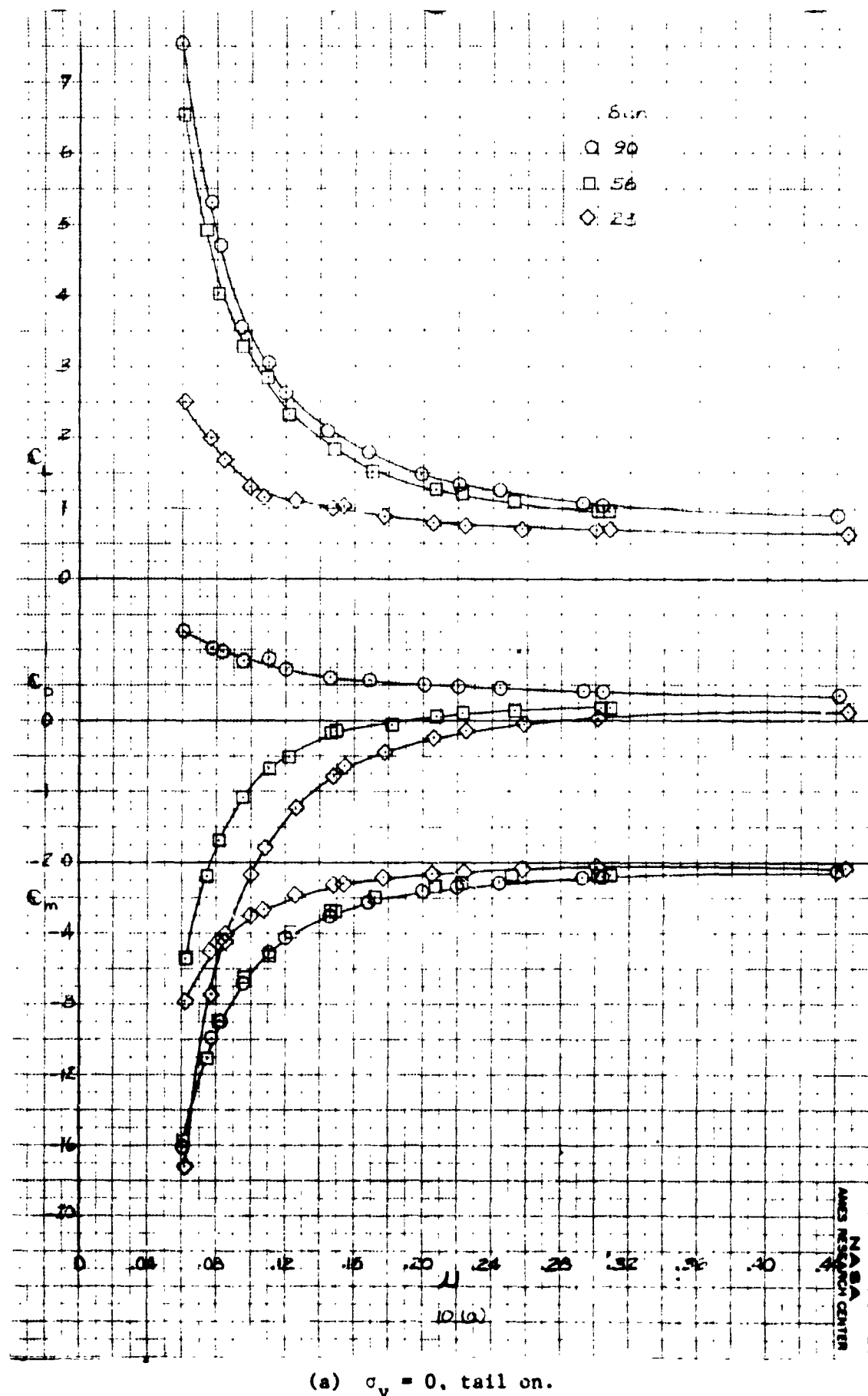
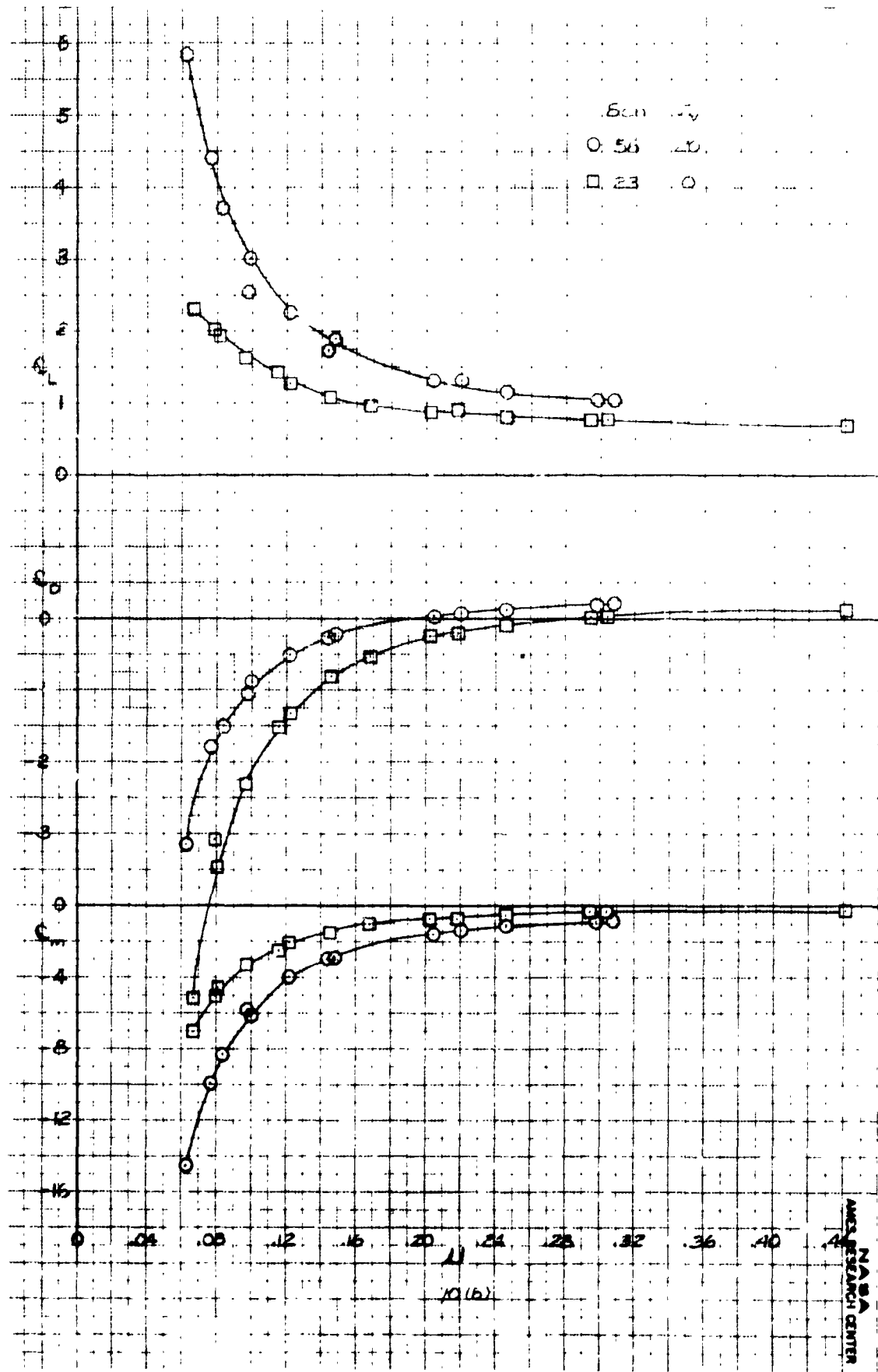
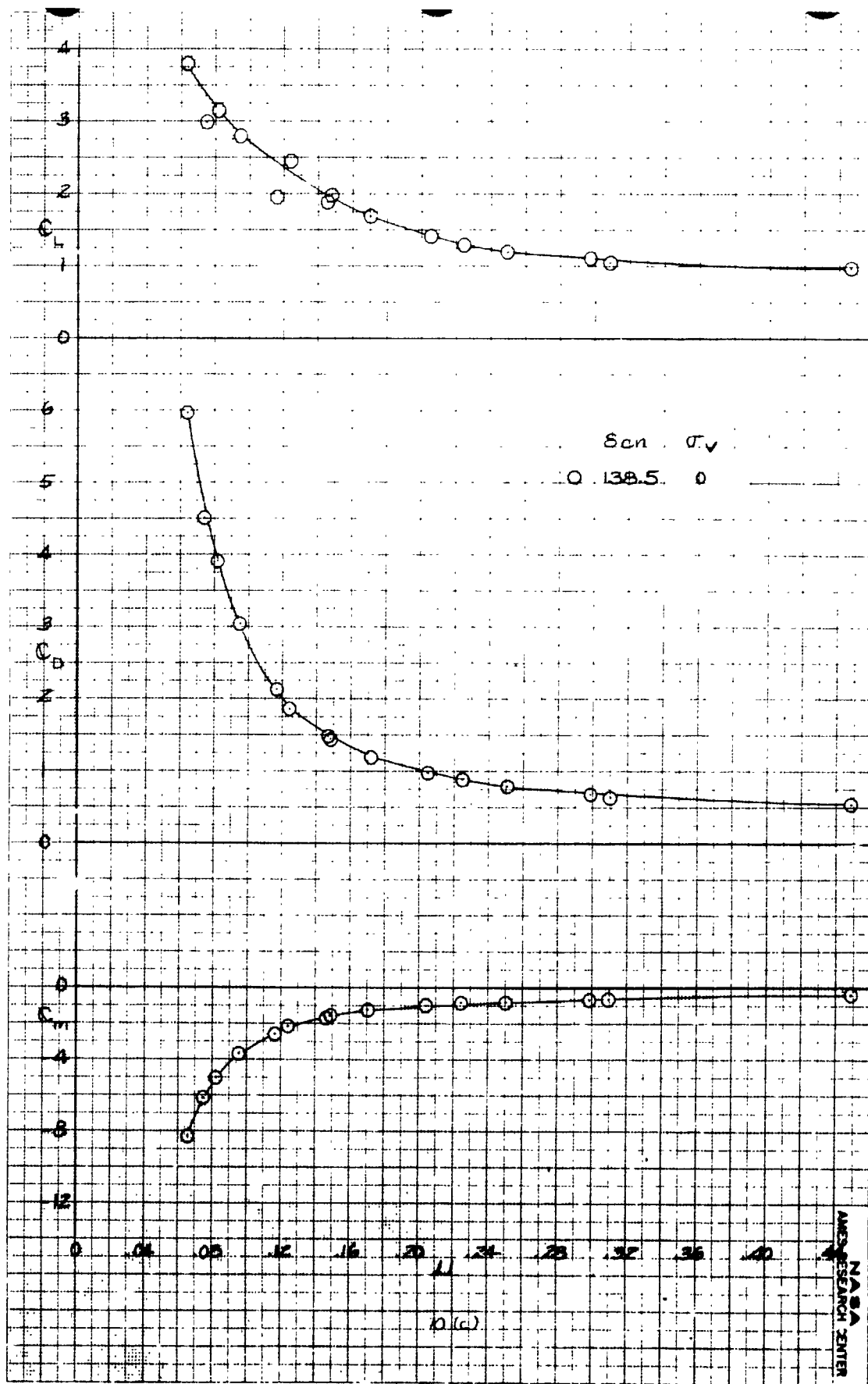


Figure 10.- The variation in longitudinal characteristics with tip-speed ratio; aft lift-cruise fans, $\beta_v = 90$, $\delta_f = 30$.



(b) Tail off.
Figure 10.- Continued.

REPRODUCIBILITY OF THE ORIGINAL PAGE IS POOR.



(c) Tail off.
Figure 10.- Concluded.

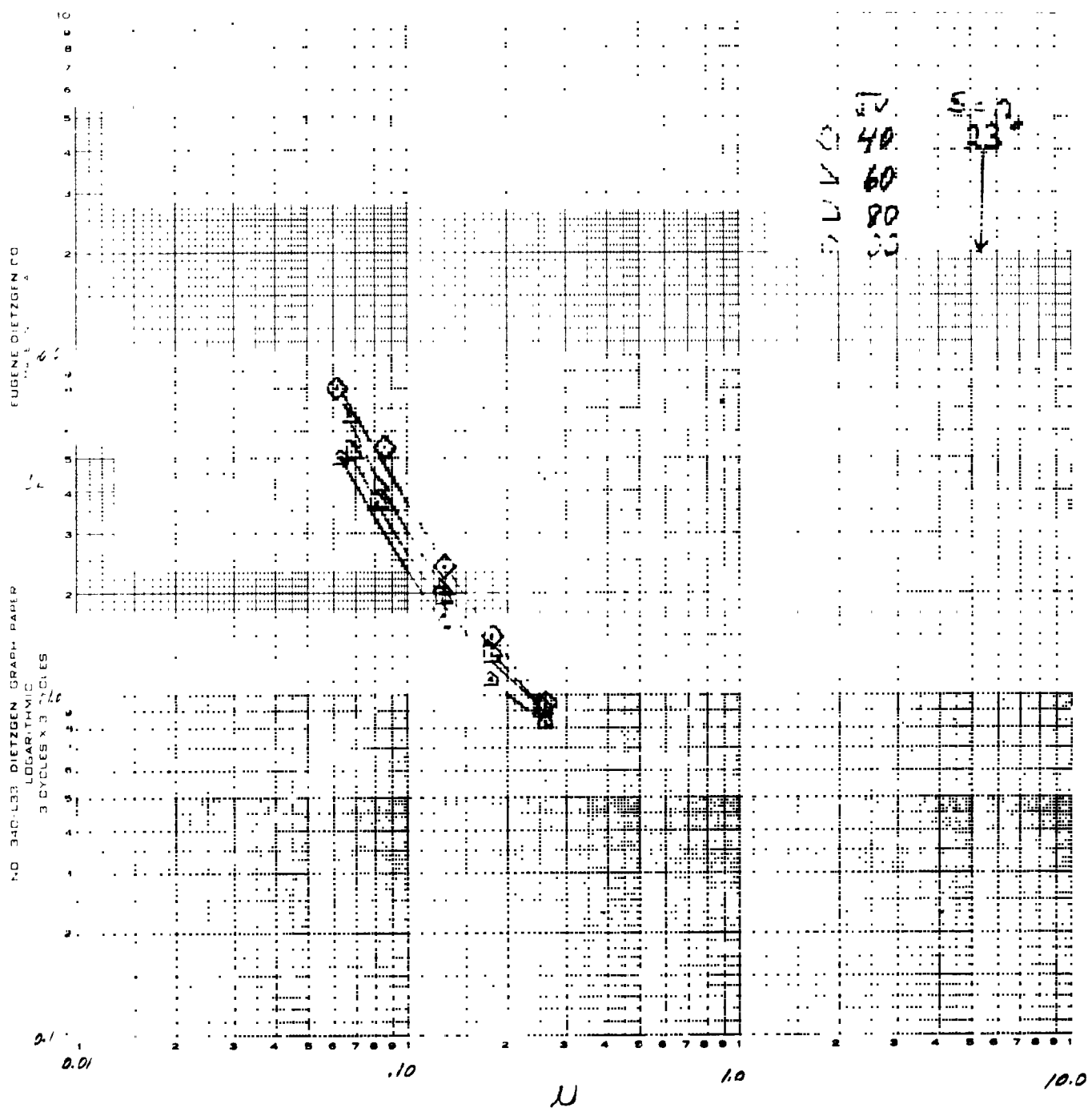
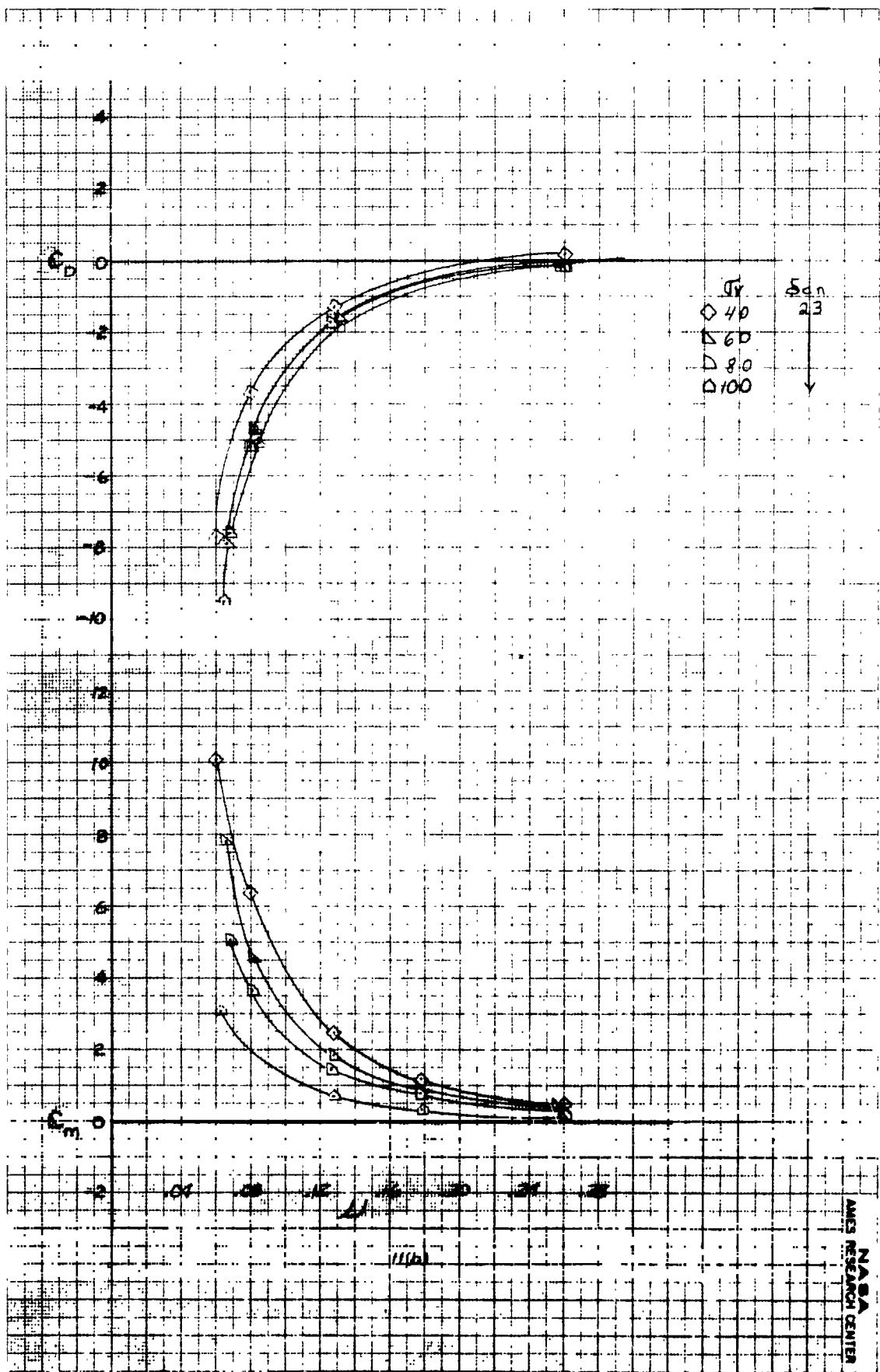
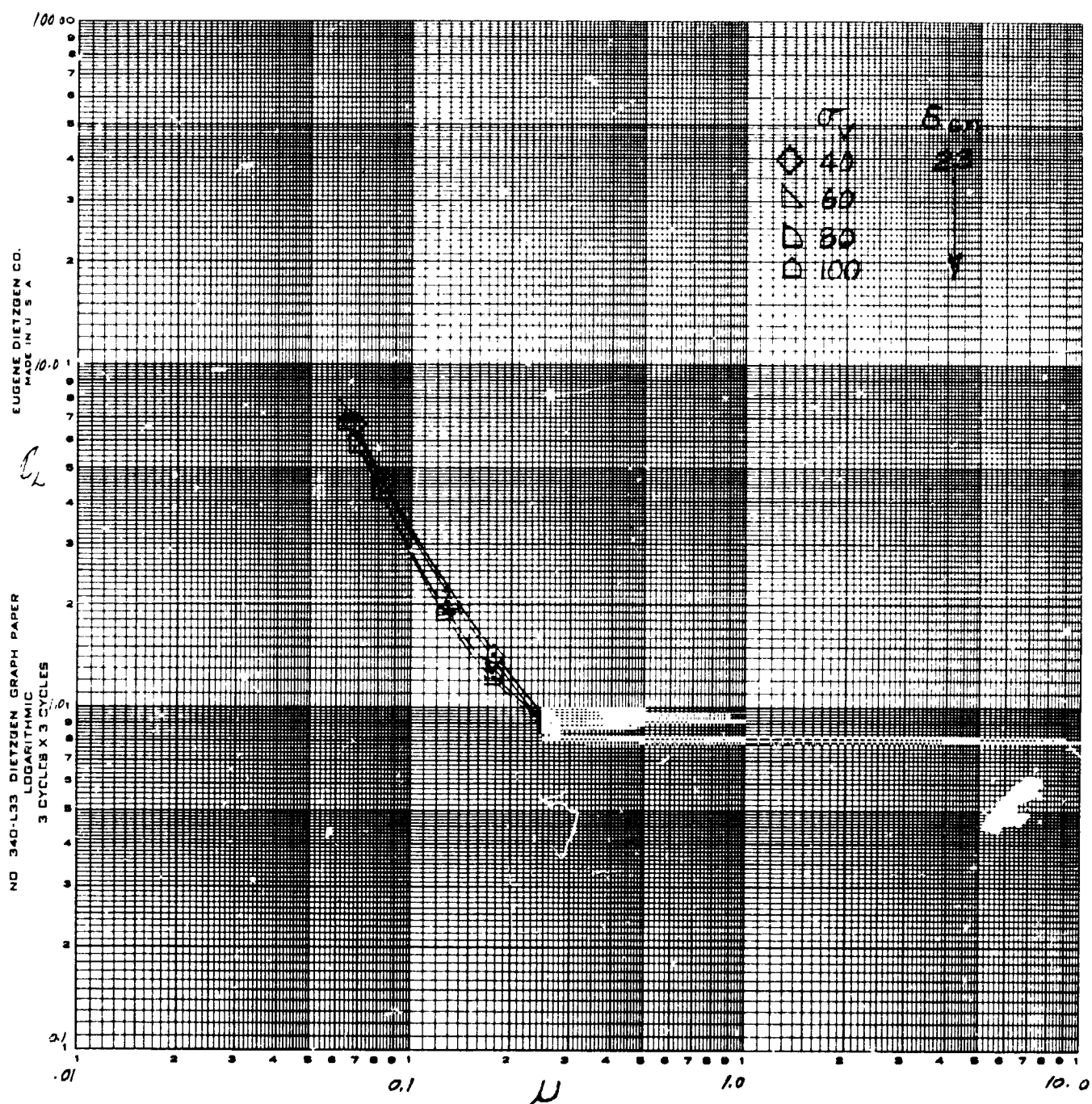


Figure 11.- The variation in longitudinal characteristics with tip-speed ratio; all four fans, tail on, $\delta_{cn} = 23$, $\delta_f = 30$.



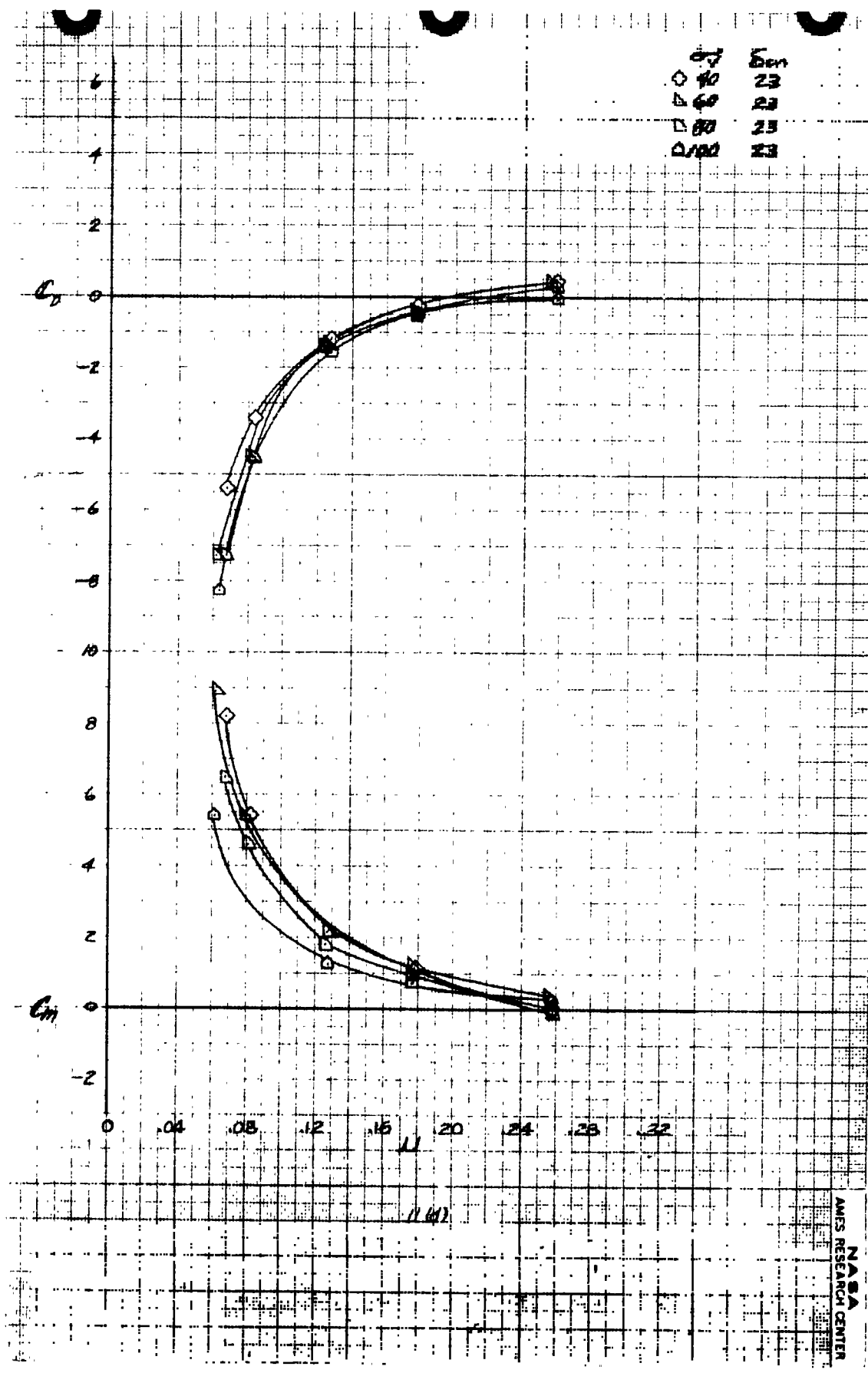
(b) $\beta_v = 0$, C_D and C_m vs μ .

Figure 11.- Continued.



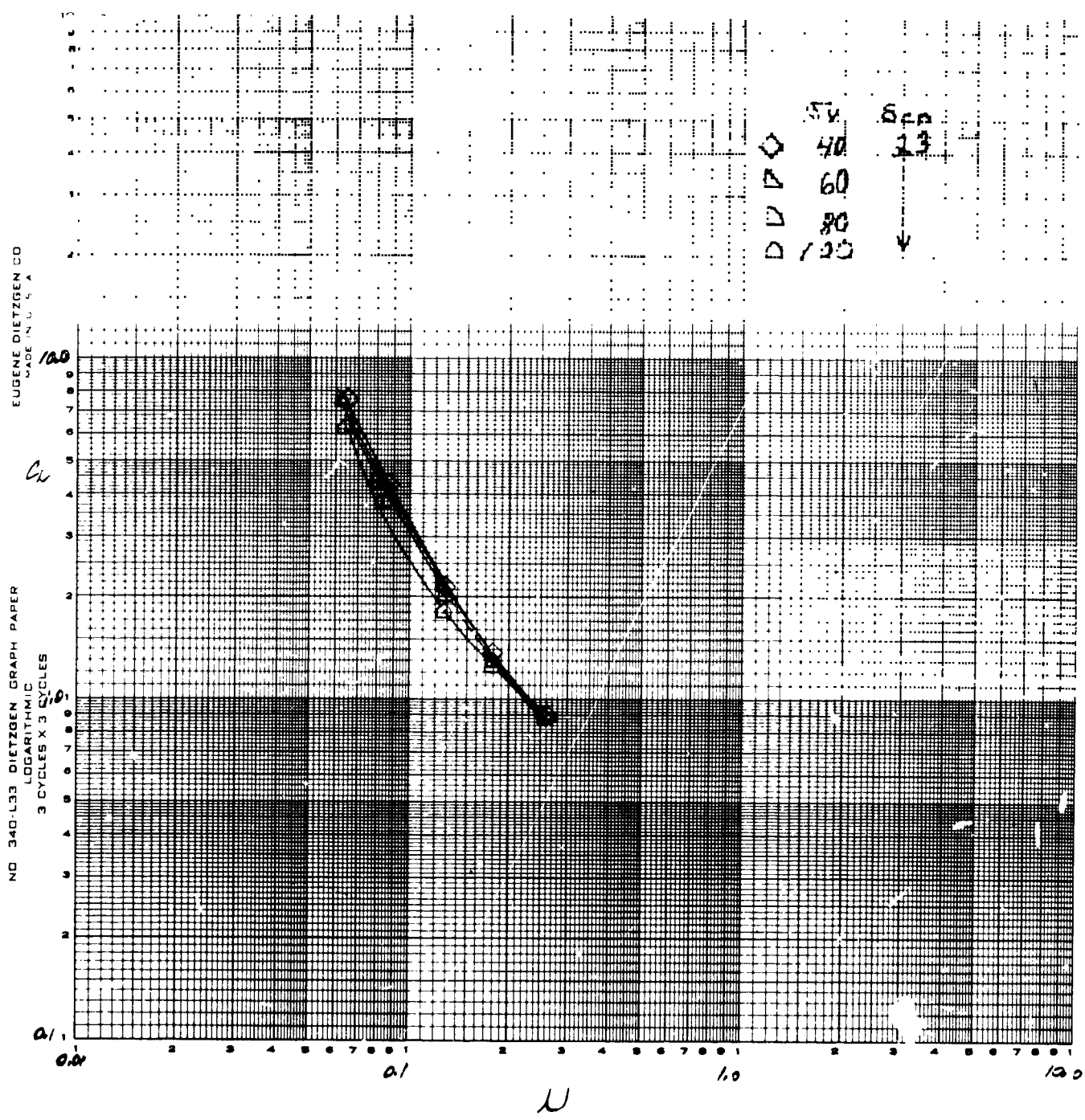
(c) $\beta_v = -8$, C_L vs μ .

Figure 11.- Continued.



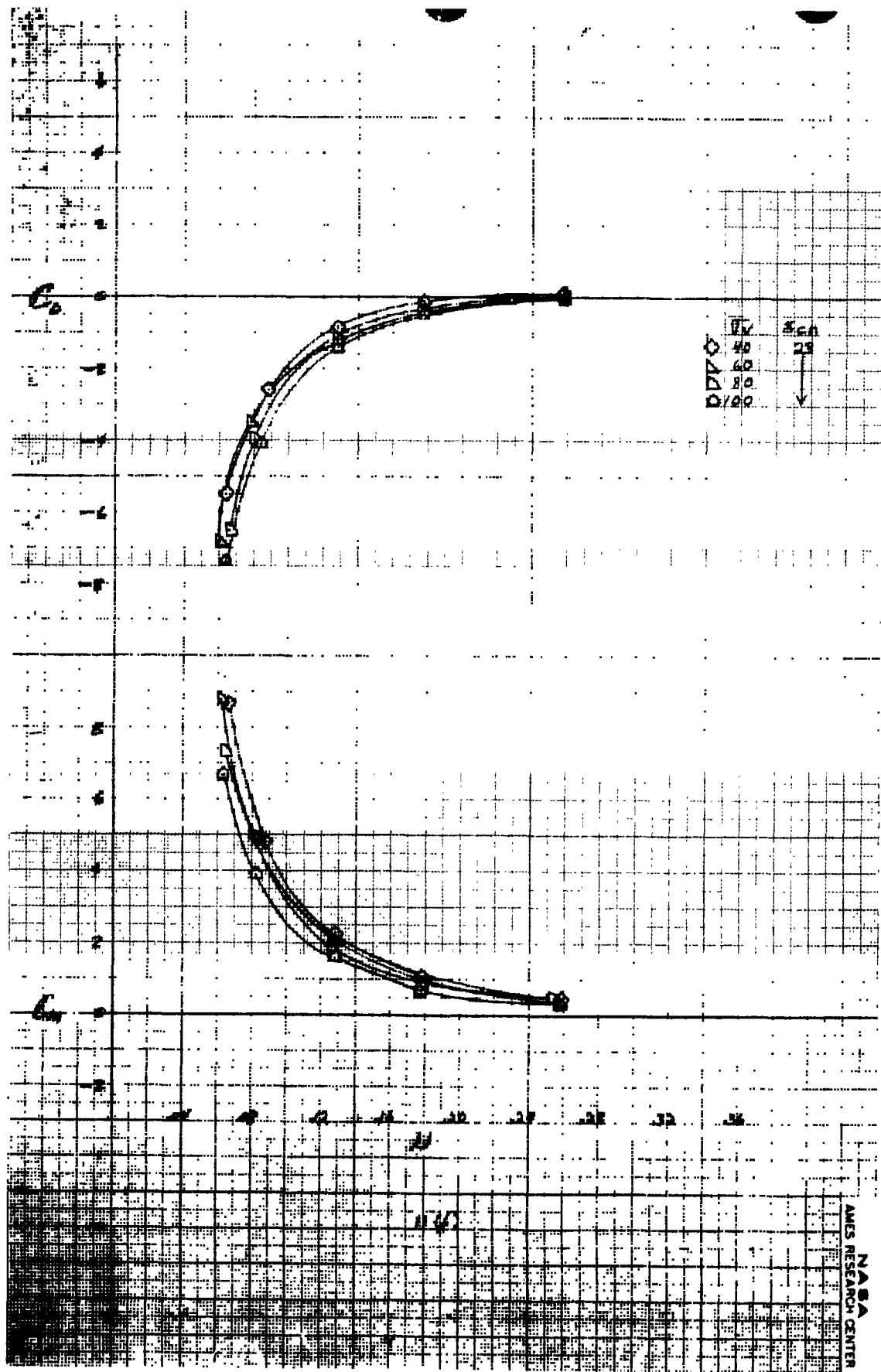
(d) $\beta_v = -8$, C_D and C_m vs u .

Figure 11.- Continued.



(e) $\beta_v = -16$, C_L vs μ .

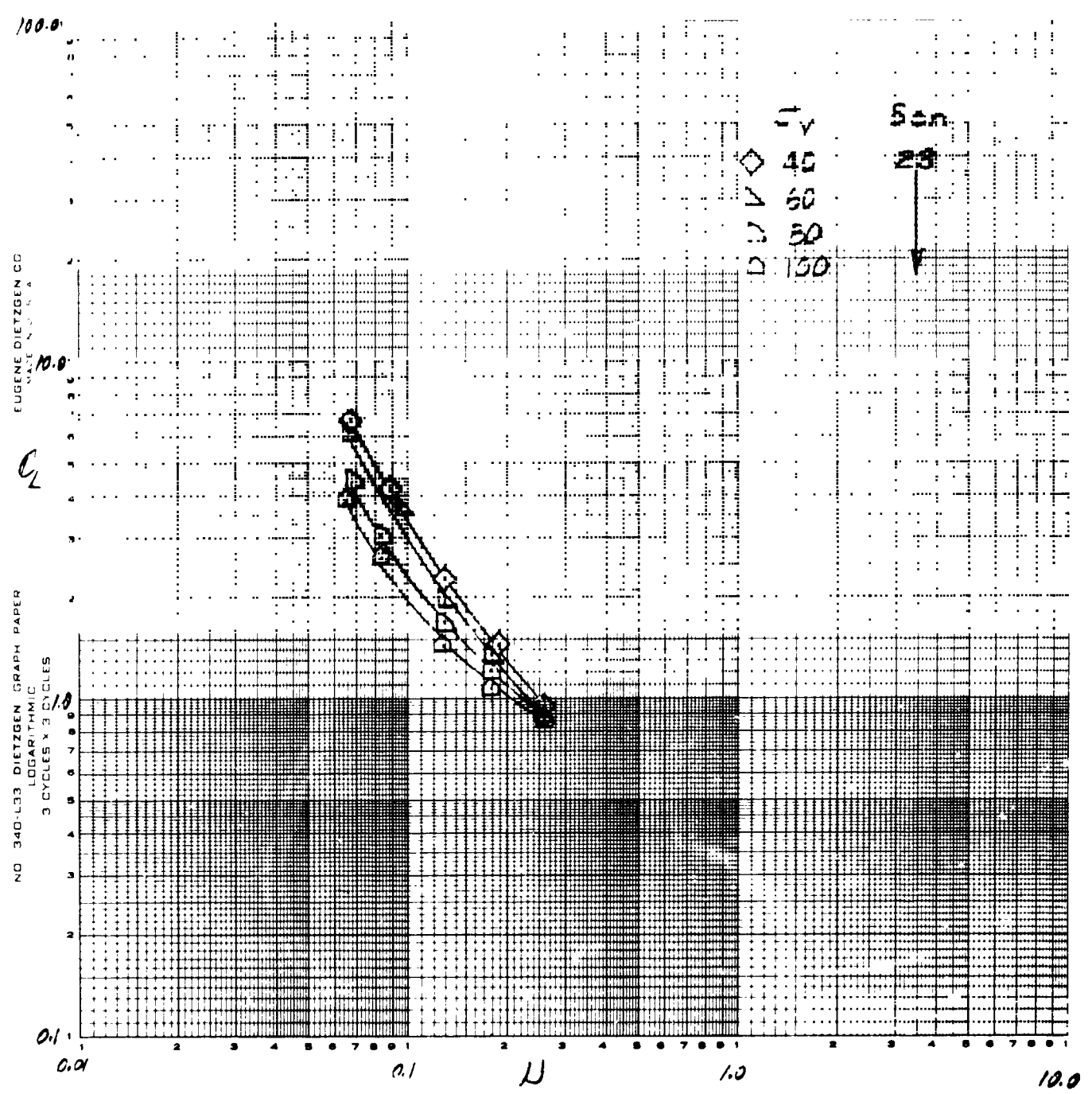
Figure 11.- Continued.



(f) $\beta_v = -16$, C_D and C_m vs μ .

Figure 11.- Continued.

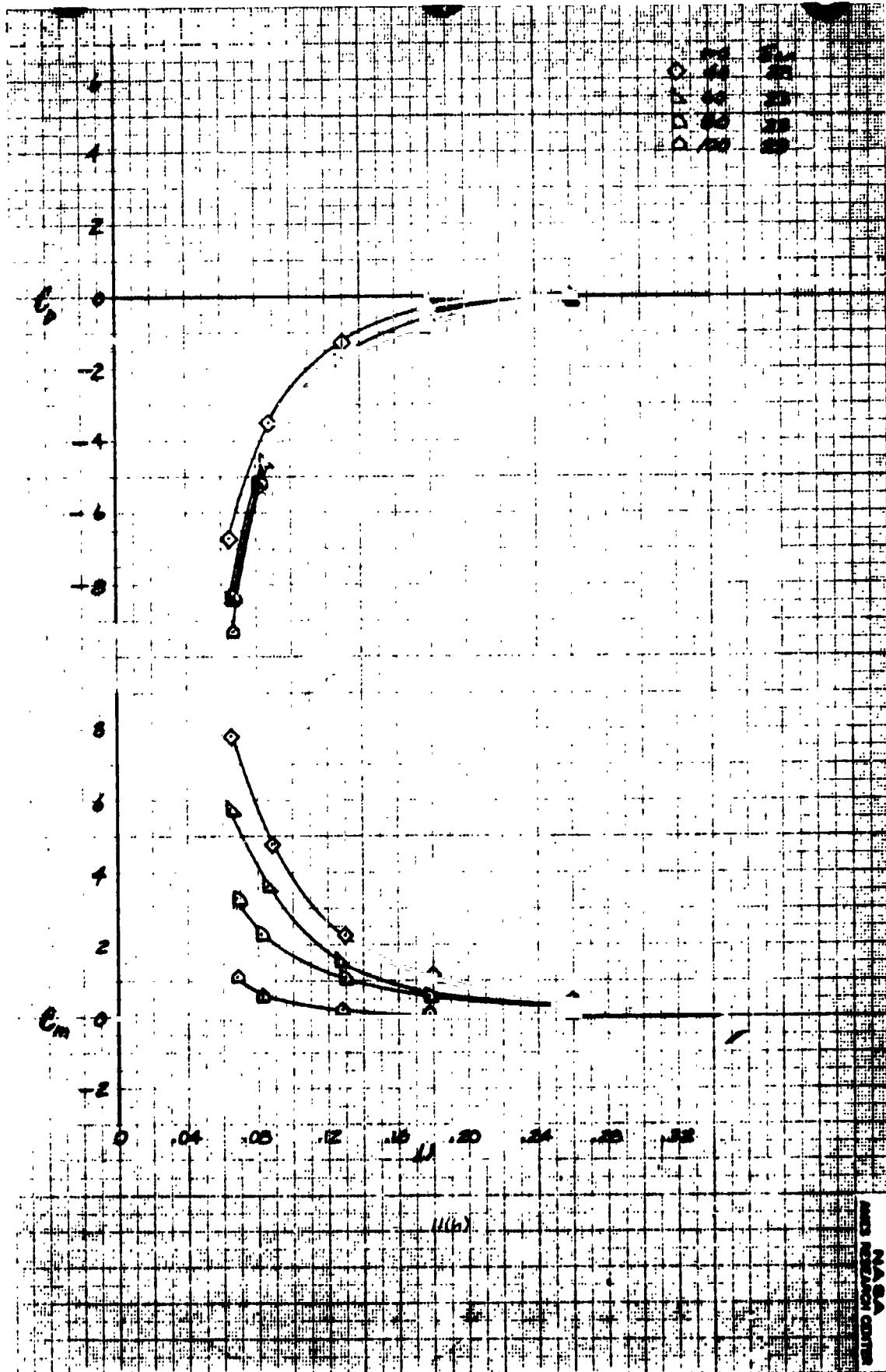
AMES RESEARCH CENTER NASA



(g) $\beta_v = +8$, C_L vs u .

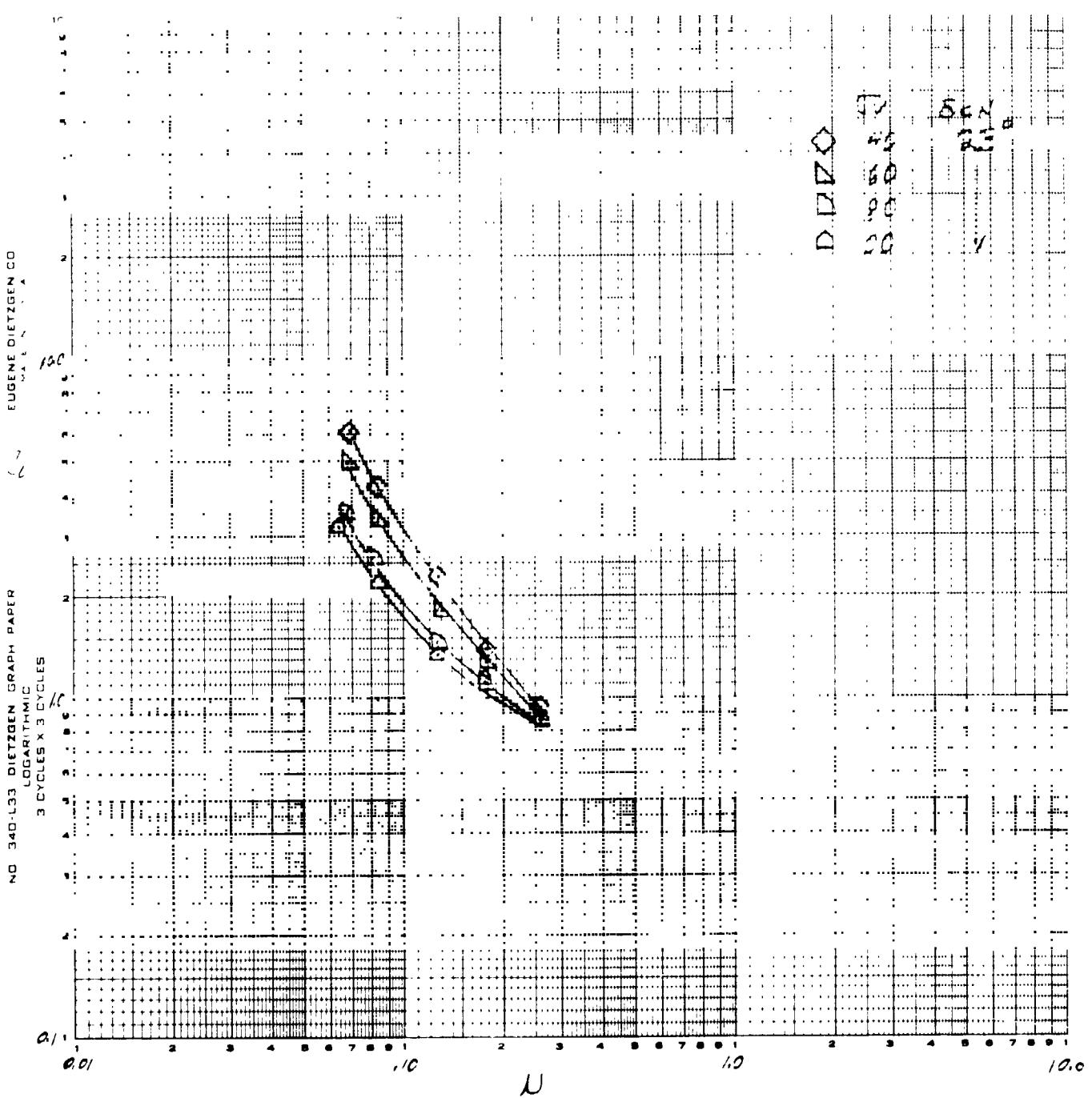
Figure 11.- Continued.

REPRODUCIBILITY OF THE ORIGINAL PAGE IS POOR.



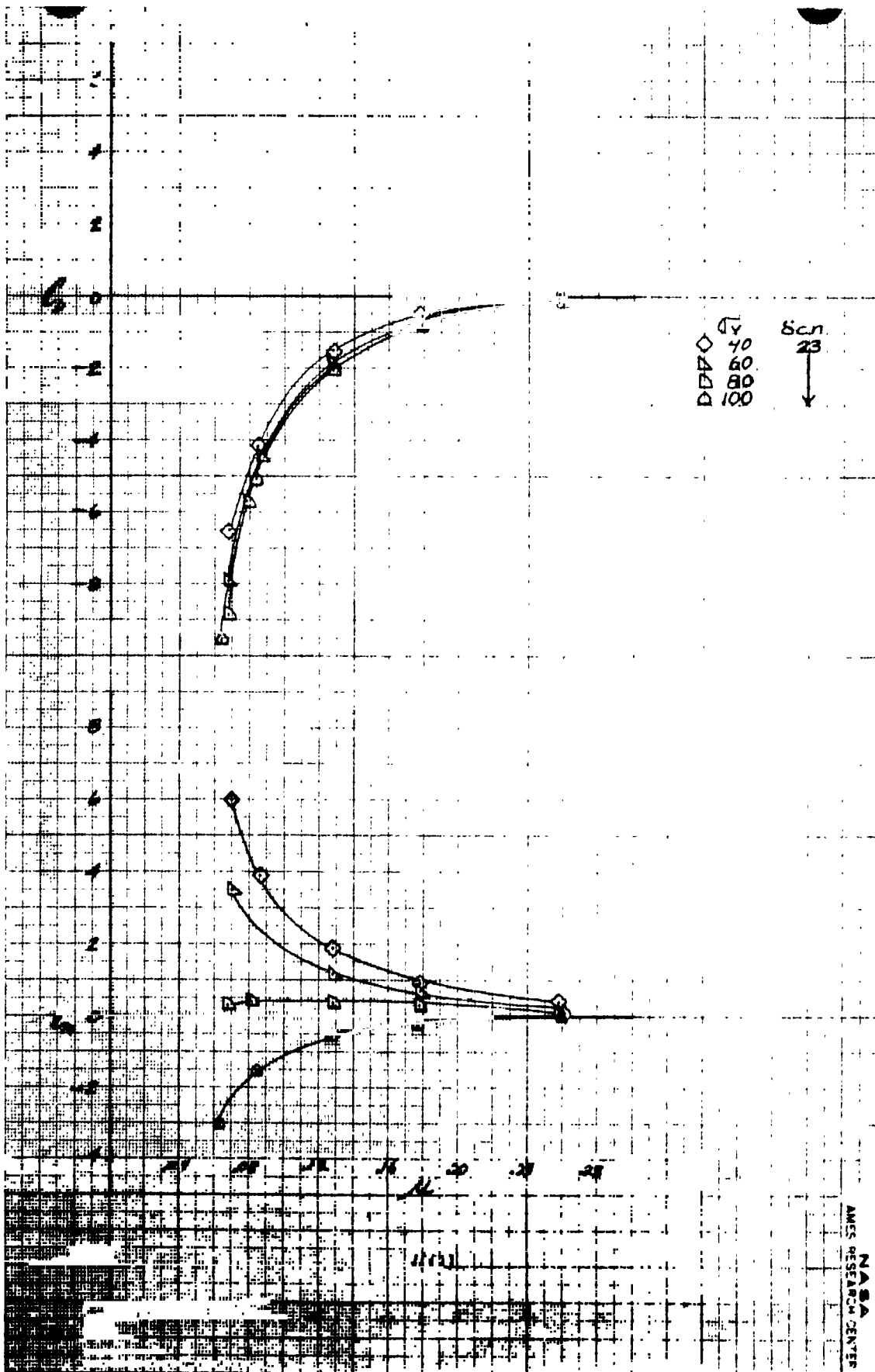
(h) $\beta_v = +8$, C_D and C_m vs u .

Figure 11.- Continued.



(i) $\beta_v = +16$, C_L vs μ .

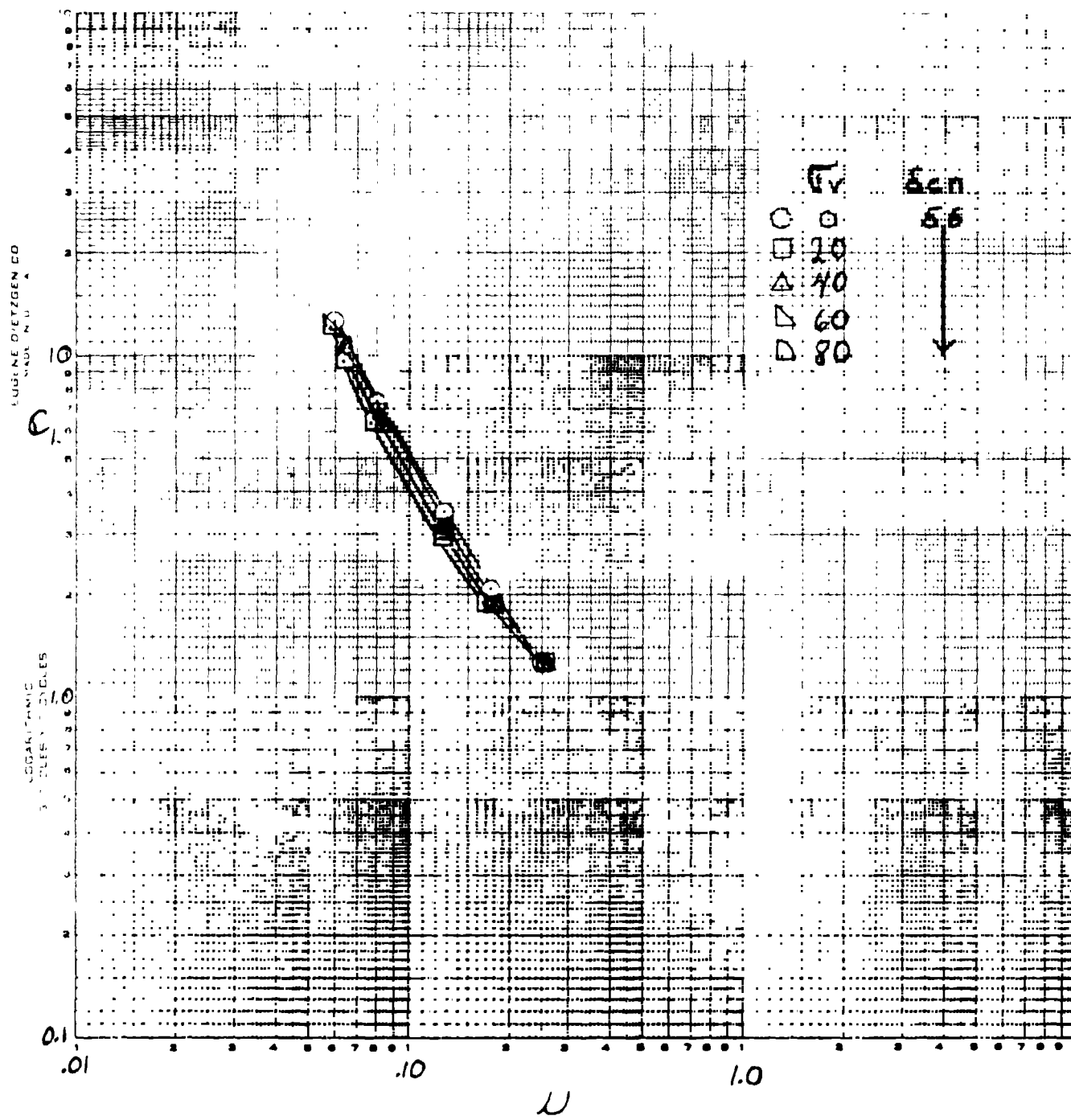
Figure 11.- Continued.



(j) $\beta_v = +16$, C_D and C_m vs μ .

Figure 11.- Concluded.

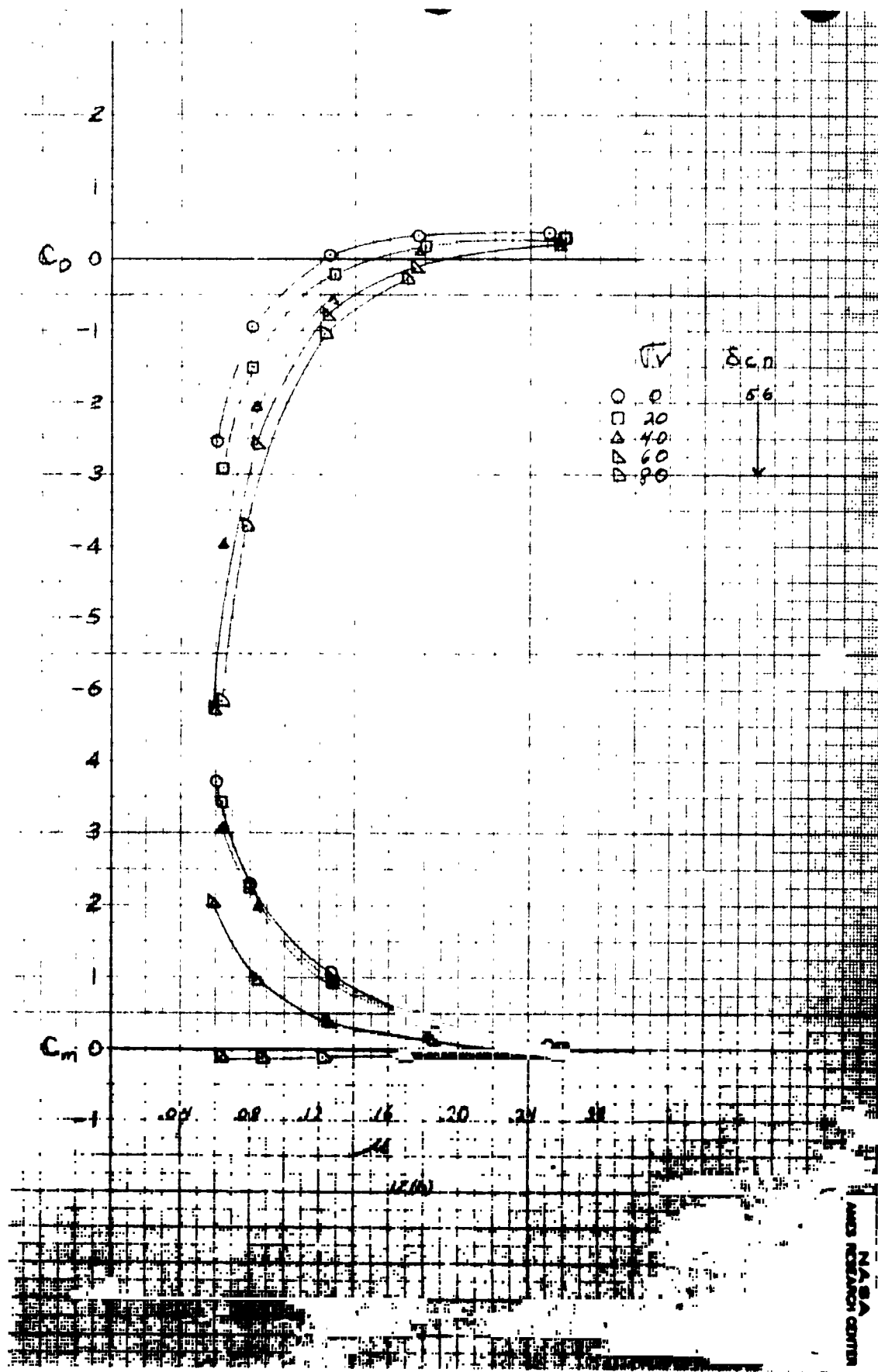
REPRODUCIBILITY OF THE ORIGINAL PAGE IS POOR.



(a) $B_v = 0$, C_L vs μ .

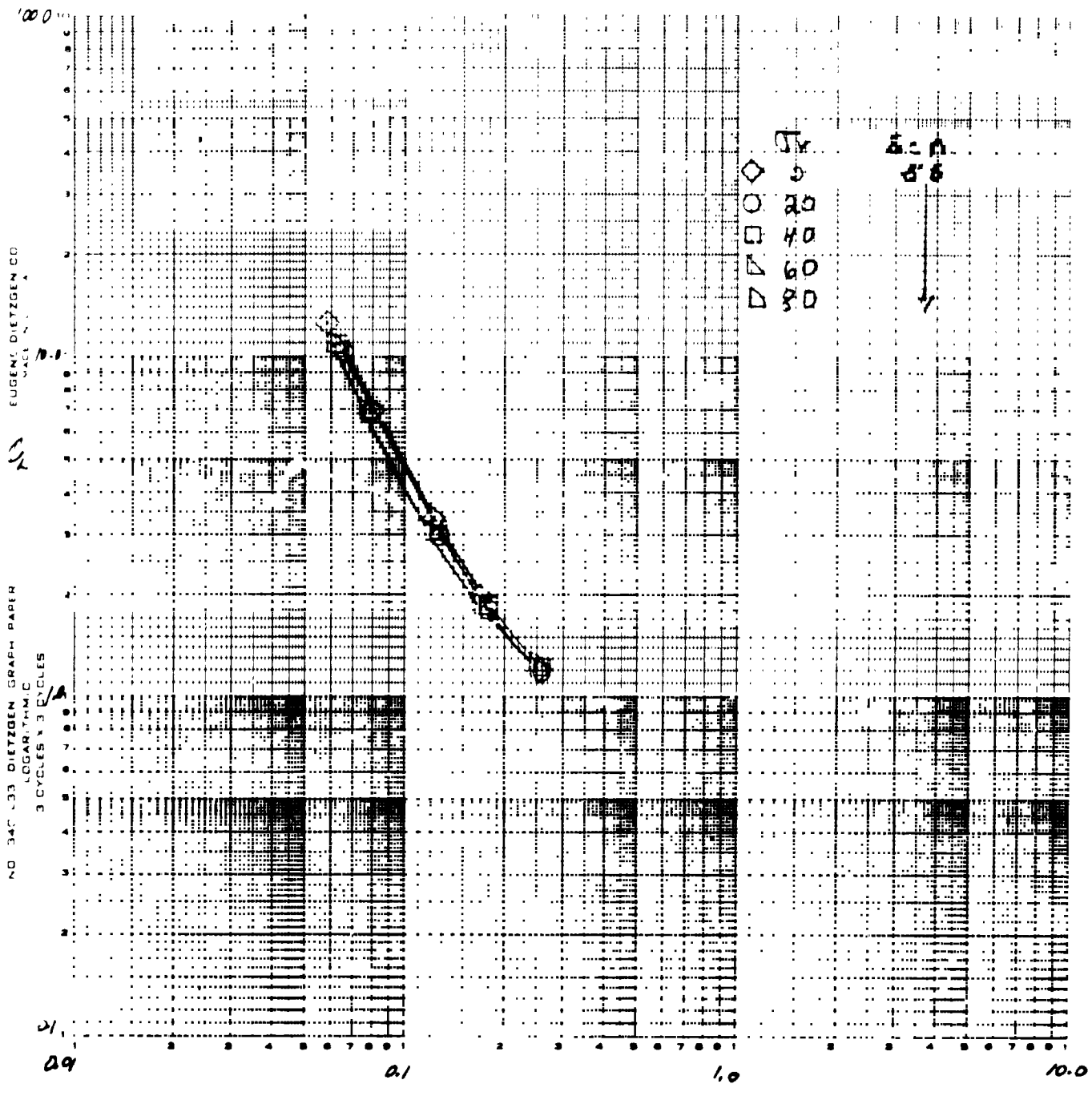
Figure 12.- The variation in longitudinal characteristics with tip-speed ratio; all four fans, tail on, $\delta_{cn} = 56$, $\delta_f = 30$.

REPRODUCIBILITY OF THE ORIGINAL PAGE IS POOR.



(b) $\beta_v = 0$, C_D and C_m vs μ .

Figure 12.- Continued.



(c) $\beta_v = -8$, C_L vs μ .

Figure 12.- Continued.

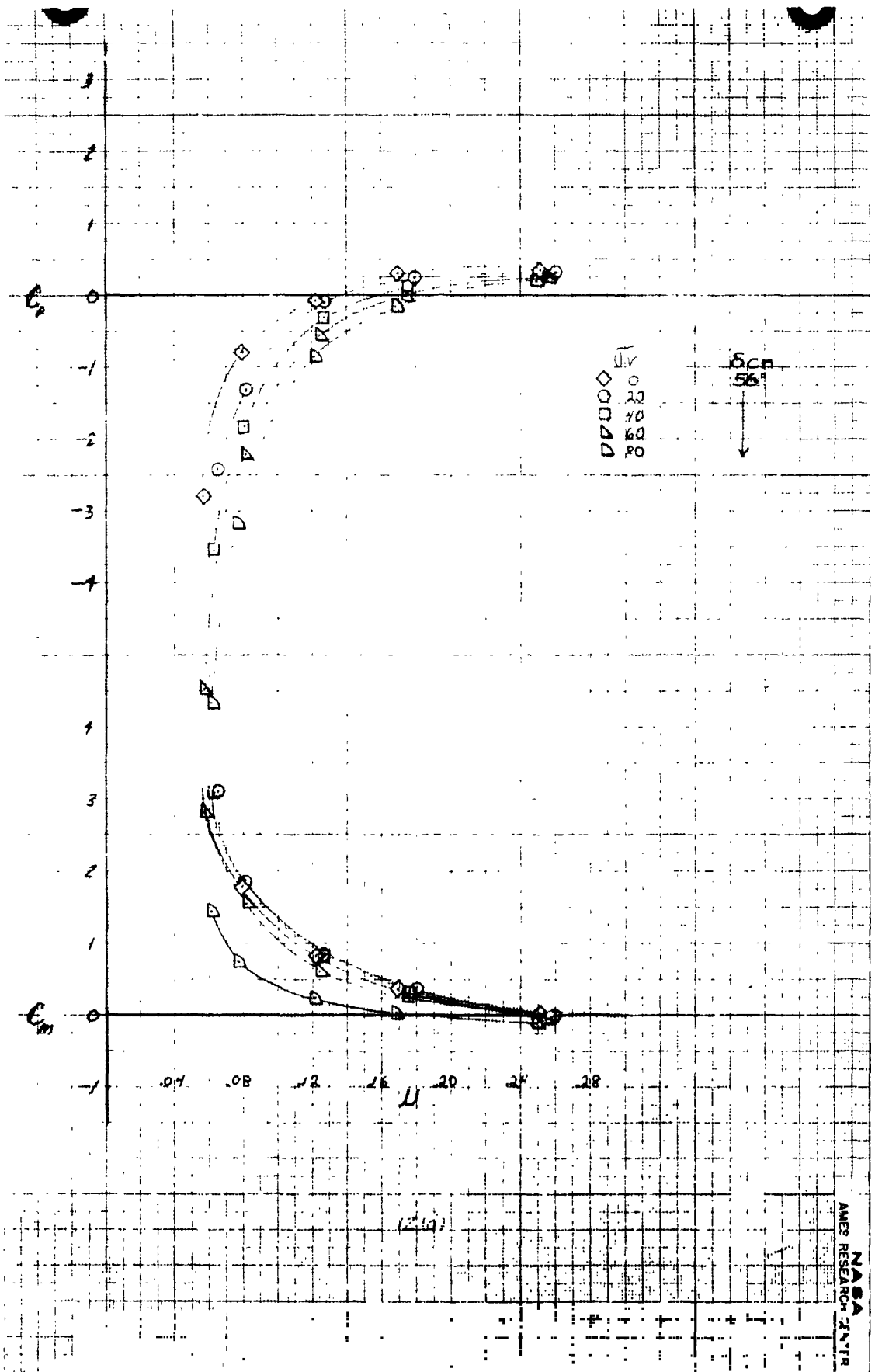
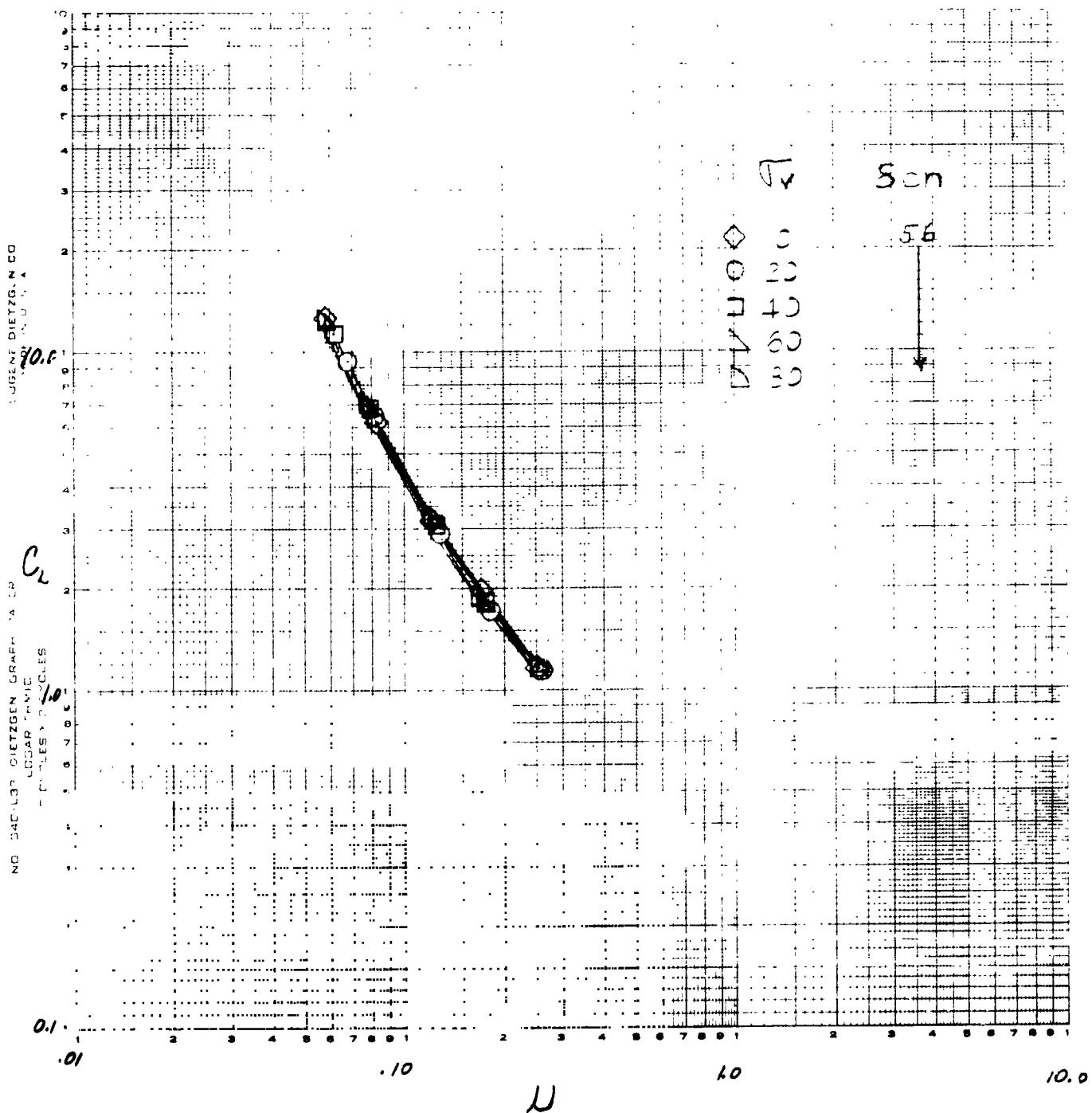


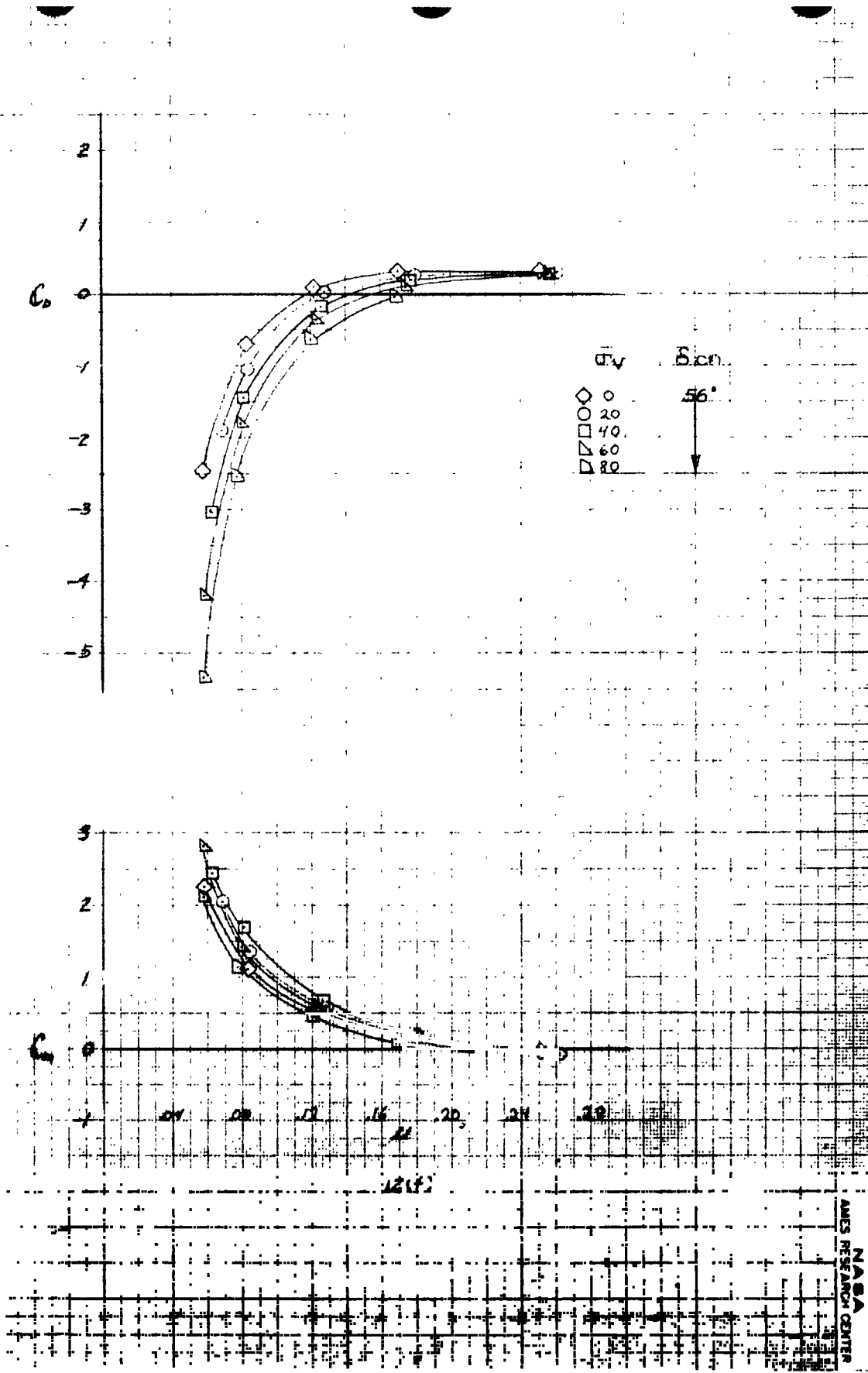
Figure 12.- Continued.

~~REPRODUCIBILITY OF THE ORIGINAL PAGE IS POOR.~~



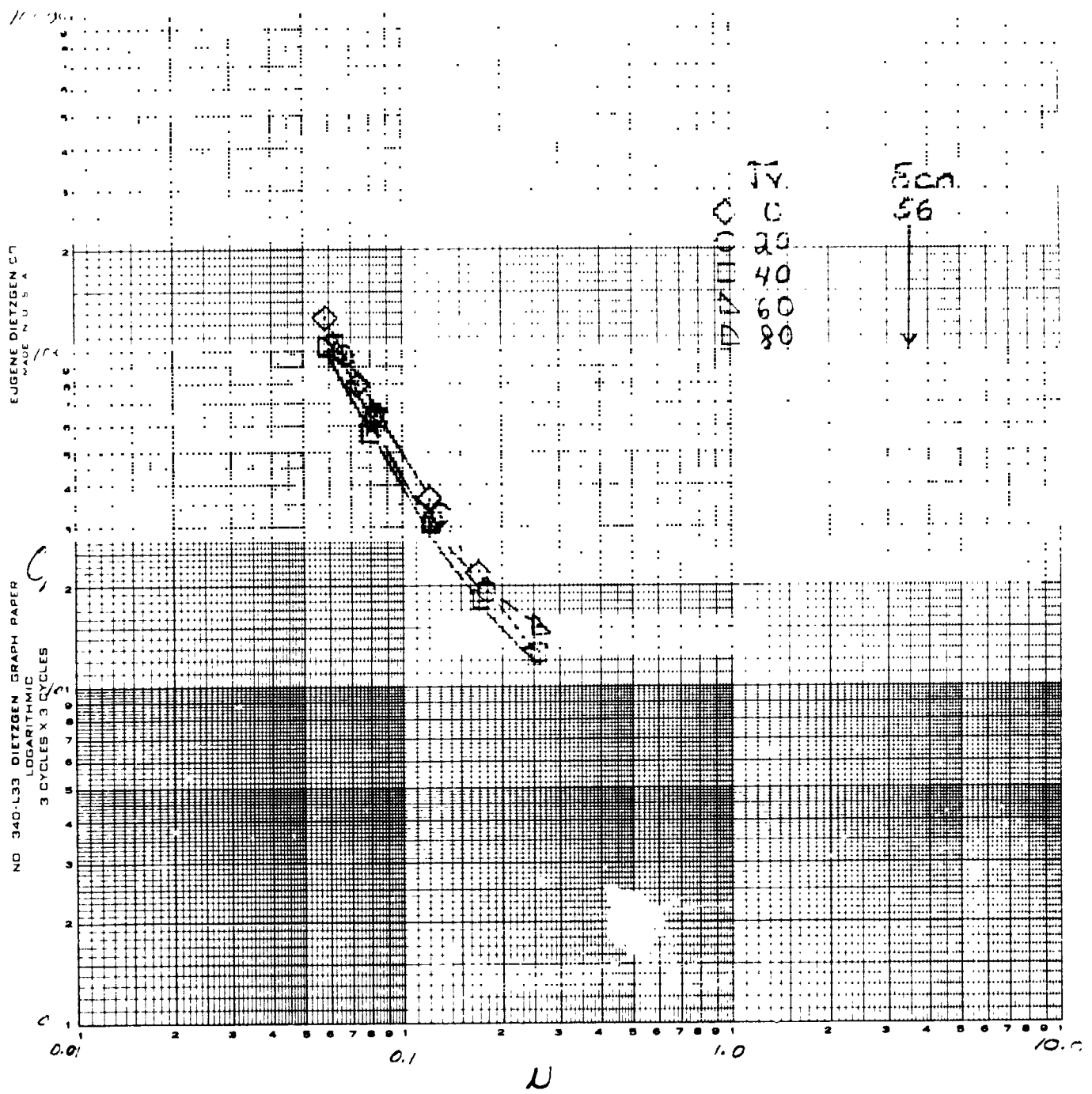
(e) $\beta_v = -16$, C_L vs u .

Figure 12.- Continued.



(f) $\beta_v = -16$, C_D and C_m vs μ .

Figure 12.- Continued.



(g) $\beta_v = +8$, C_L vs μ .

Figure 12.- Continued.

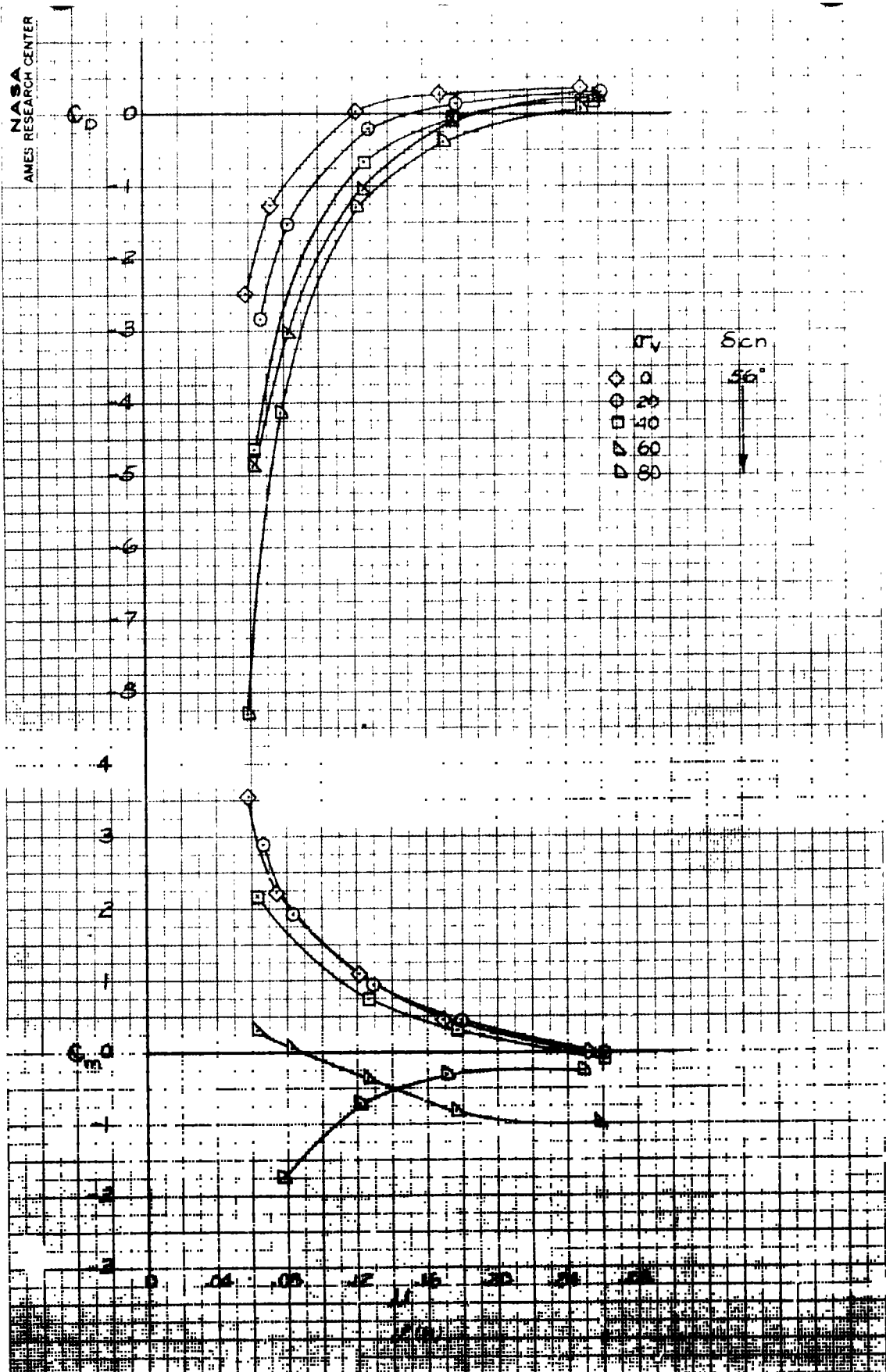
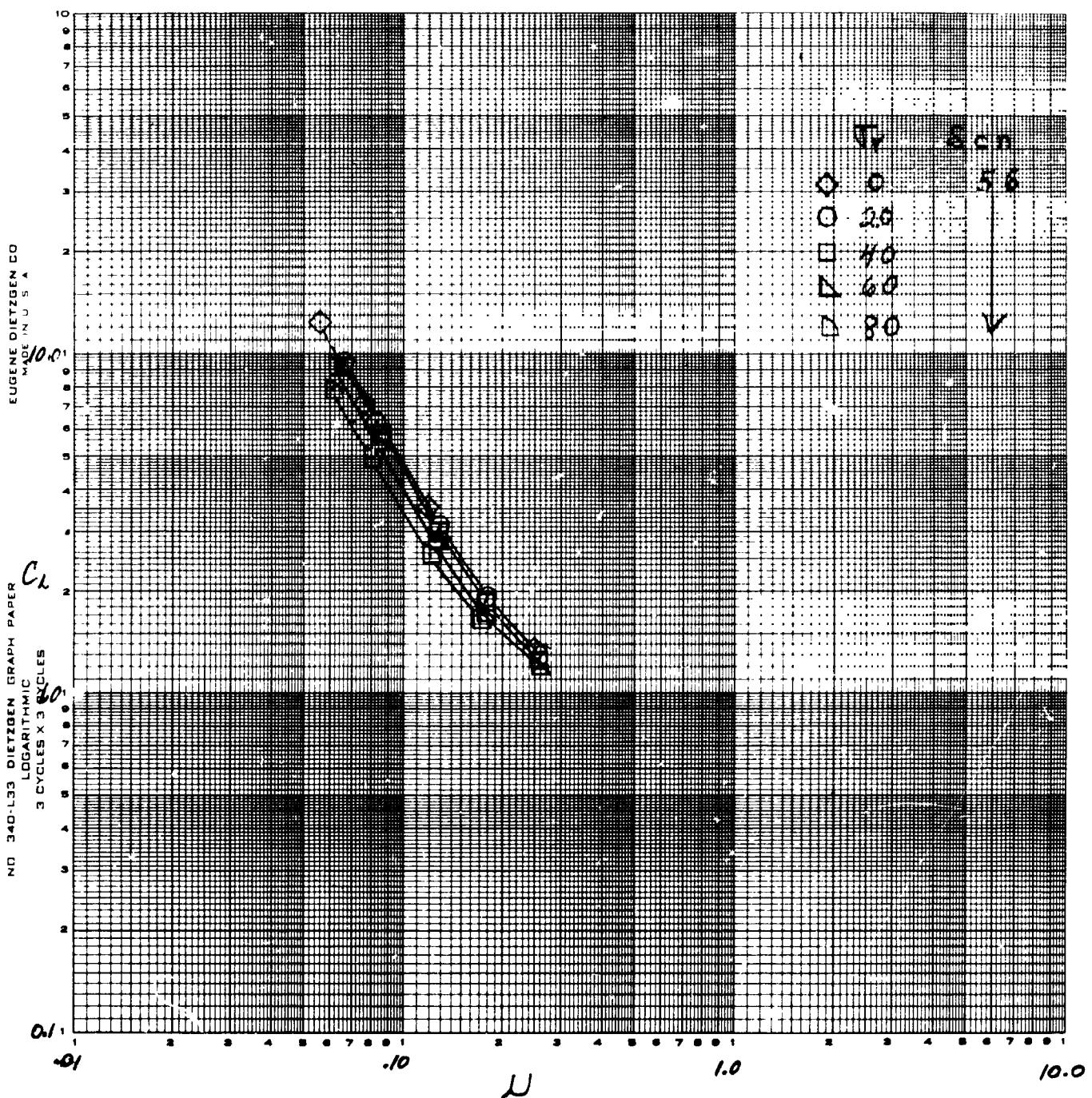


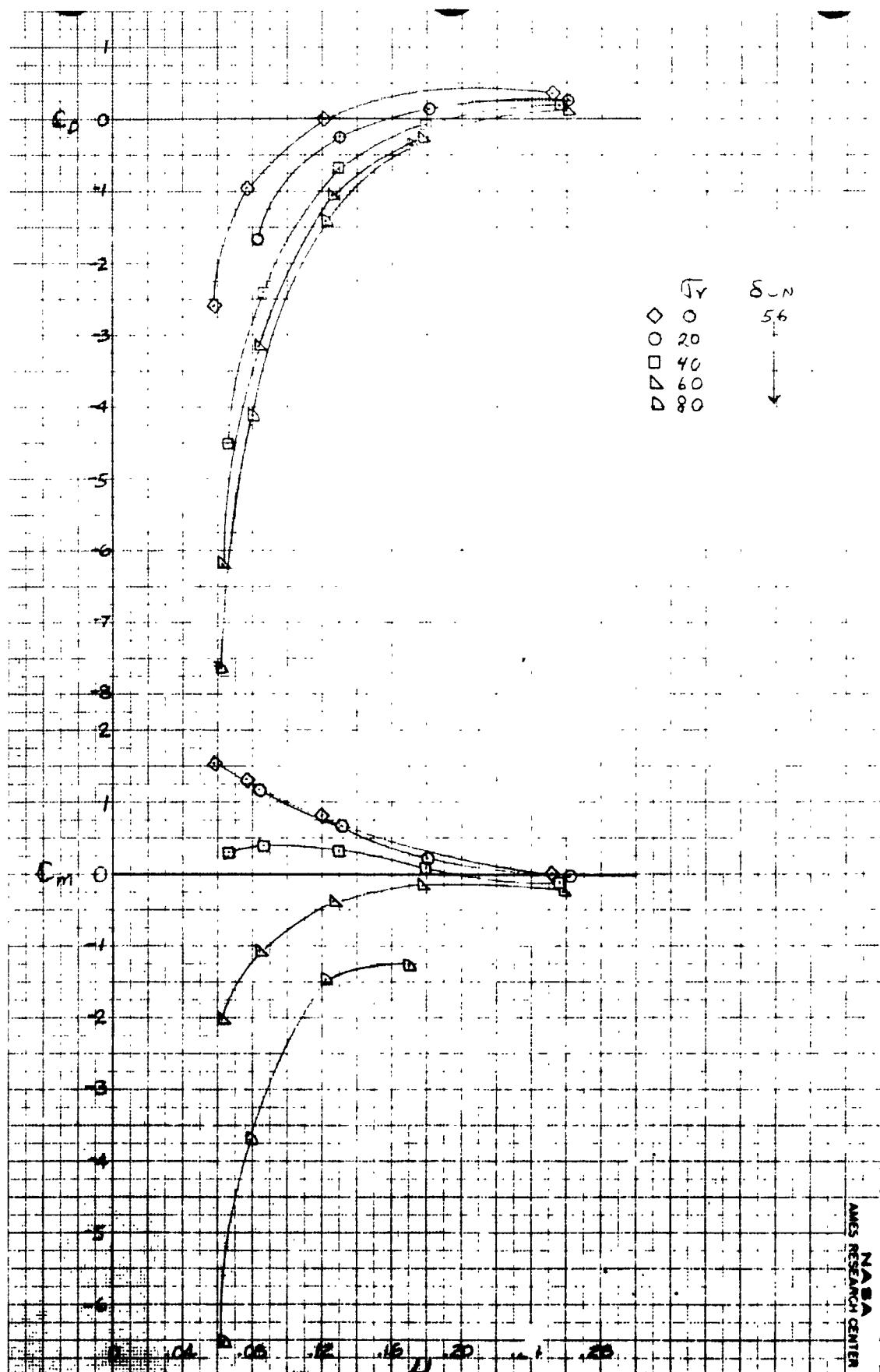
Figure 12.- Continued.



(i) $\beta_v = +16$, C_L vs μ .

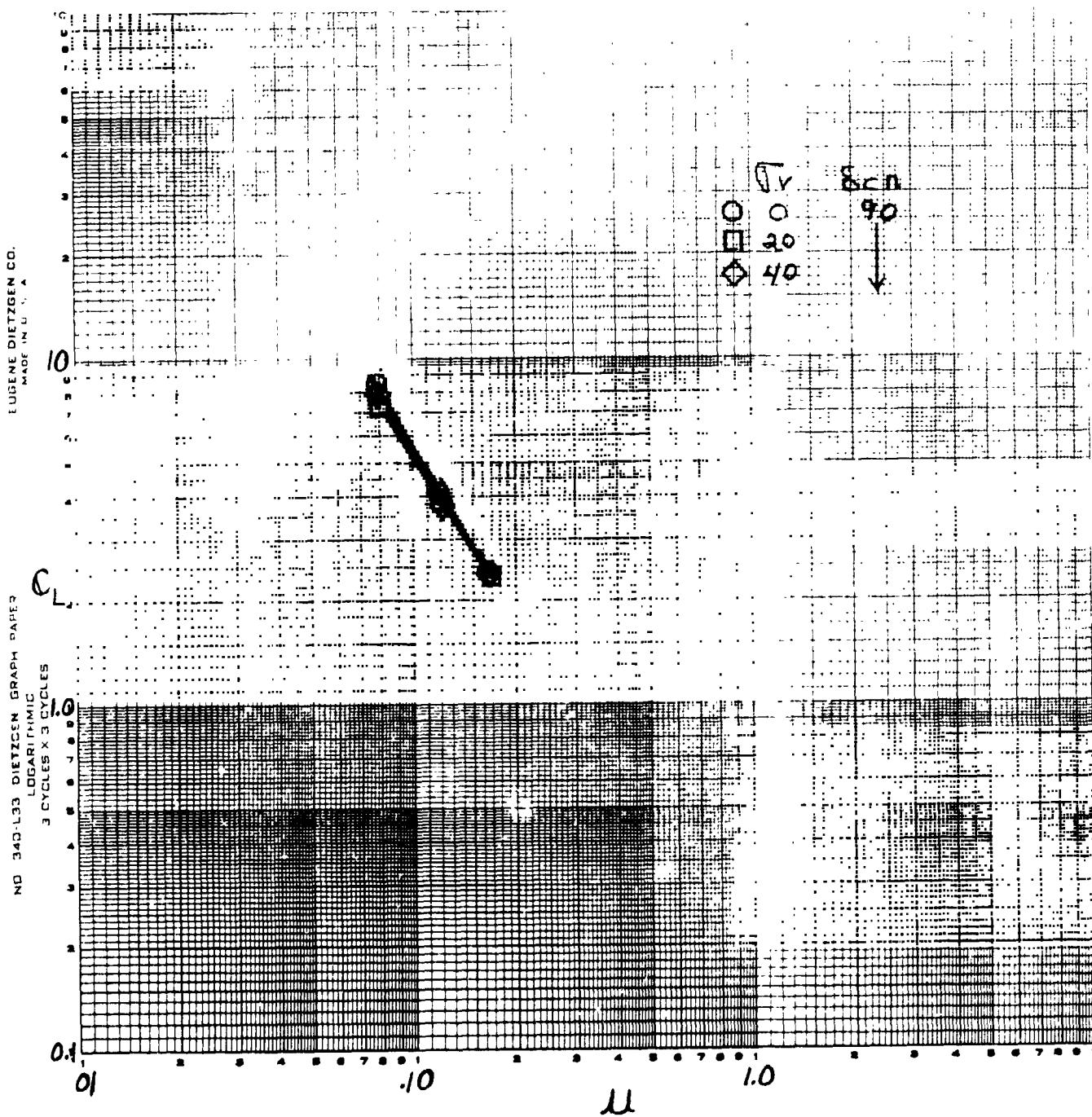
Figure 12.- Continued.

REPRODUCIBILITY OF THE ORIGINAL PAGE IS POOR.



(j) $\beta_v = +16$, C_D and C_m vs μ .

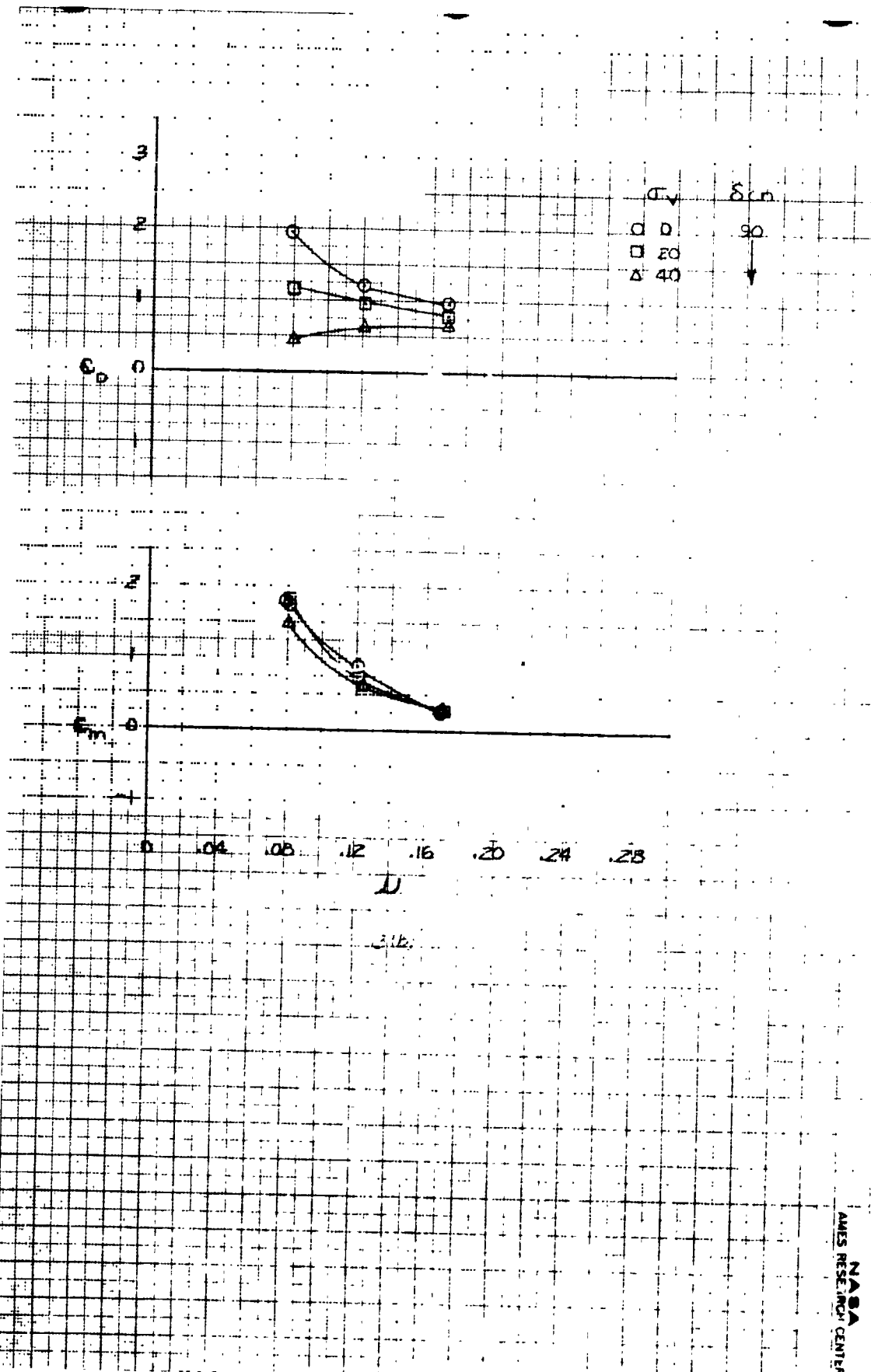
Figure 12.- Concluded.



(a) $\beta_v = 0$, C_L vs μ .

Figure 13.- The variation in longitudinal characteristics with tip-speed ratio; all four fans, tail on, $\delta_{cn} = 90$, $\delta_f = 30$.

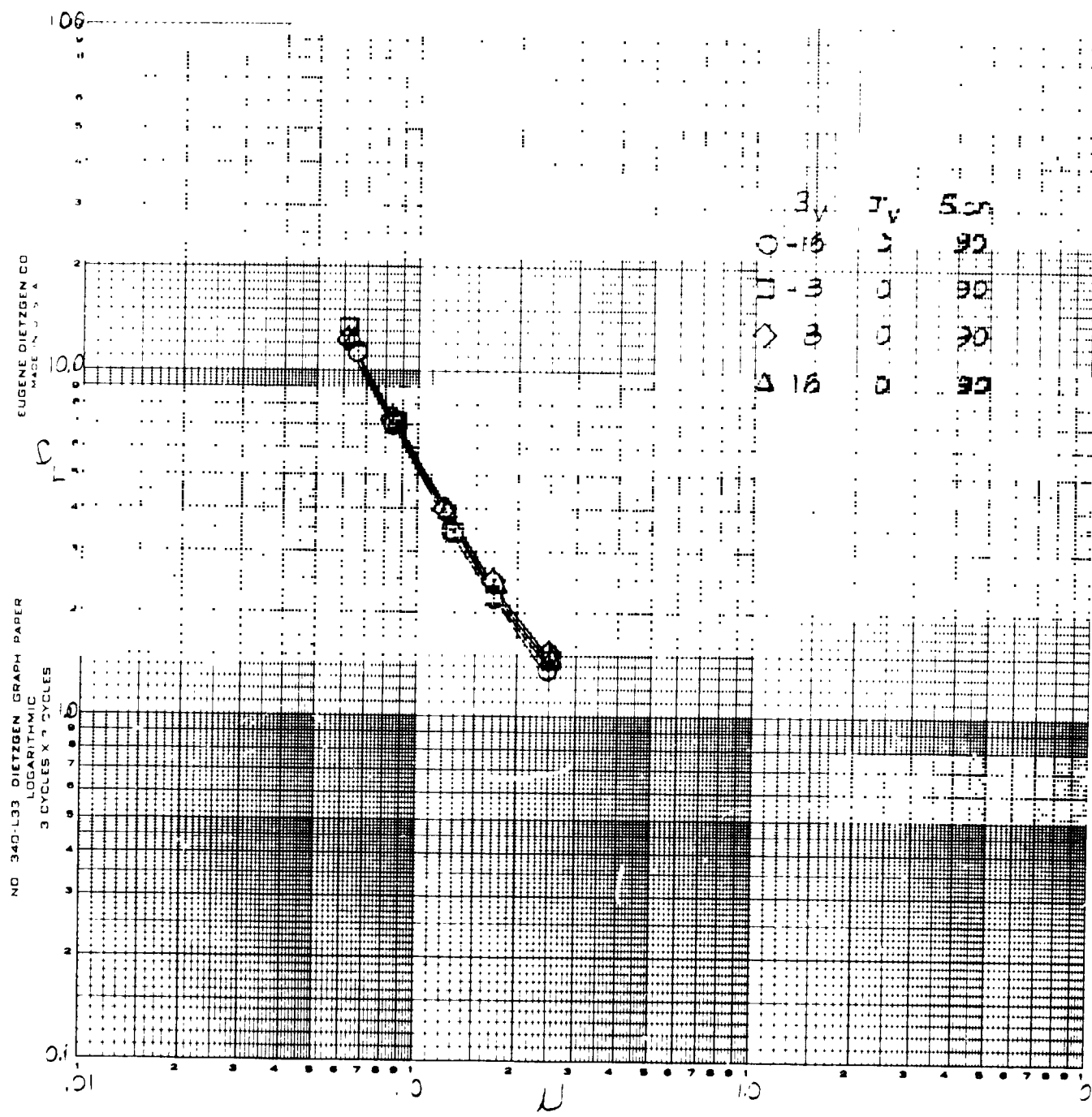
REPRODUCIBILITY OF THE ORIGINAL PAGE IS POOR.



(b) $\beta_v = 0$, C_D and C_m vs μ .

Figure 13.- Continued.

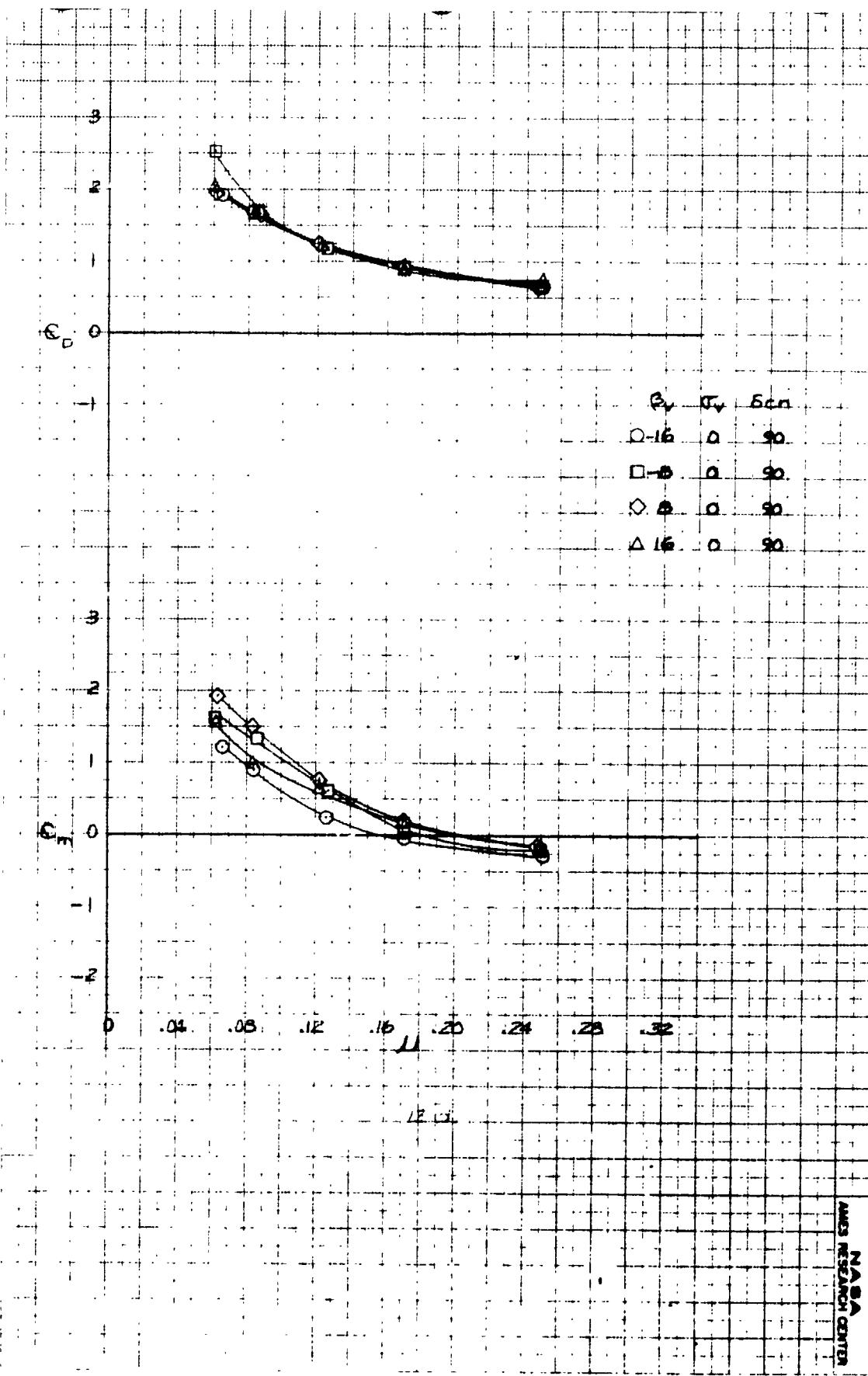
NASA
AMES RESEARCH CENTER



(c) C_L vs μ .

Figure 13.- Continued.

REPRODUCIBILITY OF THE ORIGINAL PAGE IS POOR.



(d) C_D and C_m vs μ .

Figure 13.- Concluded.

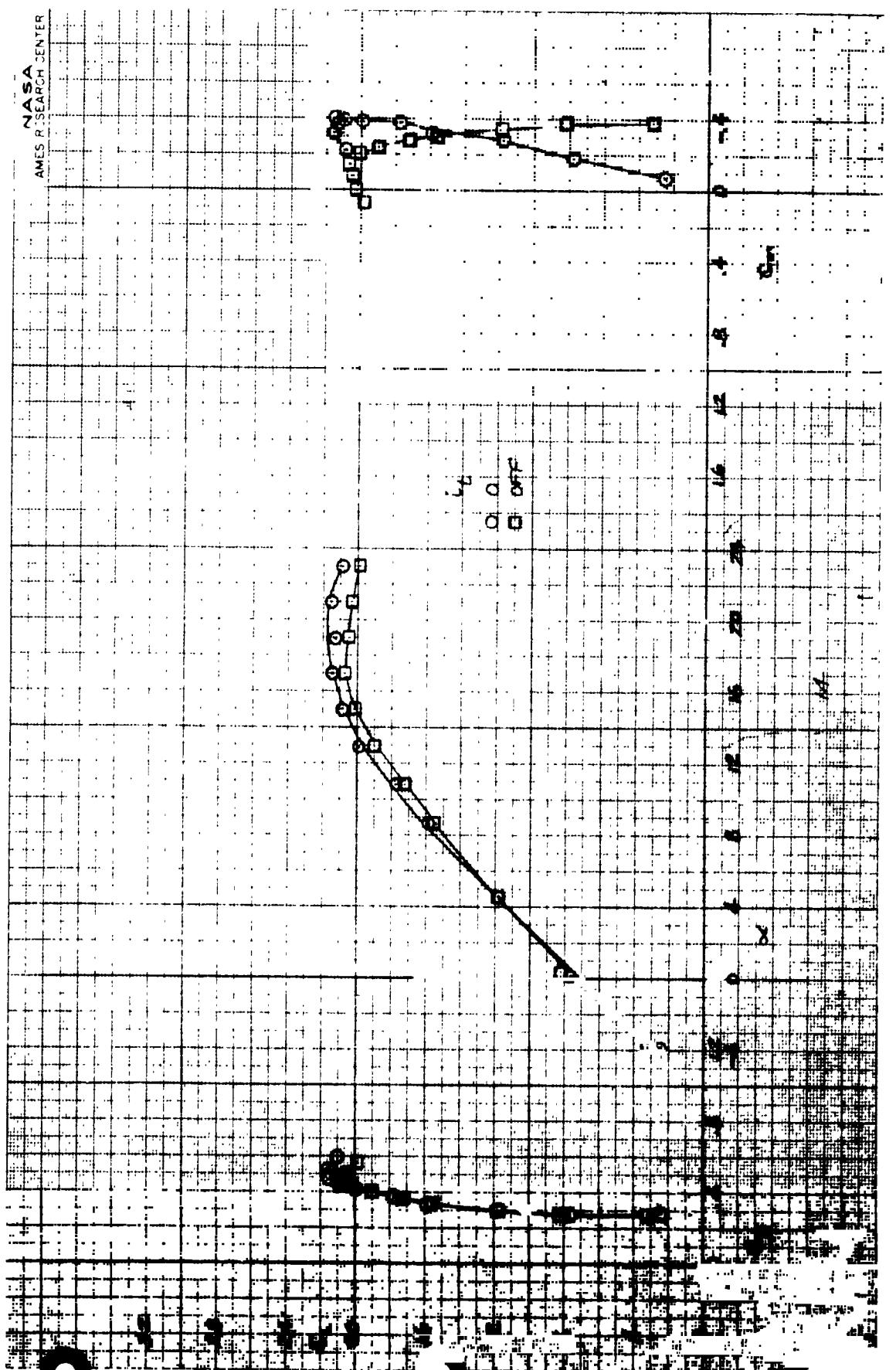
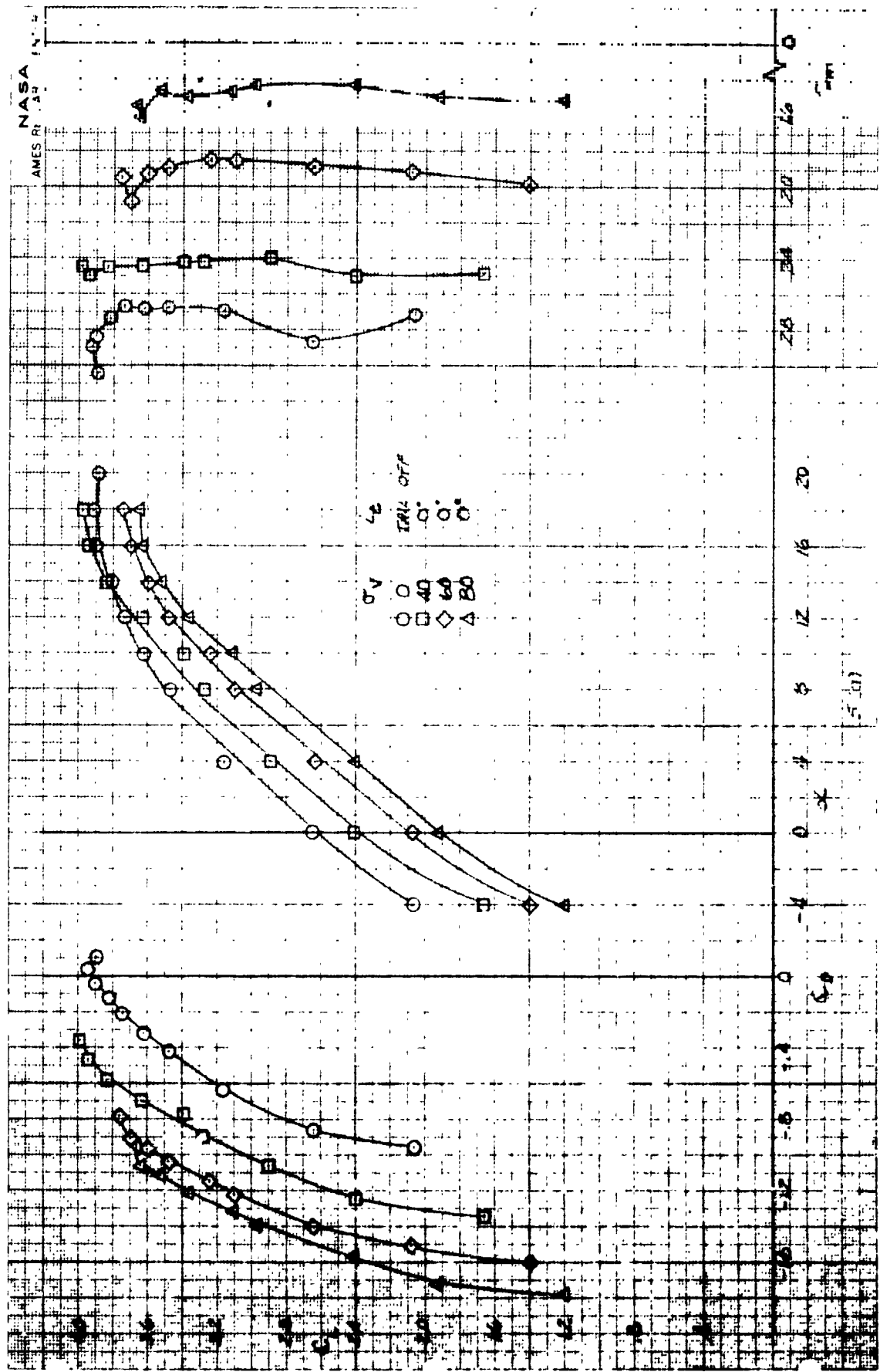


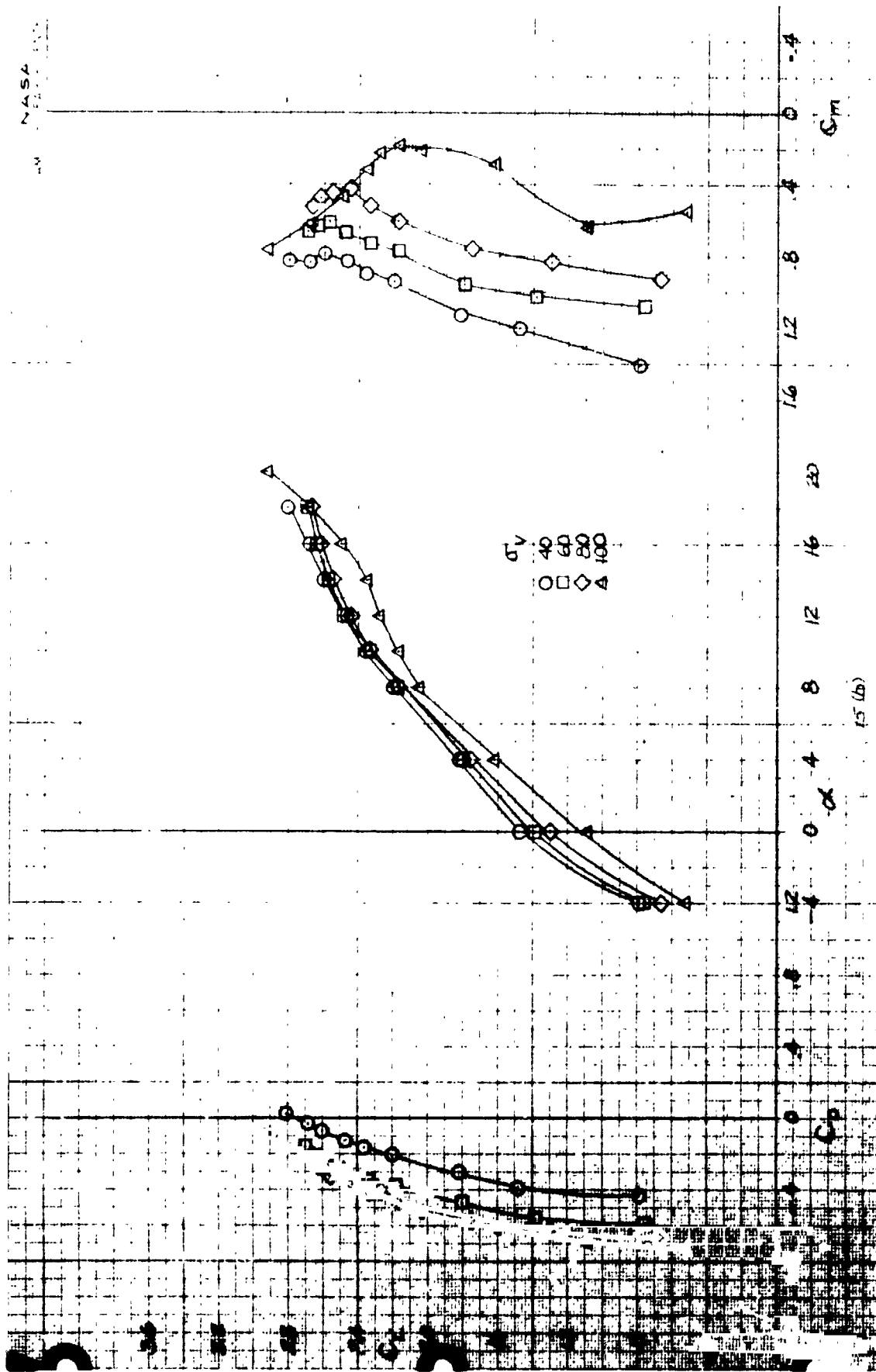
Figure 14.- The variation in longitudinal characteristics with angle of attack; power off, $\delta_v = 90^\circ$, $\dot{v}_v = 90$, front fan inlets sealed, $\delta_{cn} = 90^\circ$, $\delta_f = 30$.



(a) $u = .12$.

Figure 15.- The variation in longitudinal characteristics with angle of attack; $\beta_v = 0$, $\delta_{cn} = 23$, four fans, $t = 30$.

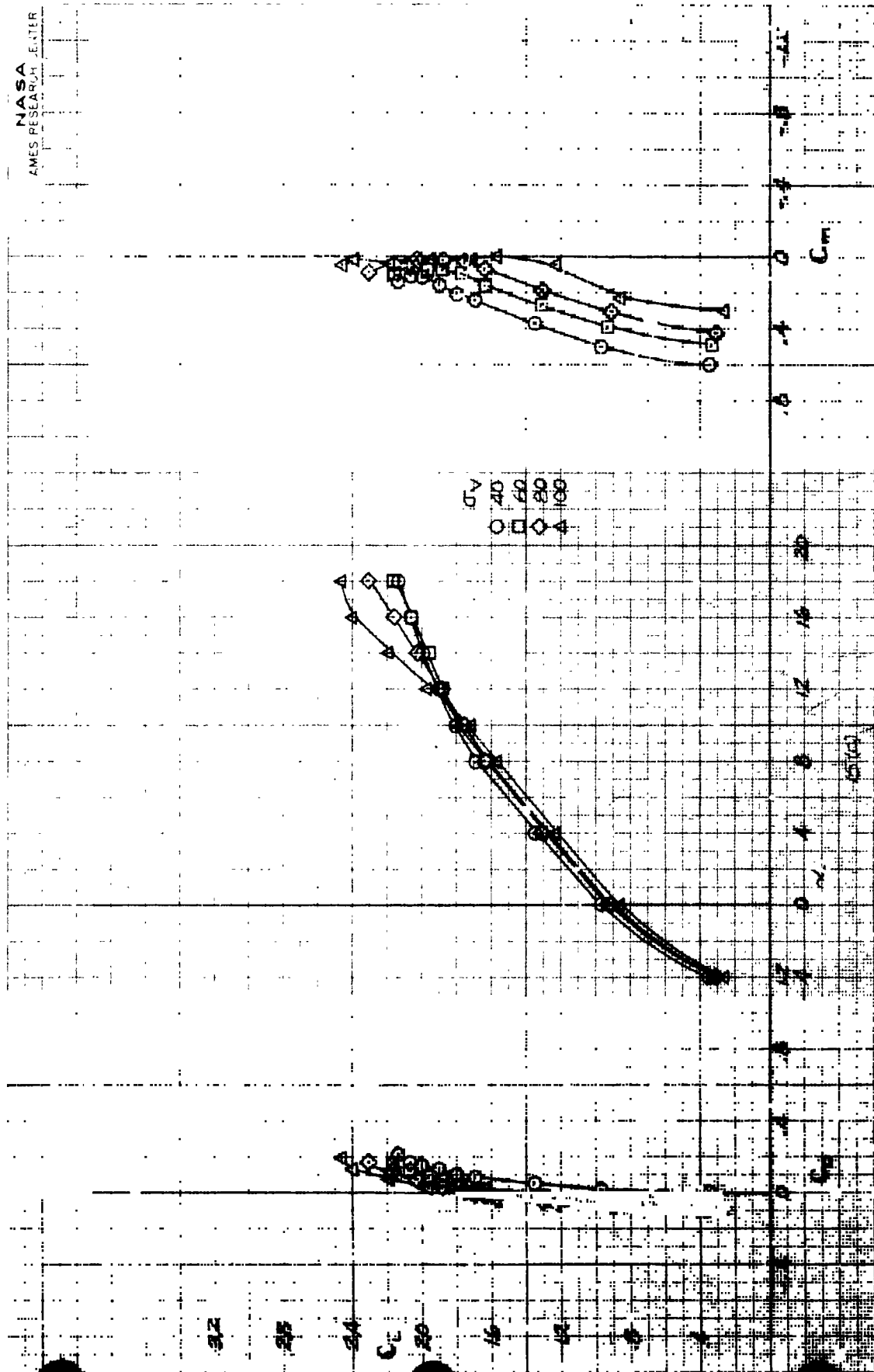
REPRODUCIBILITY OF THE ORIGINAL PAGE IS POOR.



(b) $\nu = .18$, tail on.

Figure 15.— Continued.

REPRODUCIBILITY OF THE ORIGINAL PAGE IS POOR.



(c) $\mu = .26$, tail on.

Figure 15.- Concluded.

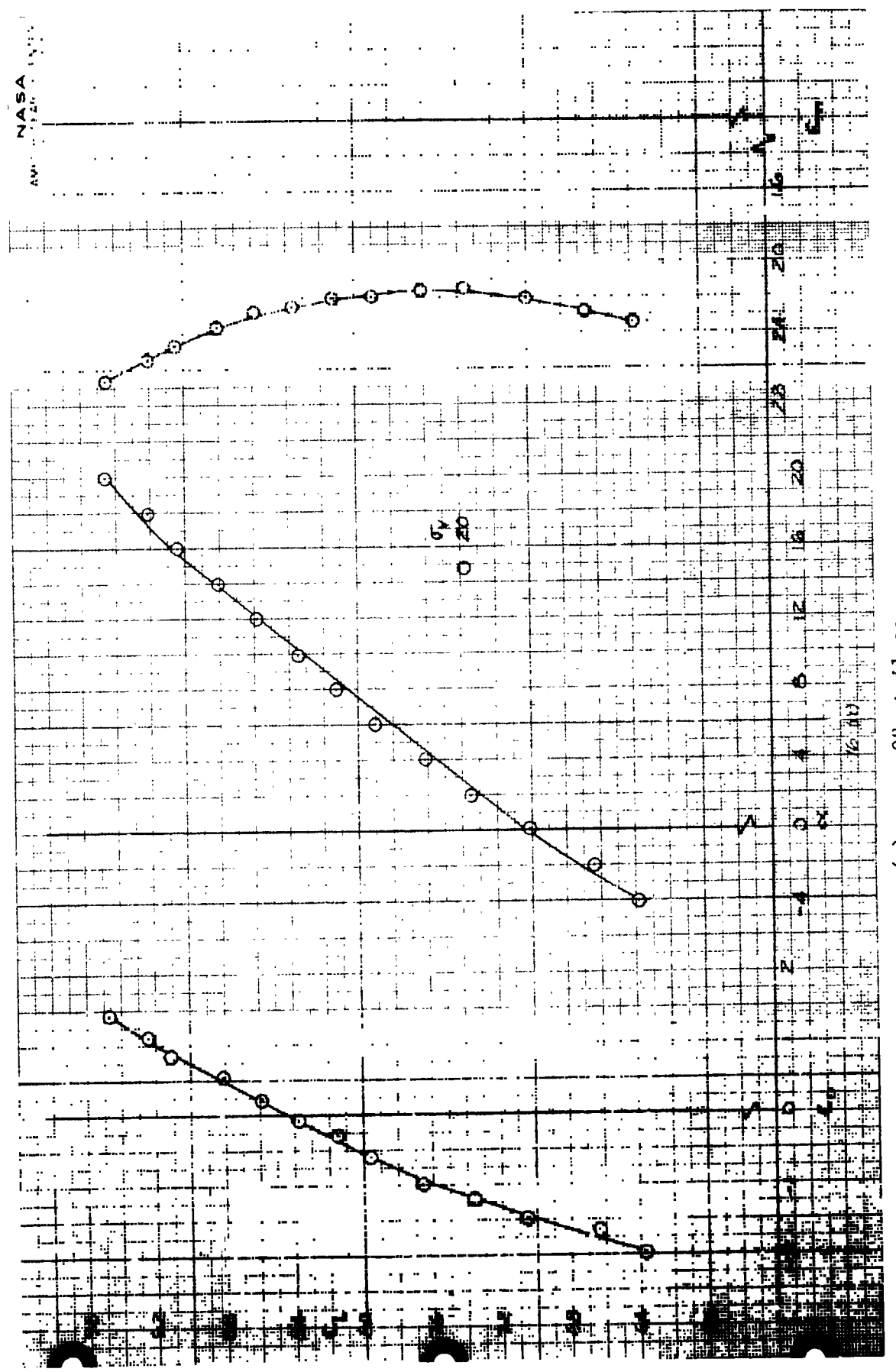


Figure 16.- The variation in longitudinal characteristics with angle of attack; $\beta_v = 0$, $\delta_{cn} = 56$, four fans, $\delta_f = 30$.

REPRODUCIBILITY OF THE ORIGINAL PAGE IS POOR.

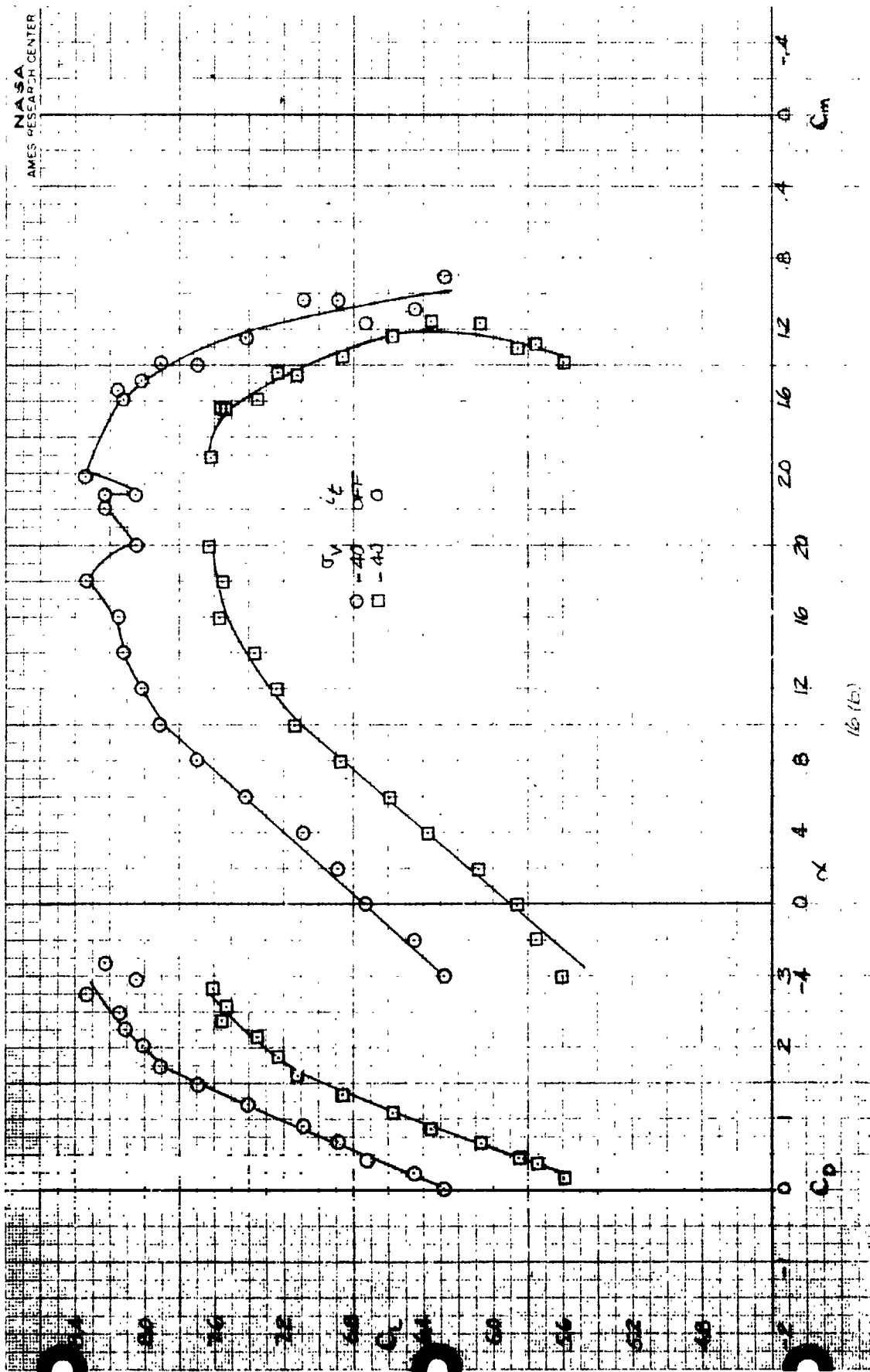
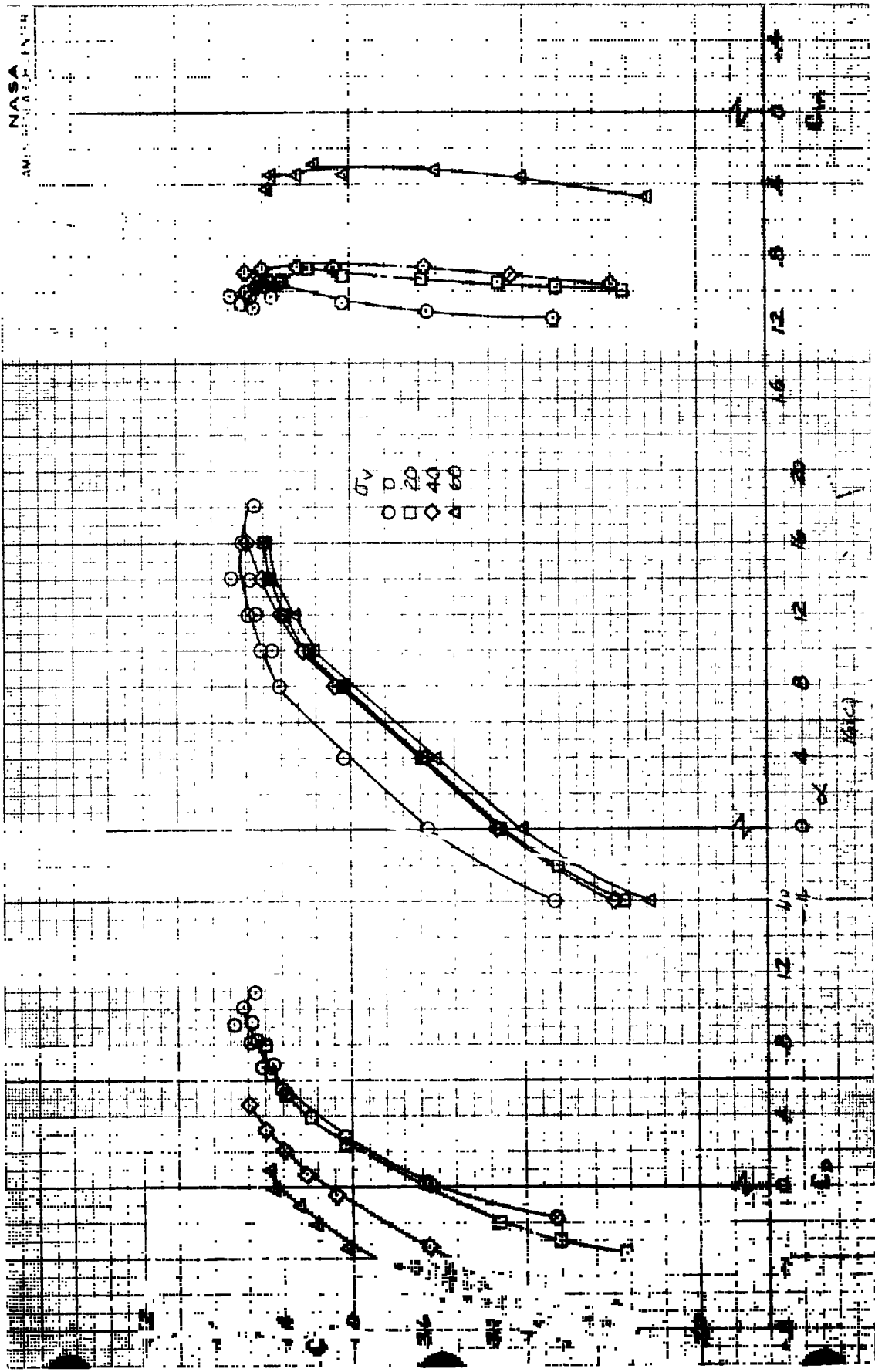


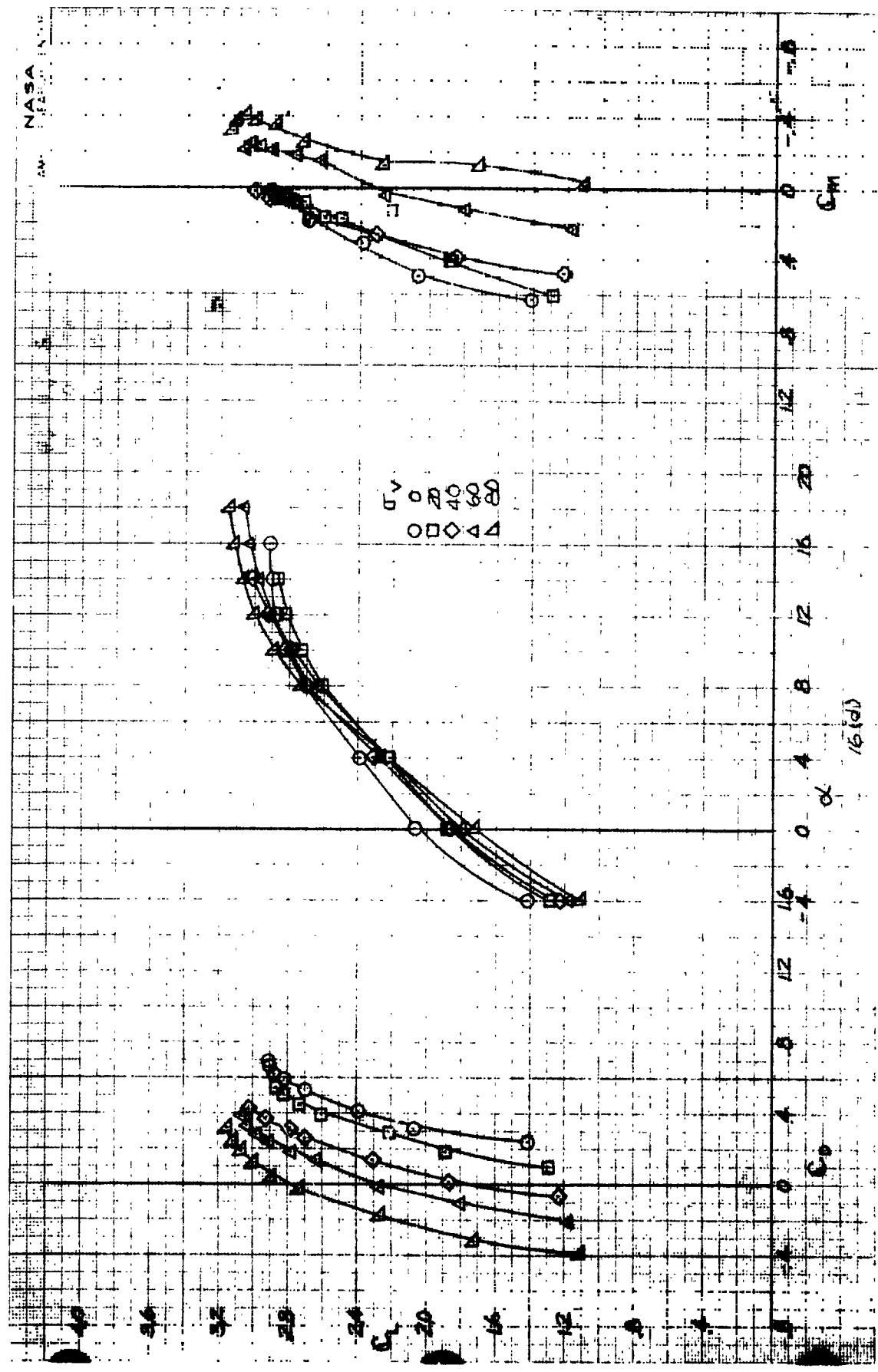
Figure 16.- Continued.



(c) $\mu = .12$, tail on.

Figure 16.- Continued

REPRODUCIBILITY OF THE ORIGINAL PAGE IS POOR.



(d) $\mu = .18$, tail on.

Figure 16.- Continued.

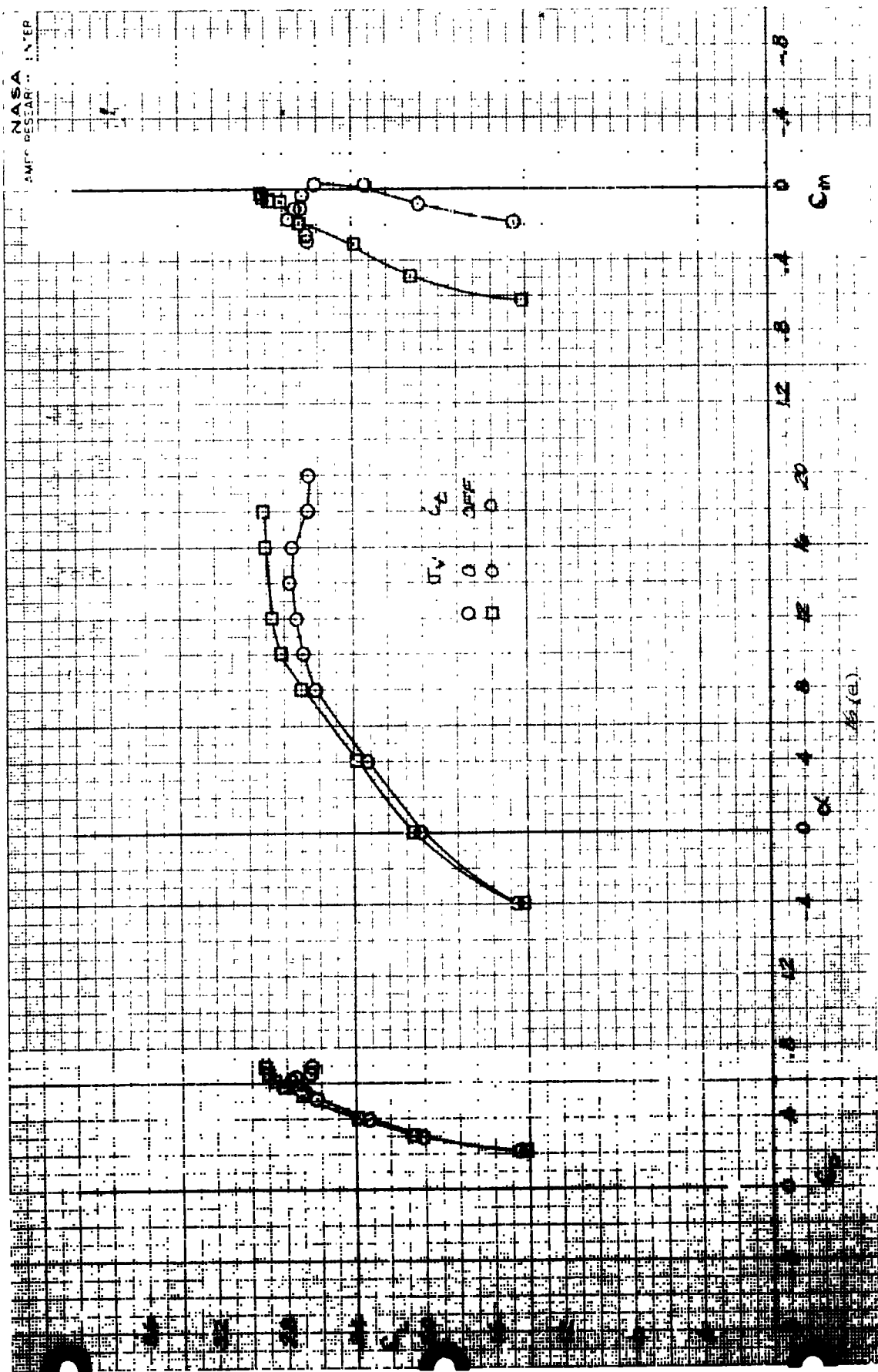
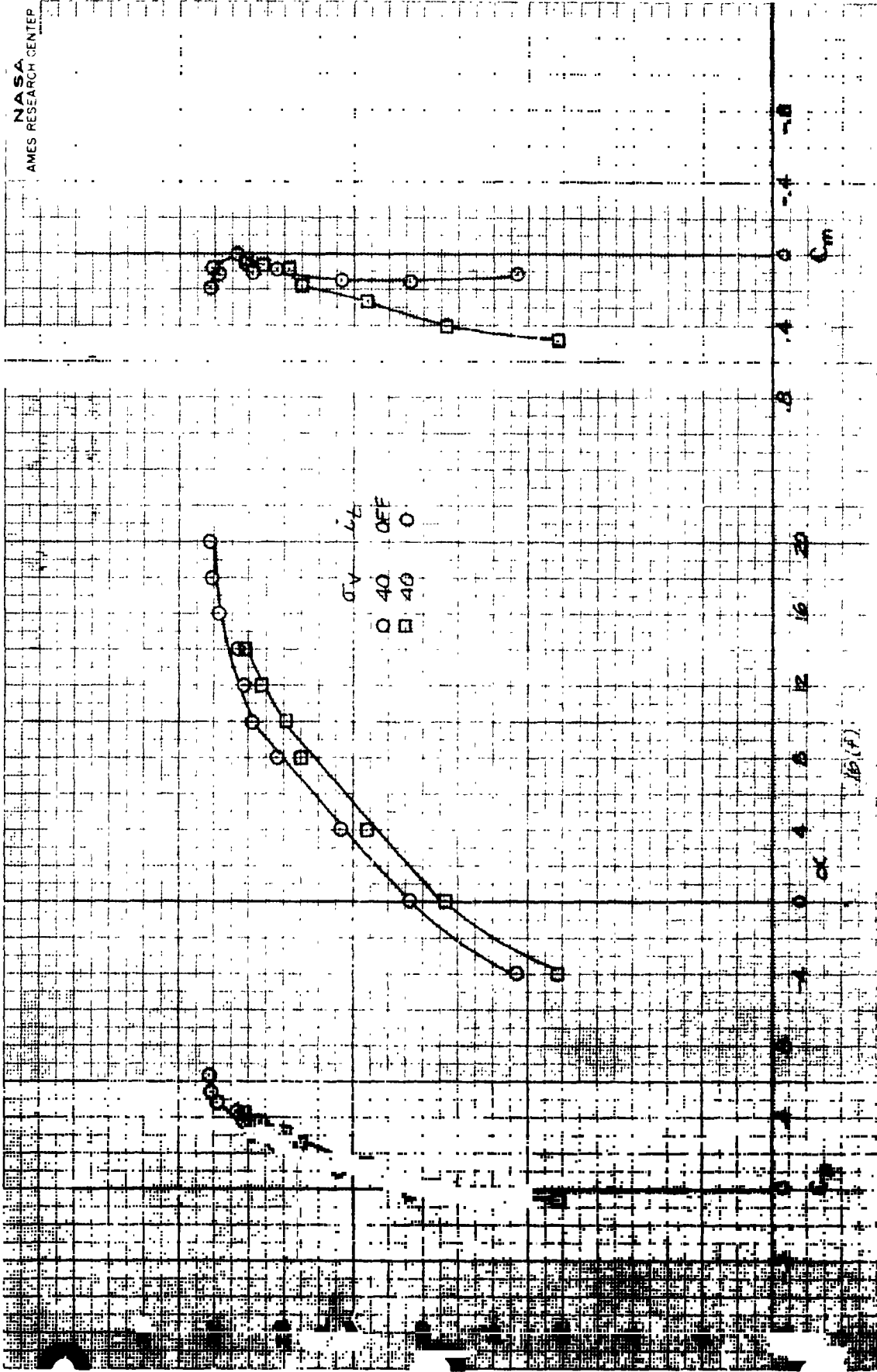


Figure 16.- Continued.

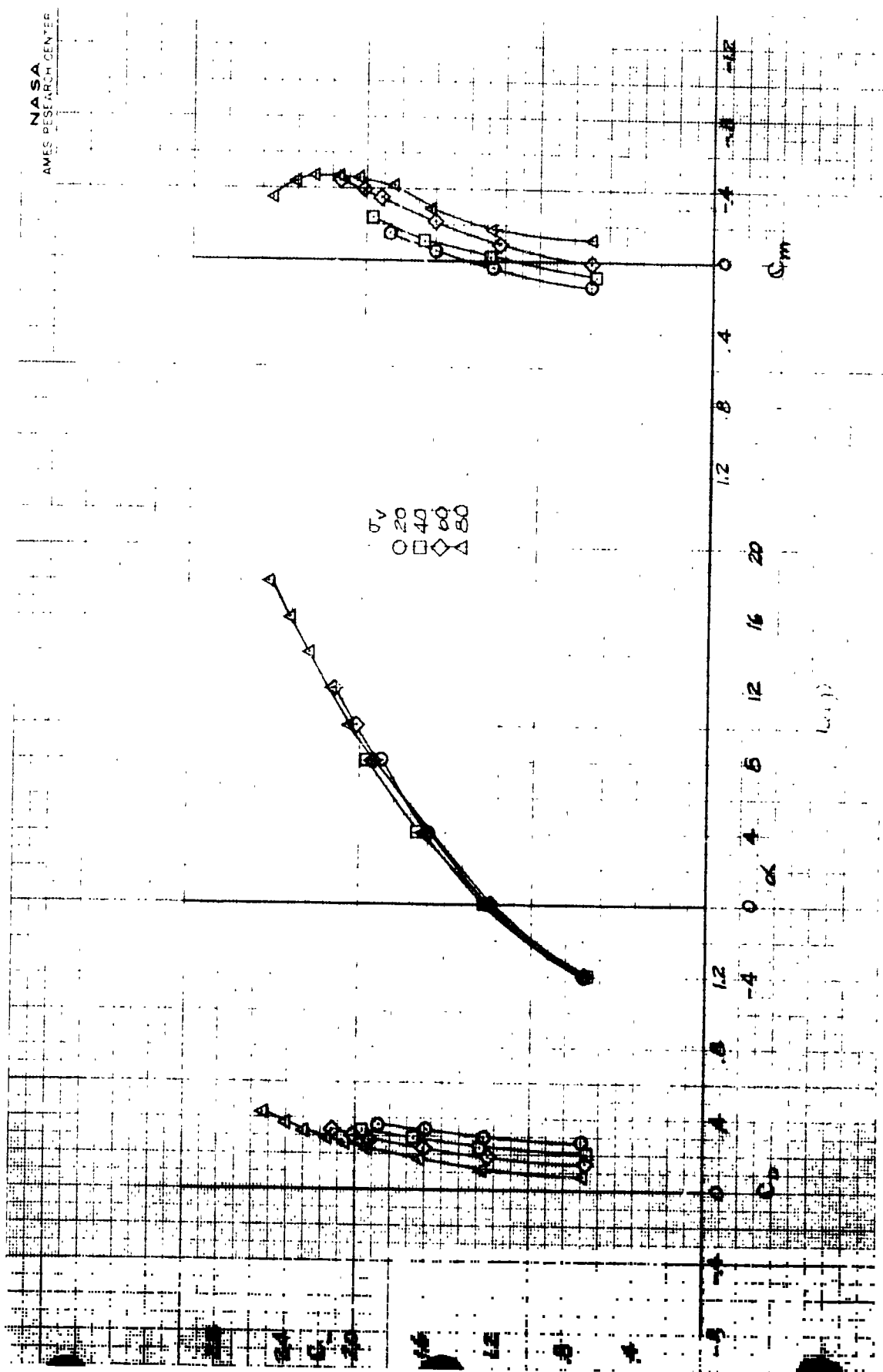
REPRODUCIBILITY OF THE ORIGINAL PAGE IS POOR.



(F) $\nu = .18$, $\sigma_v = 40$.

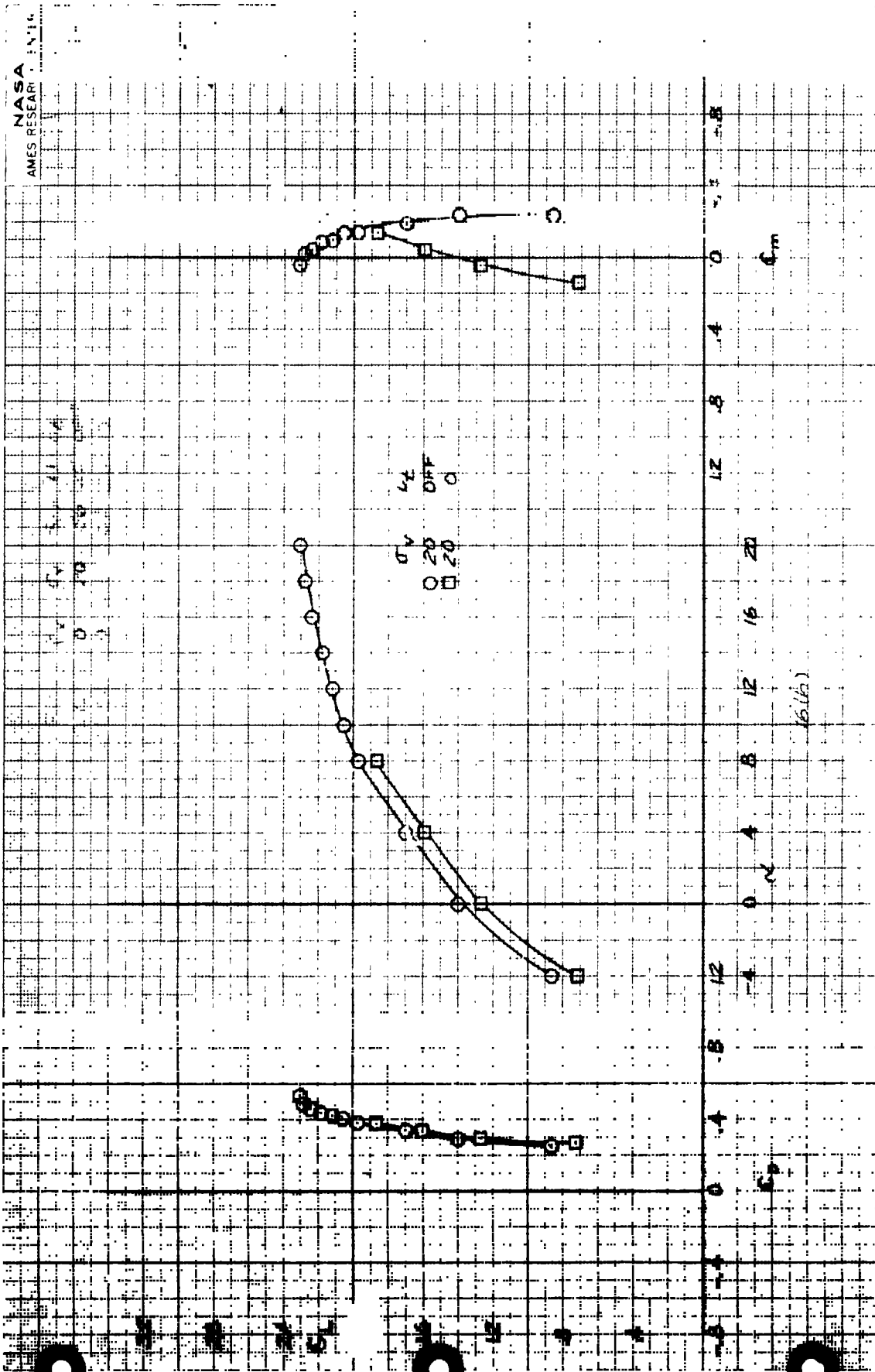
Figure 16. - Continued.

REPRODUCIBILITY OF THE ORIGINAL PAGE IS POOR.



(g) $\mu = .26$, tail on.

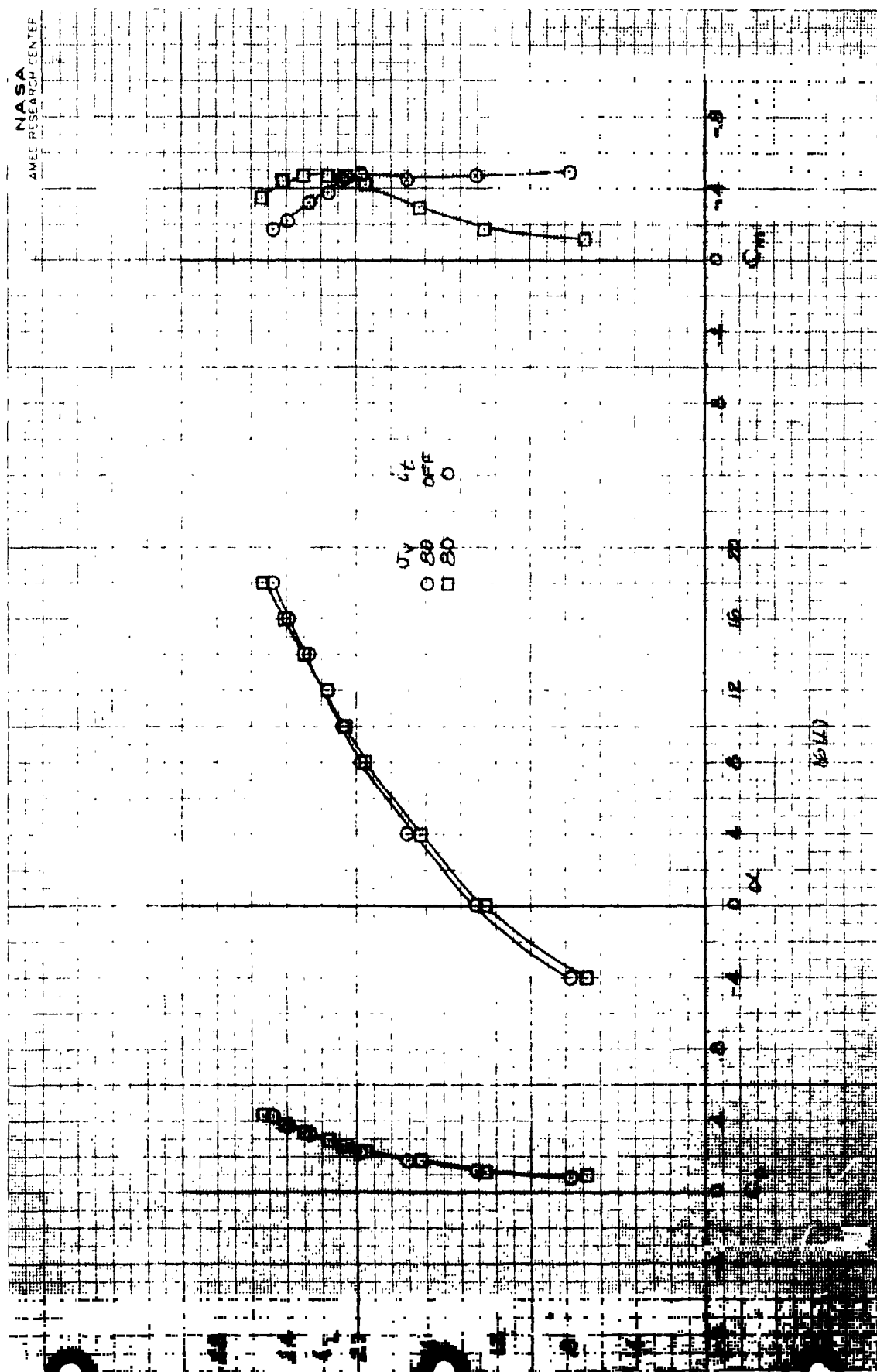
Figure 16.- Continued.



(h) $\mu = .26$, $v = 20$.

Figure 16.- Continued.

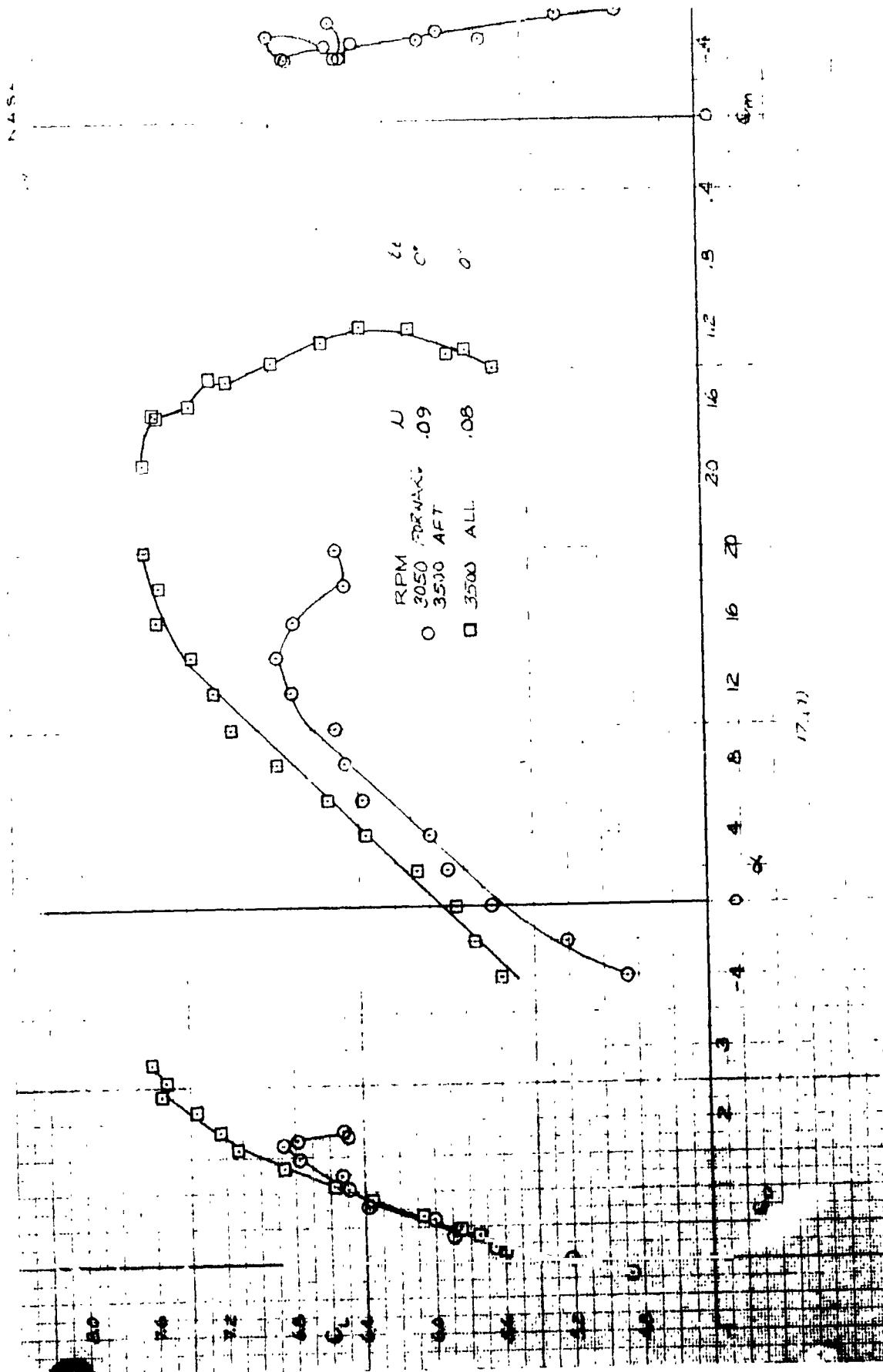
REPRODUCIBILITY OF THE ORIGINAL PAGE IS POOR.



(i) $\nu = .26$, $\alpha_v = 80$.

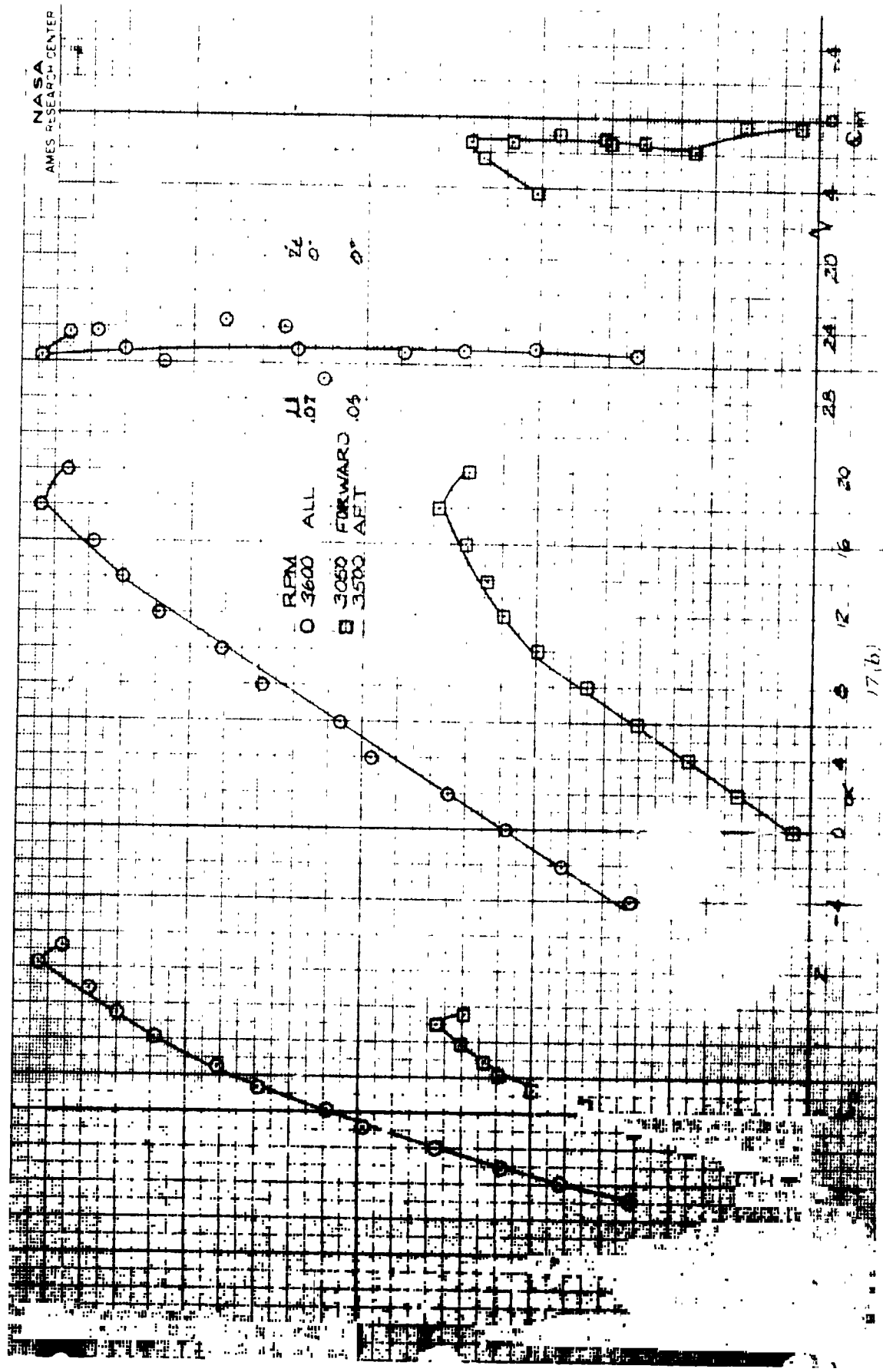
Figure 16.- Concluded.

REPRODUCIBILITY OF THE ORIGINAL PAGE IS POOR.



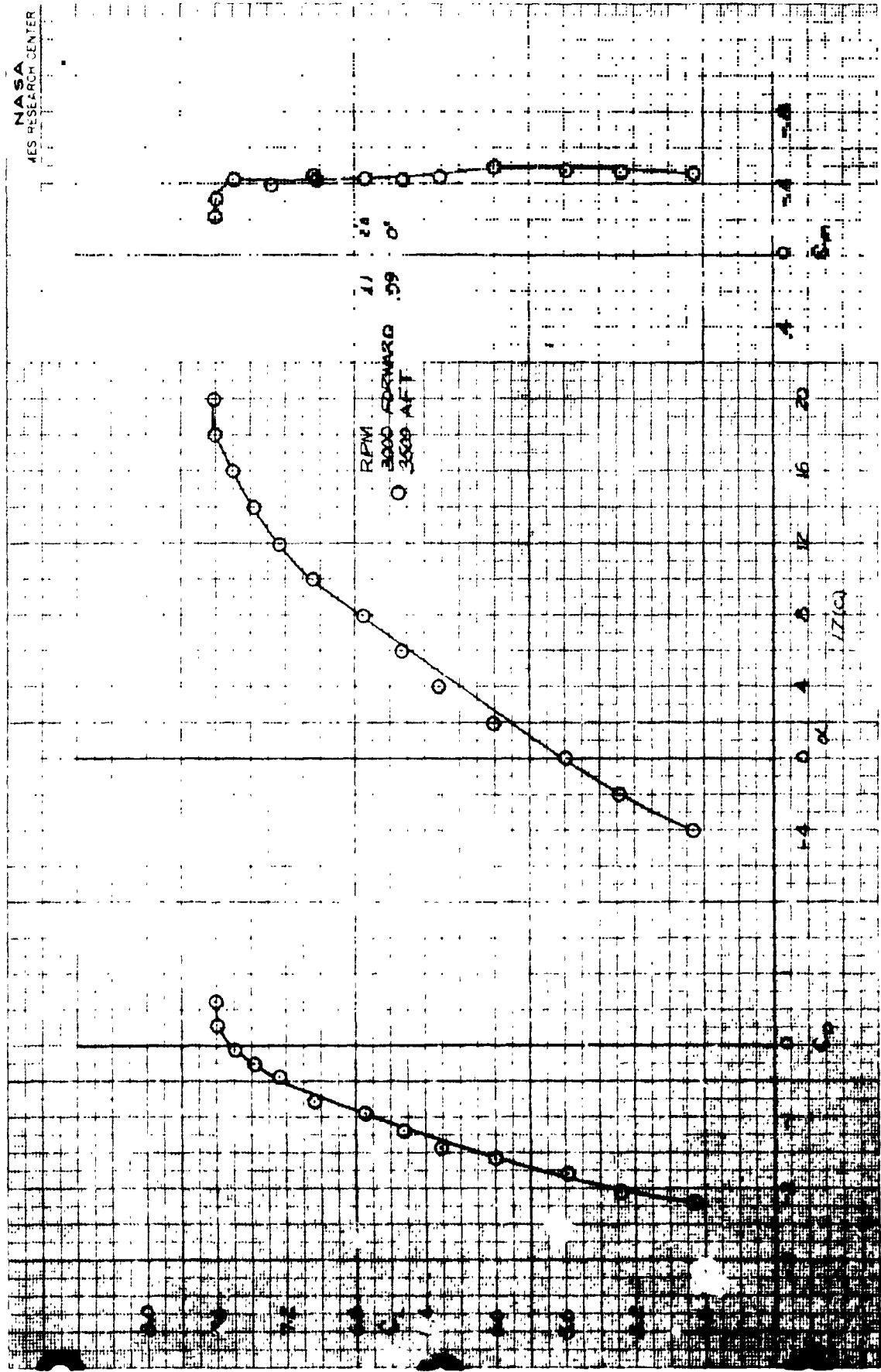
(a) $v = -40$.

Figure 17.- The effect of varying lift fan RPM on longitudinal characteristics; $v_v = 0$, $v_{in} = 56$, tail on, four fans, $v_t = 30$.



(b) $\zeta_v = 0$.

Figure 17.- Continued.



(c) $\gamma_v = 40.$

Figure 17.- Concluded.

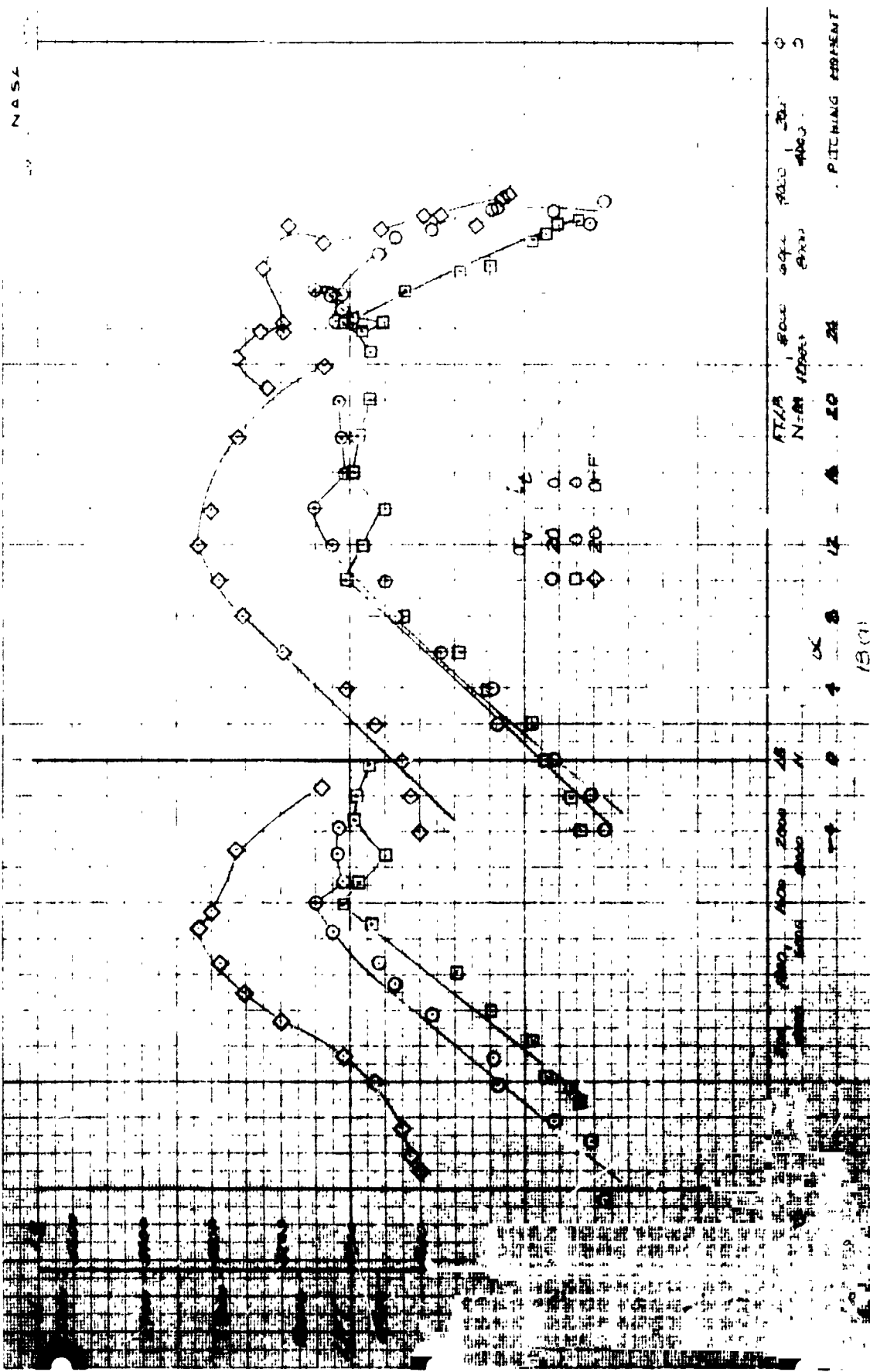


Figure 18.- The variation in longitudinal characteristics with angle of attack; $\mu = 0$, $c_n = 20$, four trans, $f = 30$.

REPRODUCIBILITY OF THE ORIGINAL PAGE IS POOR.

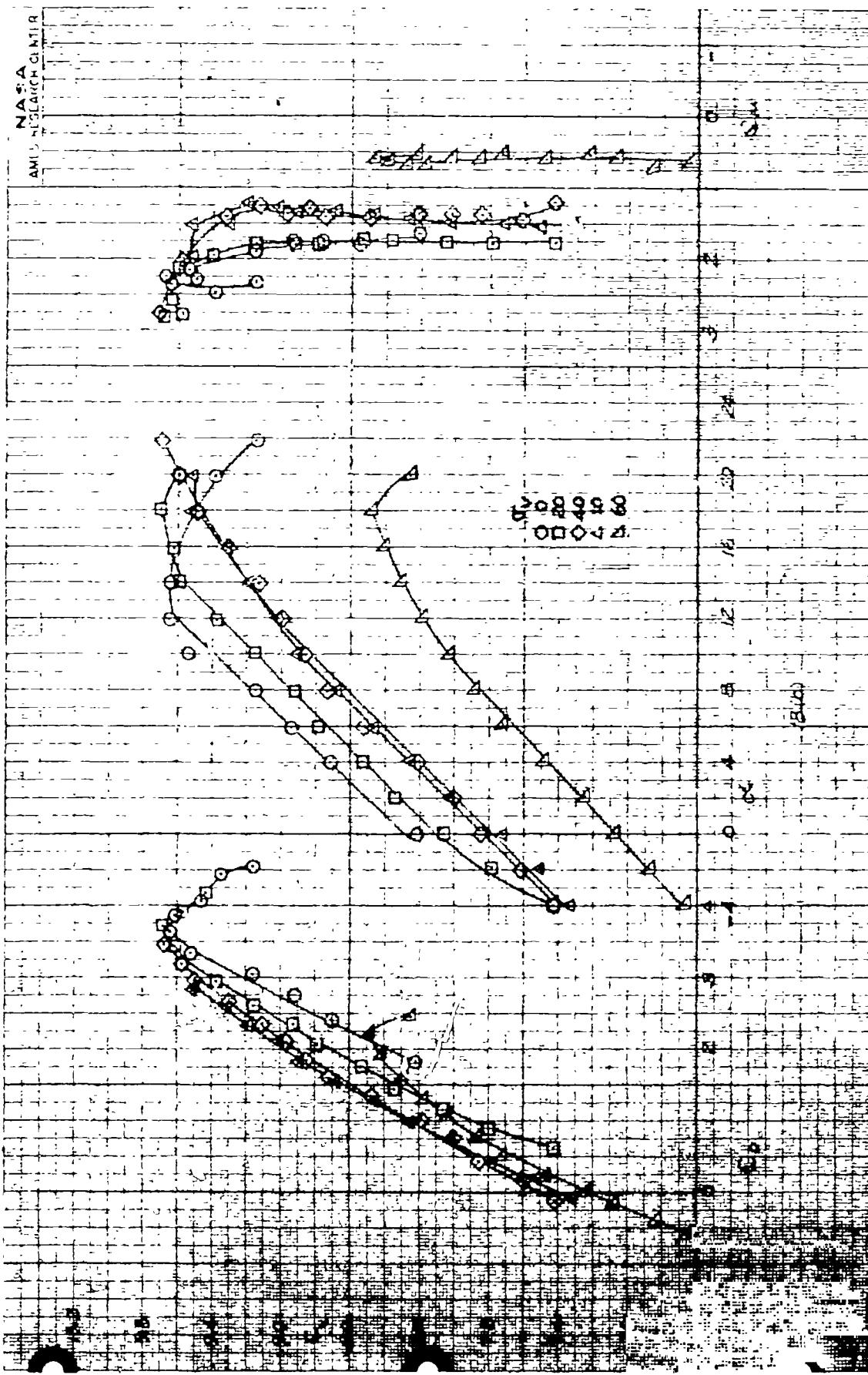
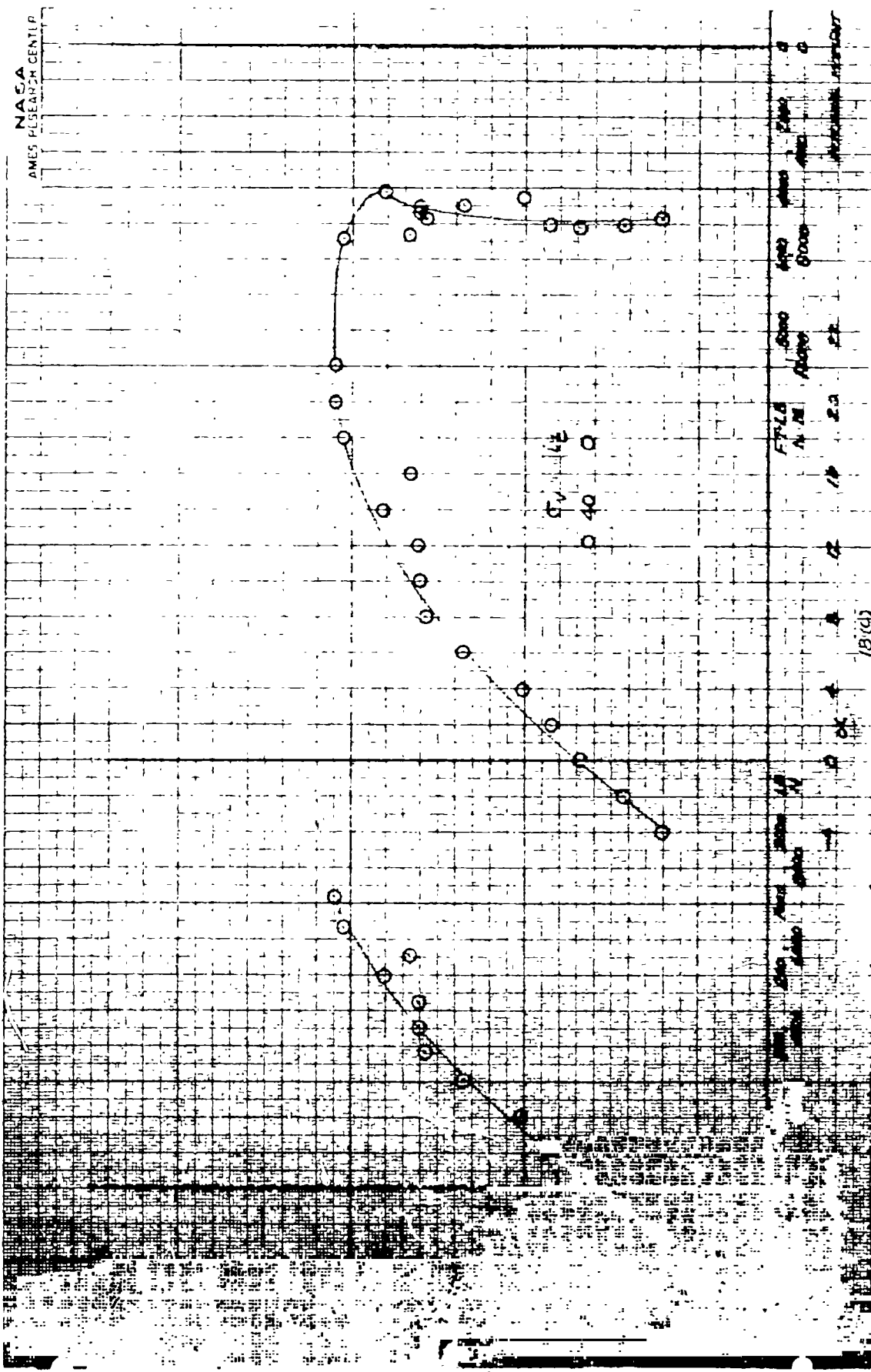
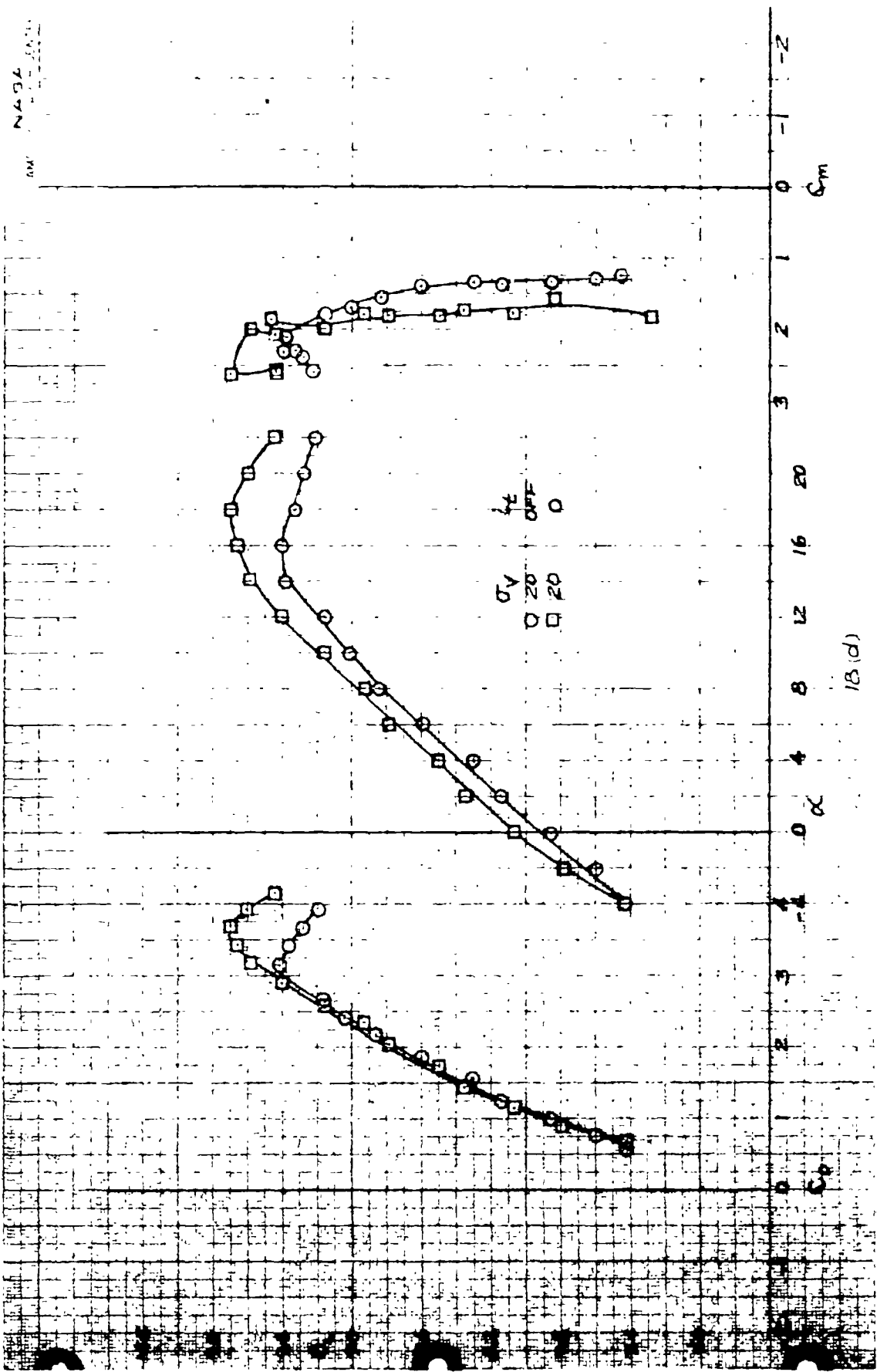


Figure 18.- Continued.



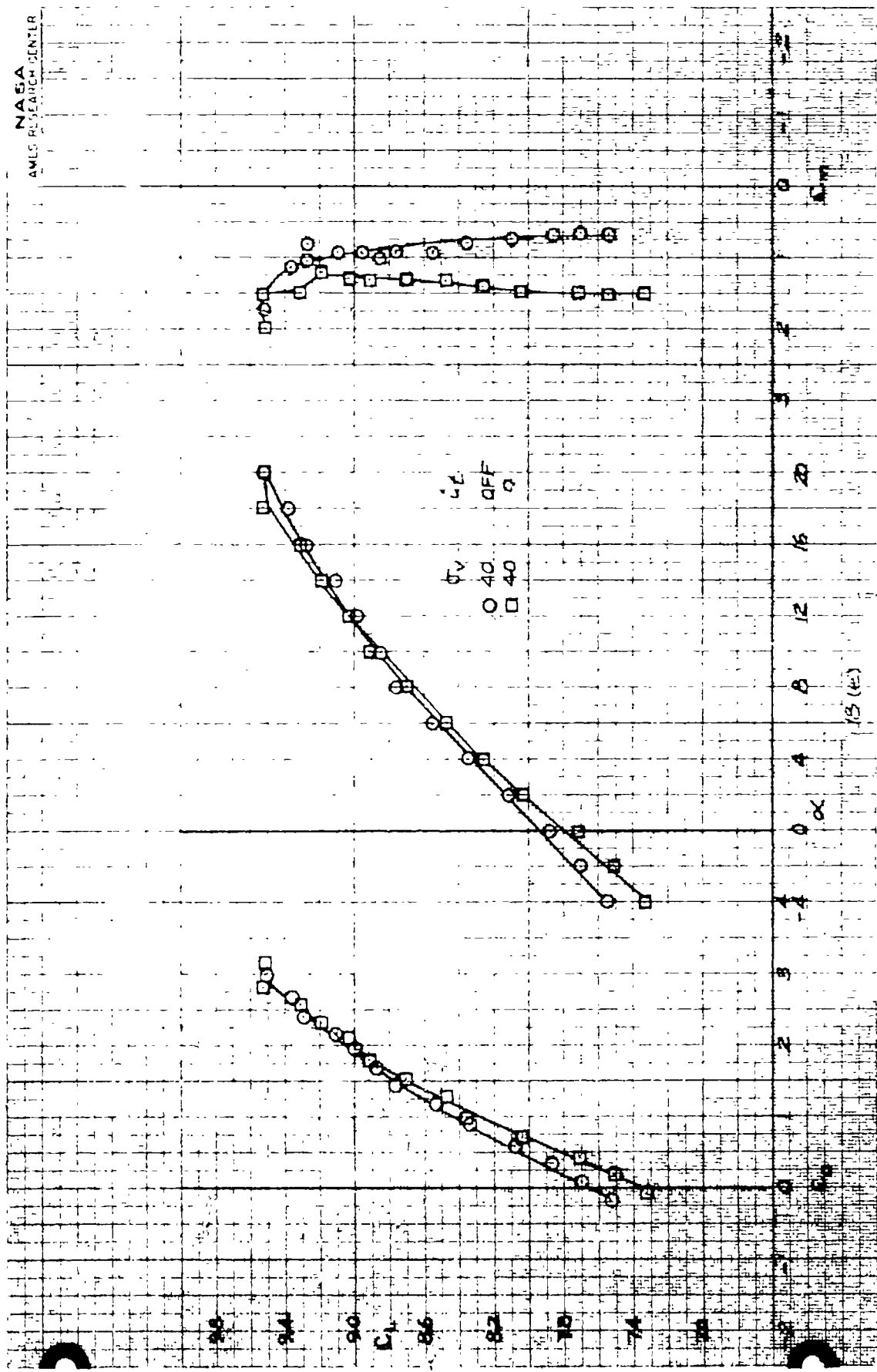
(c) $\mu = .06$, $\alpha_v = 40^\circ$.

Figure 18.- Continued.



(d) $\nu = .08$, $\sigma_v = 20$.

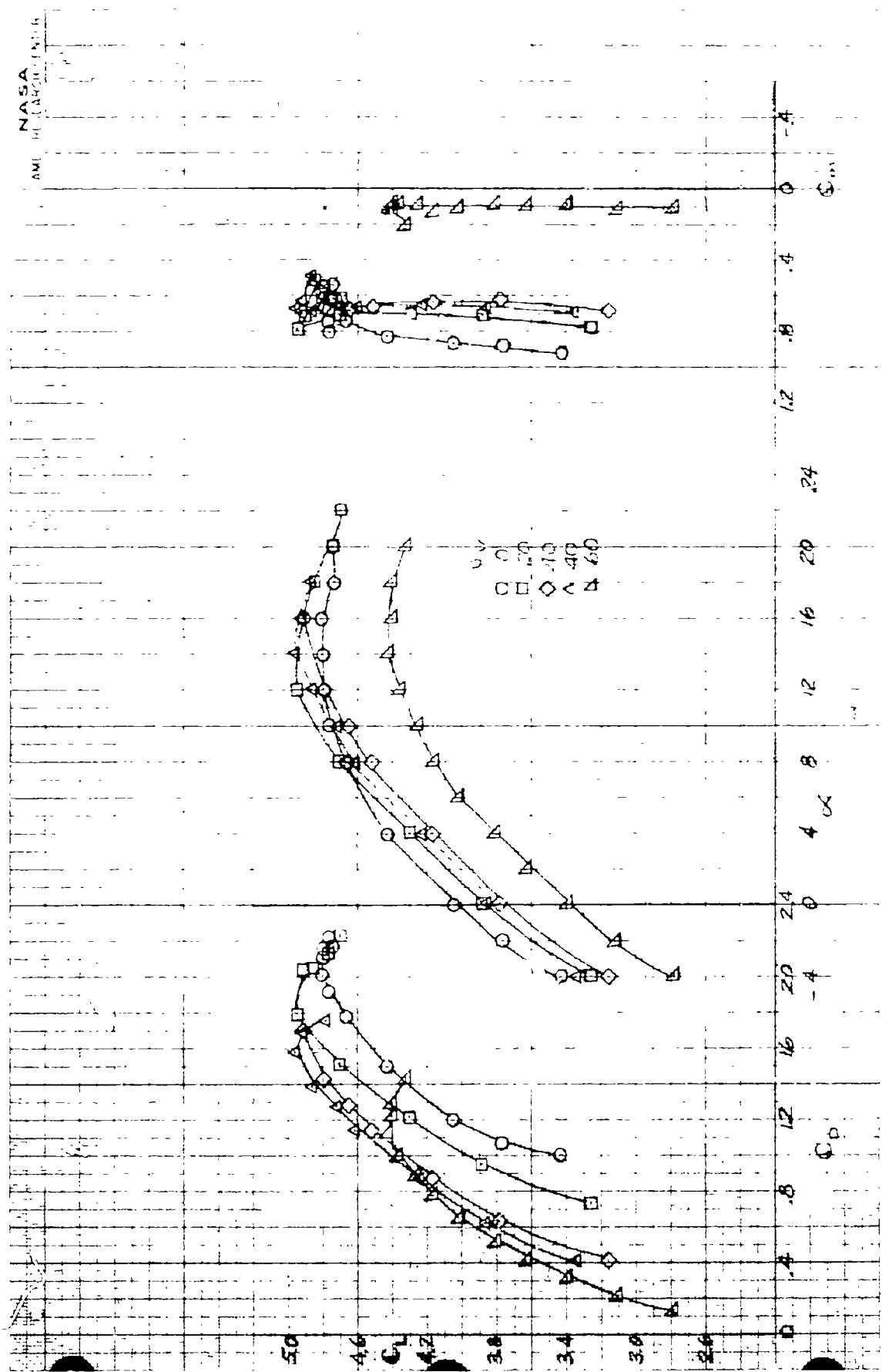
Figure 18.— Continued.

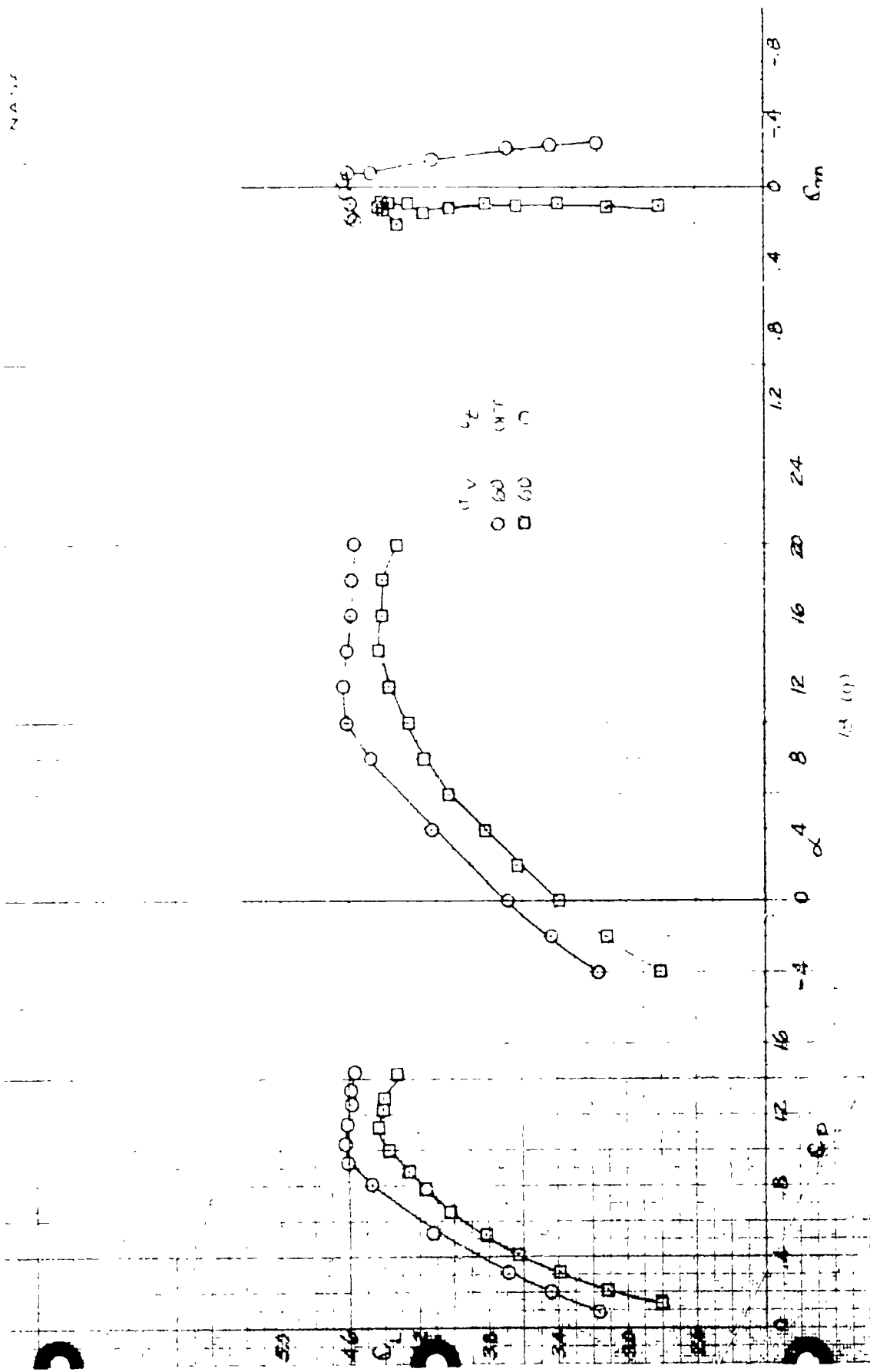


(e) $\mu = .08$, $v = 40.$

Figure 18,- Continued.

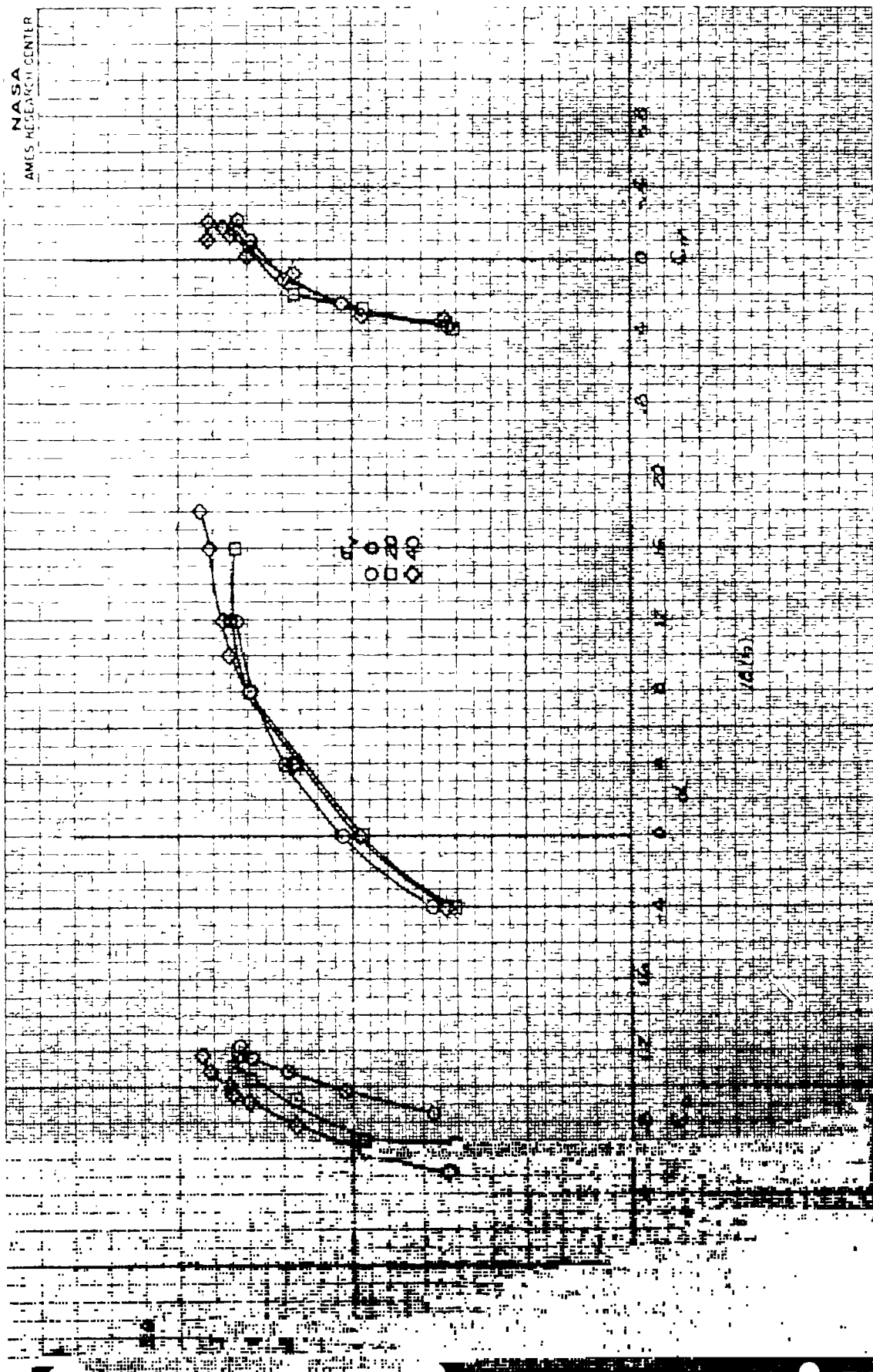
REPRODUCIBILITY OF THE ORIGINAL PAGE IS POOR.





(g) $\alpha = 12$, $\lambda = 60$.

Figure 18.- Continued



(h) $\mu = .17$, tail on.

Figure 18.- Continued.

REPRODUCIBILITY OF THE ORIGINAL PAGE IS POOR

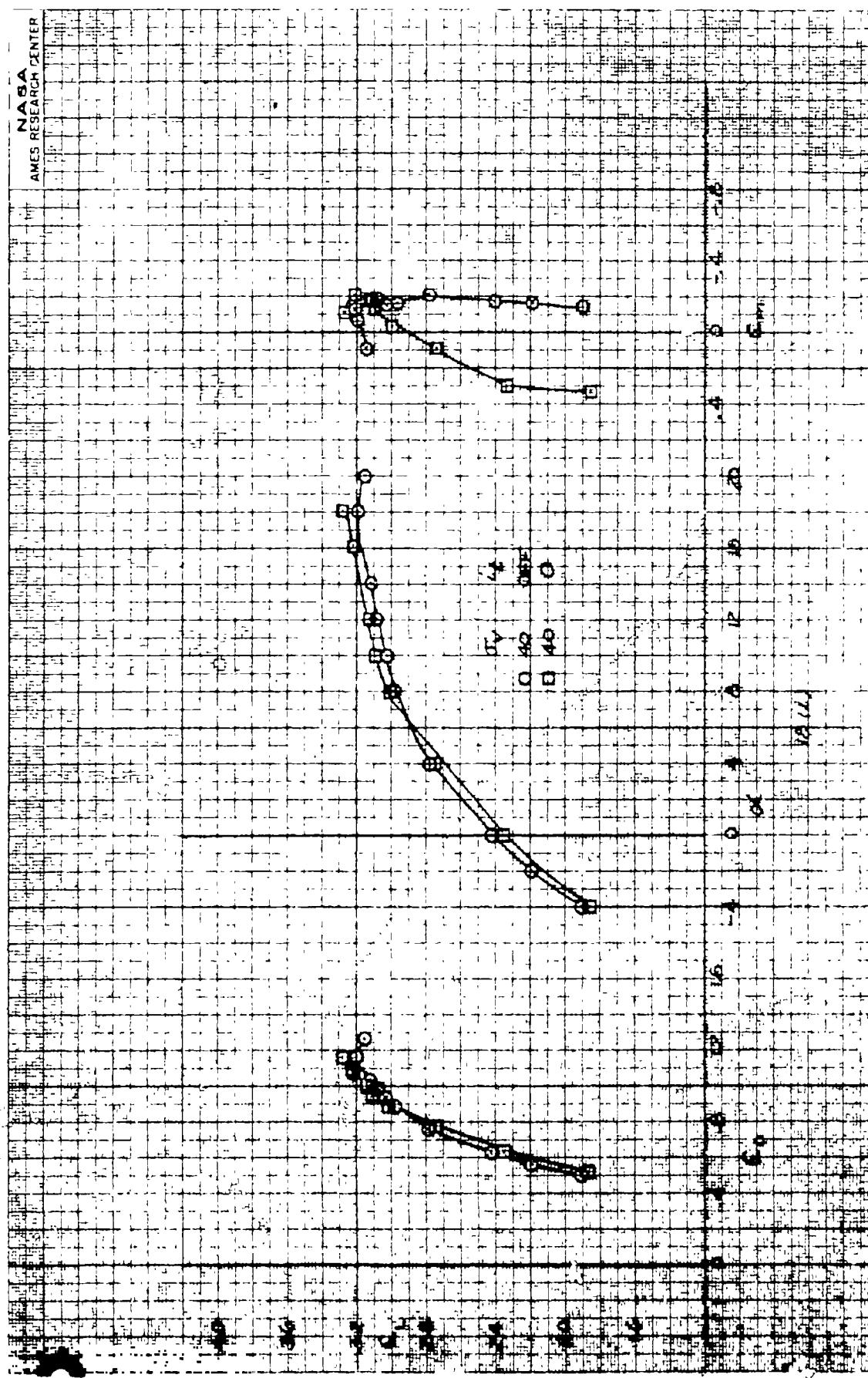


Figure 18.- Concluded.

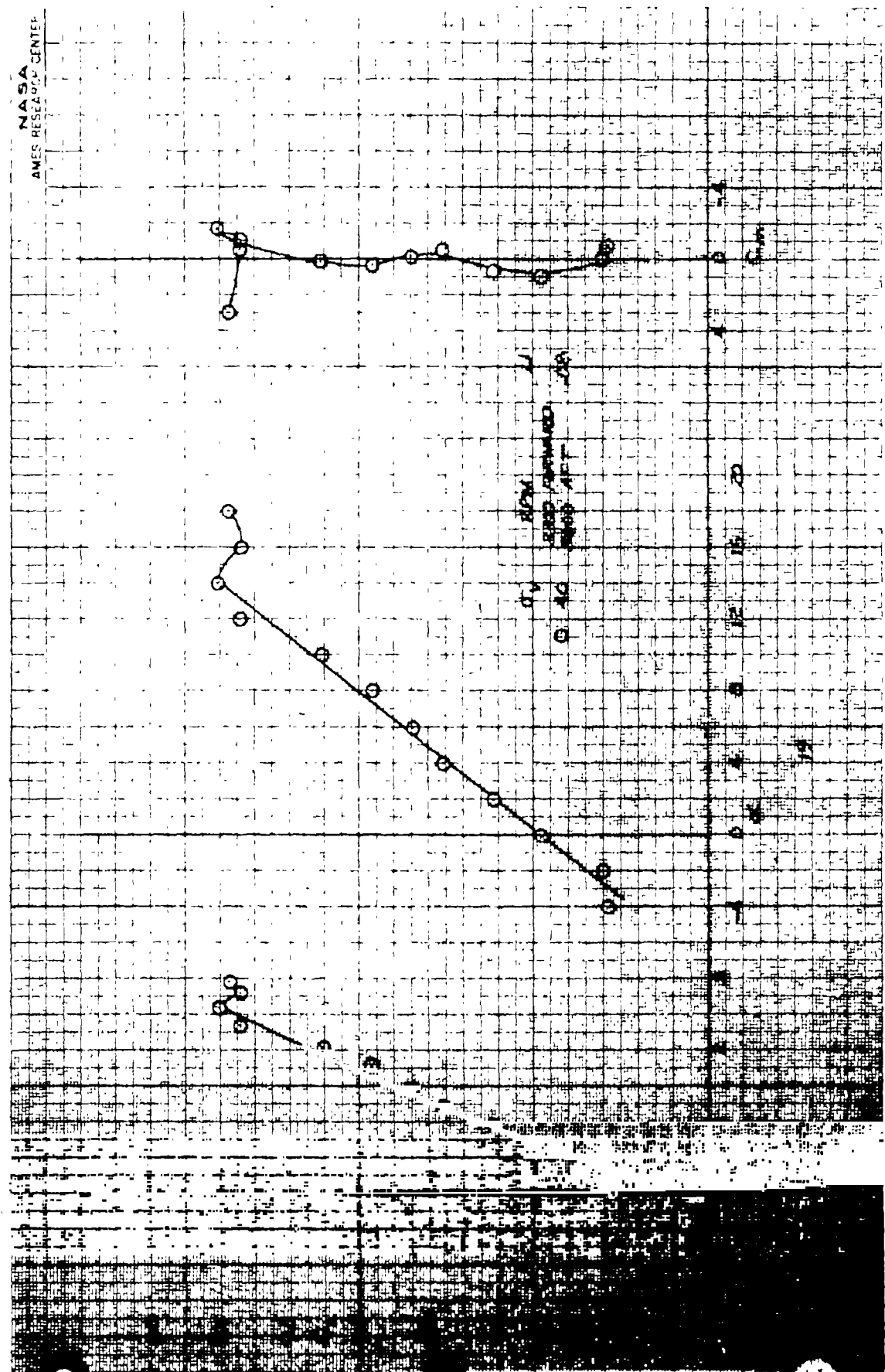
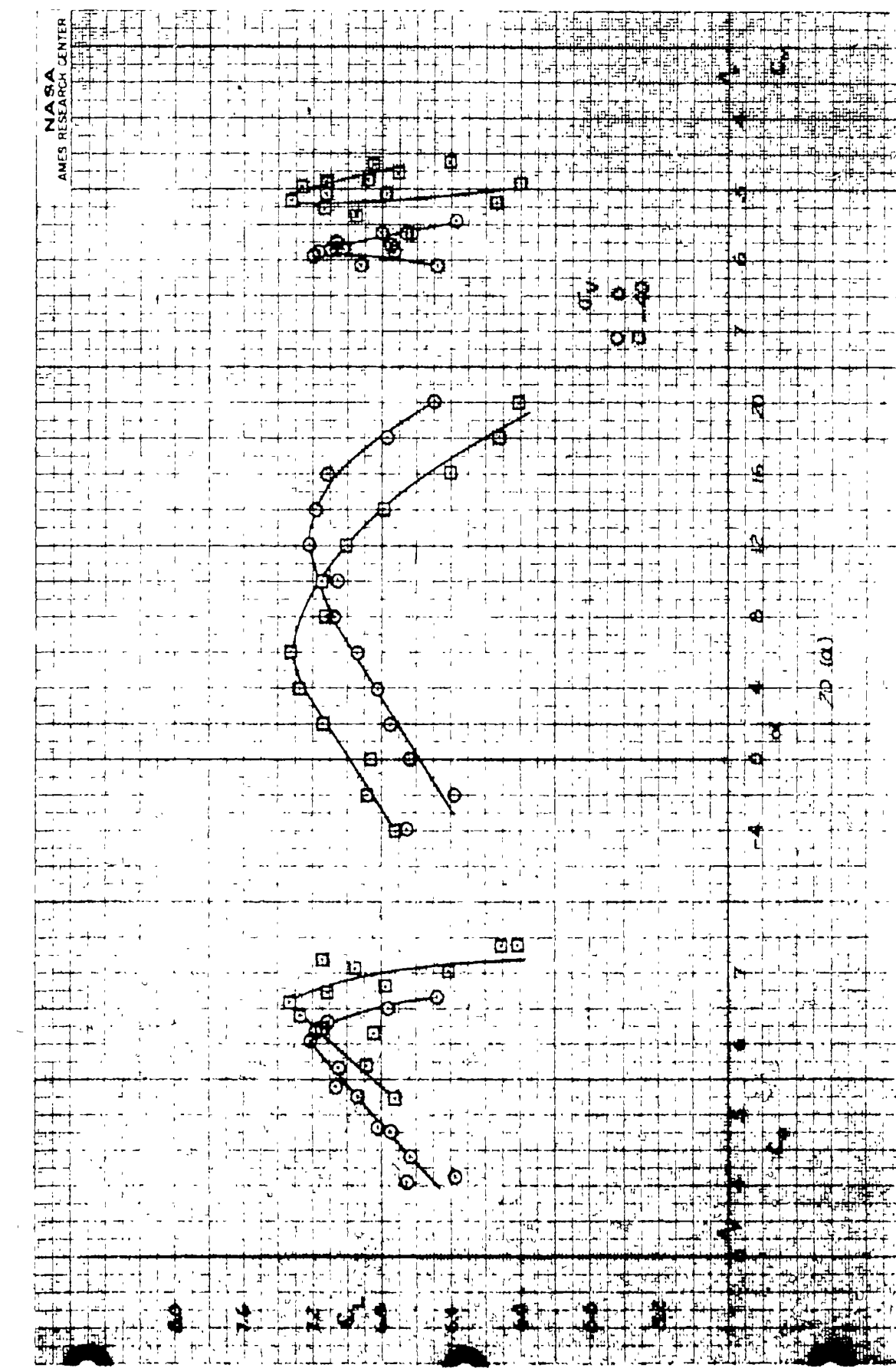
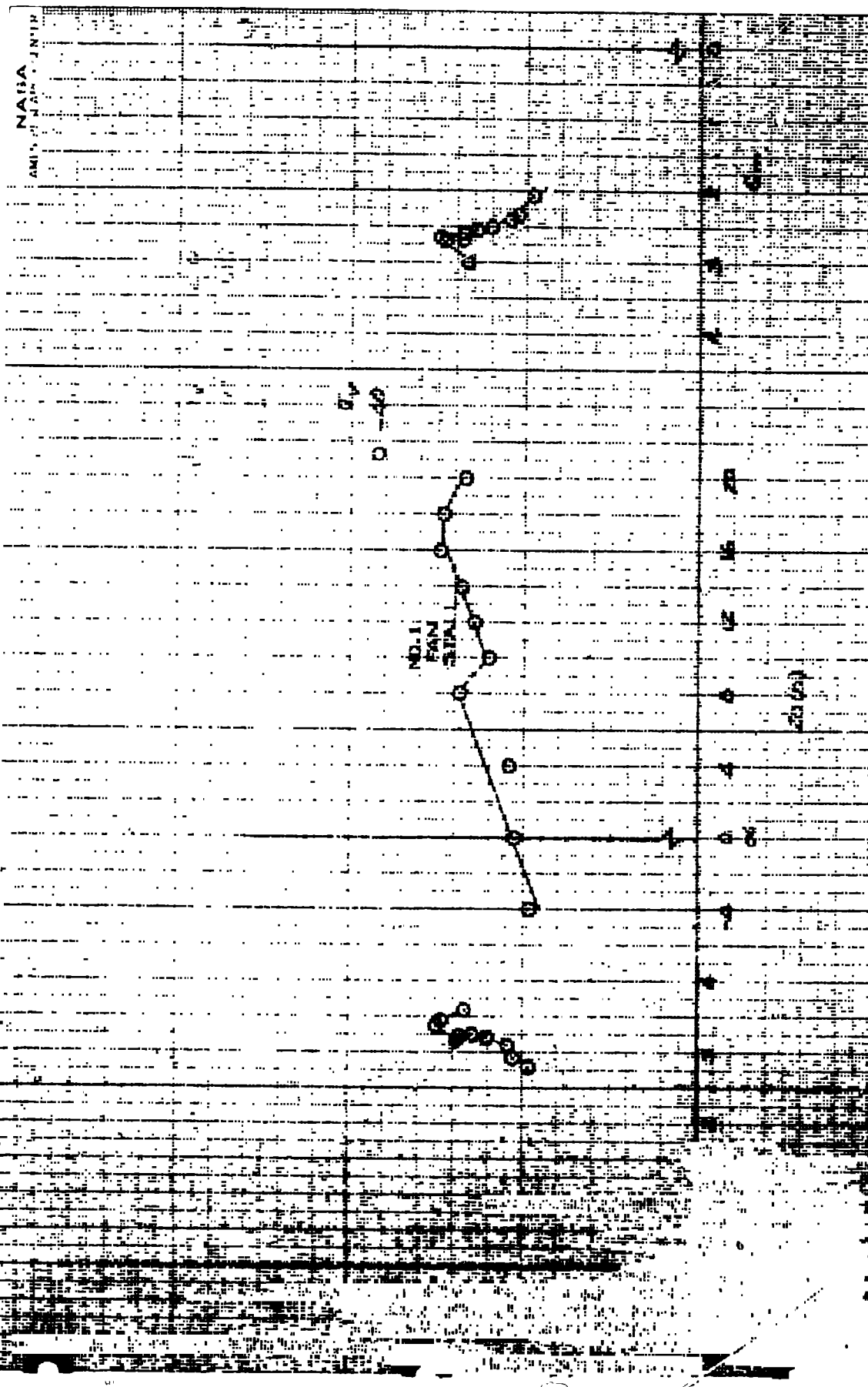


Figure 19.— The effect of varying lift-fan RPM on longitudinal characteristics; $\delta_v = 0$, $\delta_{cn} = 90$, tail on, four fans, $\delta_f = 30$.



(a) $\mu = .08$.

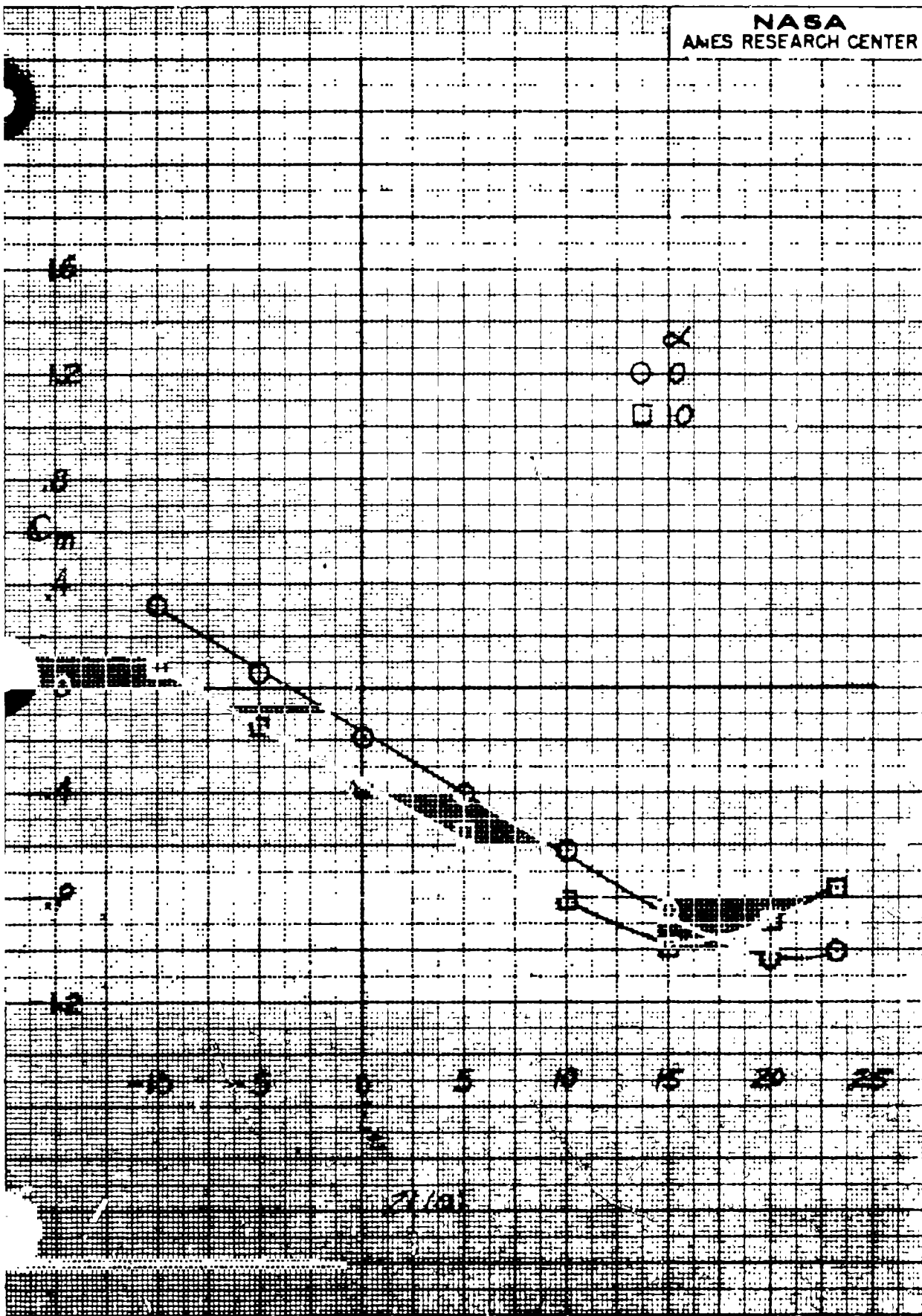
Figure 20.- The variation in longitudinal characteristics with angle of attack; $\beta_v = 0$, $\delta_{cn} = 138.5$, tail off, four fans, $\delta_f = 30$.



(b) $u = .12.$

Figure 20.- Concluded.

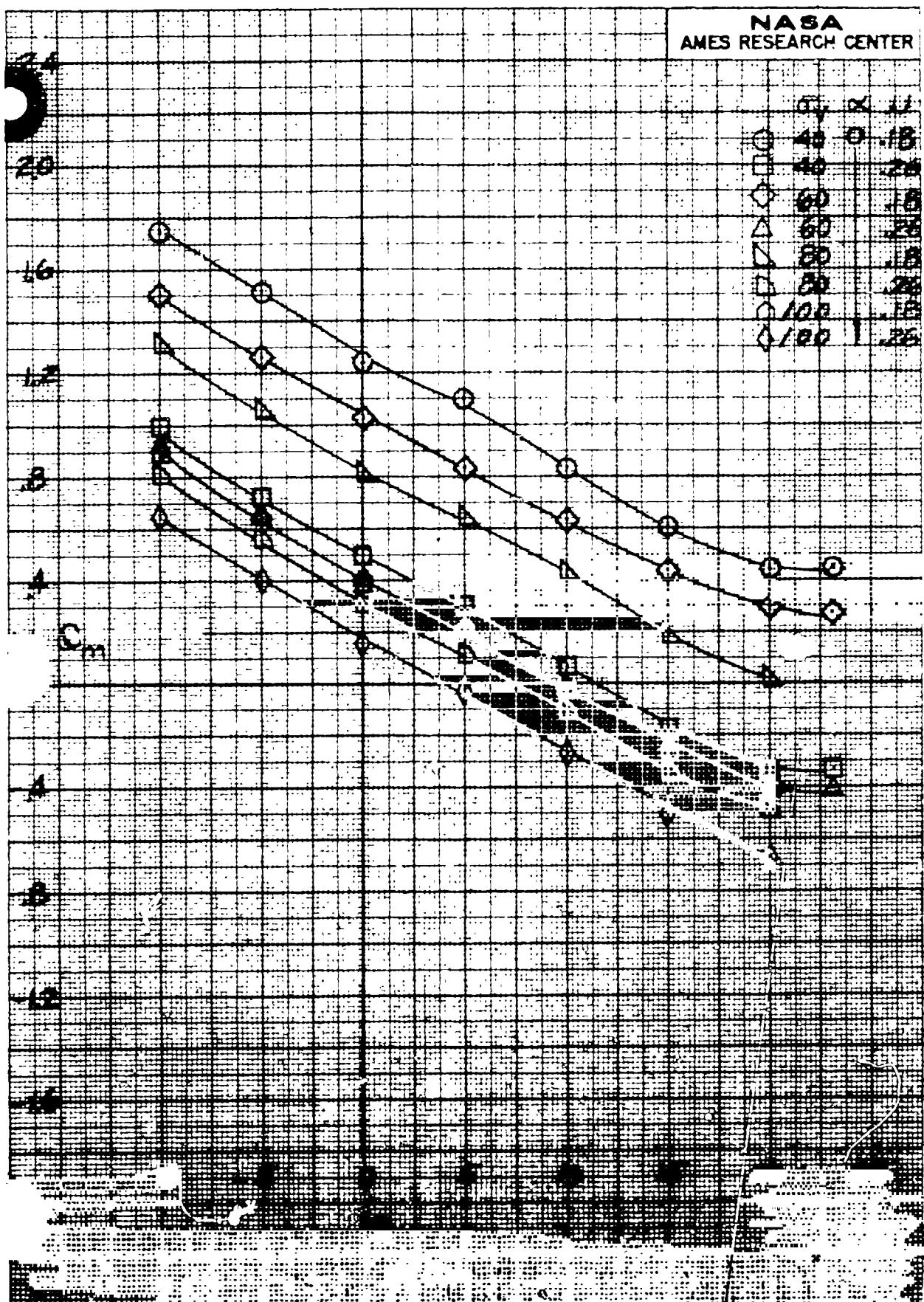
NASA
AMES RESEARCH CENTER



(a) Power off, $\delta_v = 90^\circ$, $\sigma_v = 90^\circ$, front inlets sealed, $\delta_{cn} = 90^\circ$.

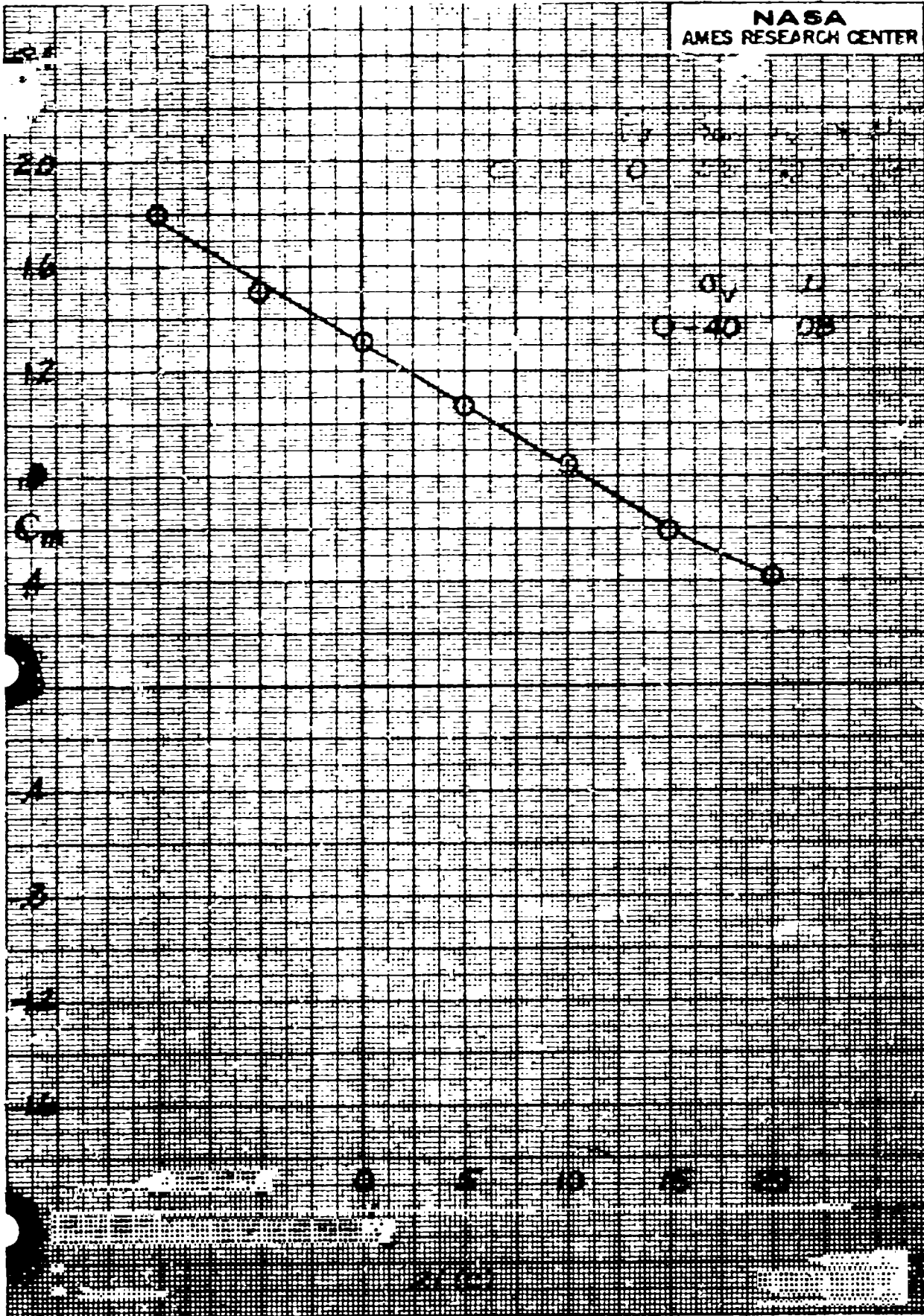
Figure 21.- Horizontal tail effectiveness; $\delta_x = 30^\circ$.

NASA
AMES RESEARCH CENTER



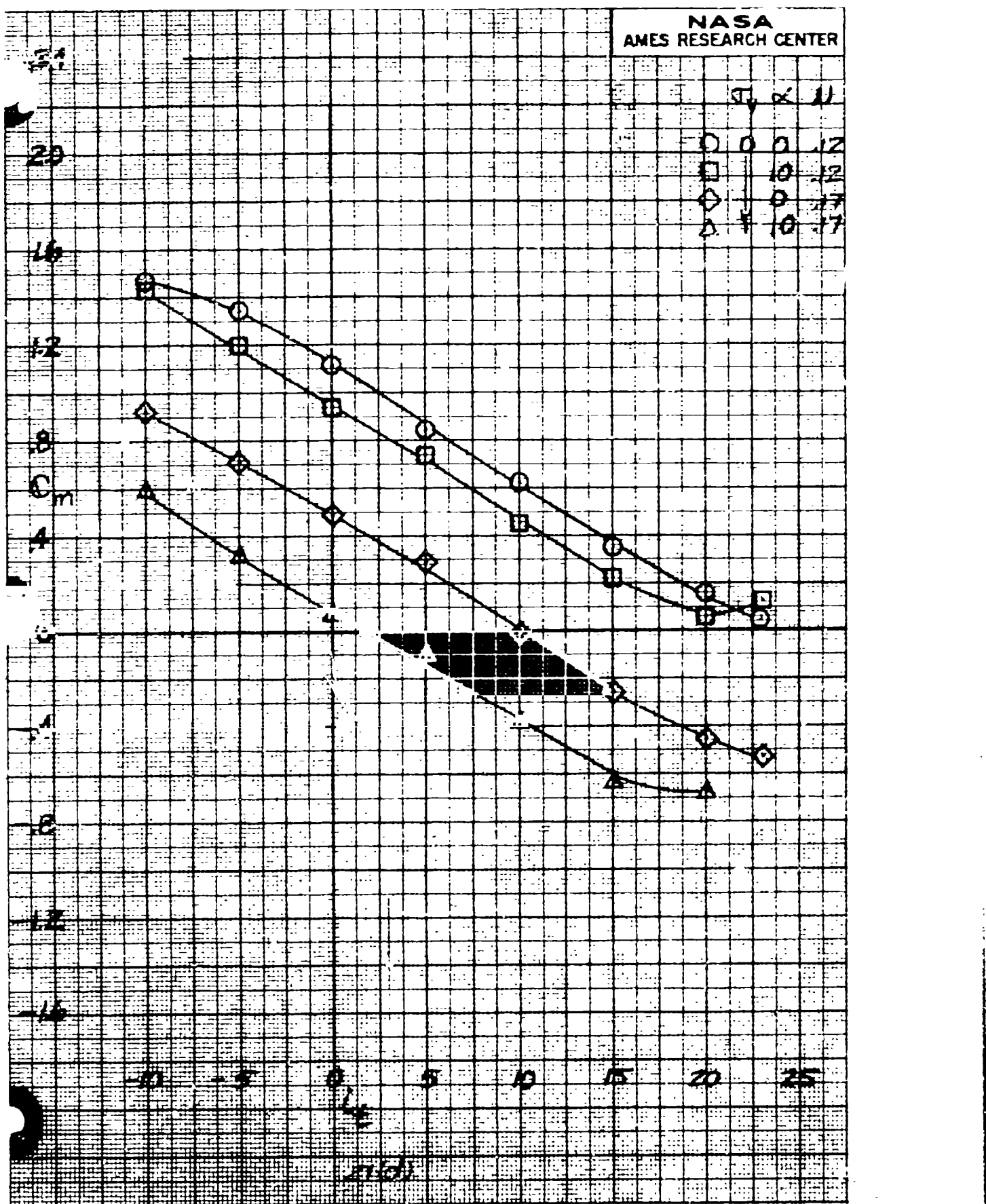
$$(b) \quad \beta_{v_0} = 0, \quad \delta_{\text{exp}} = 23, \quad a = 0.$$

Figure 23 - Continued



$$(c) \quad \beta_v = 0, \quad \delta_{cn} = 56, \quad \alpha = 0.$$

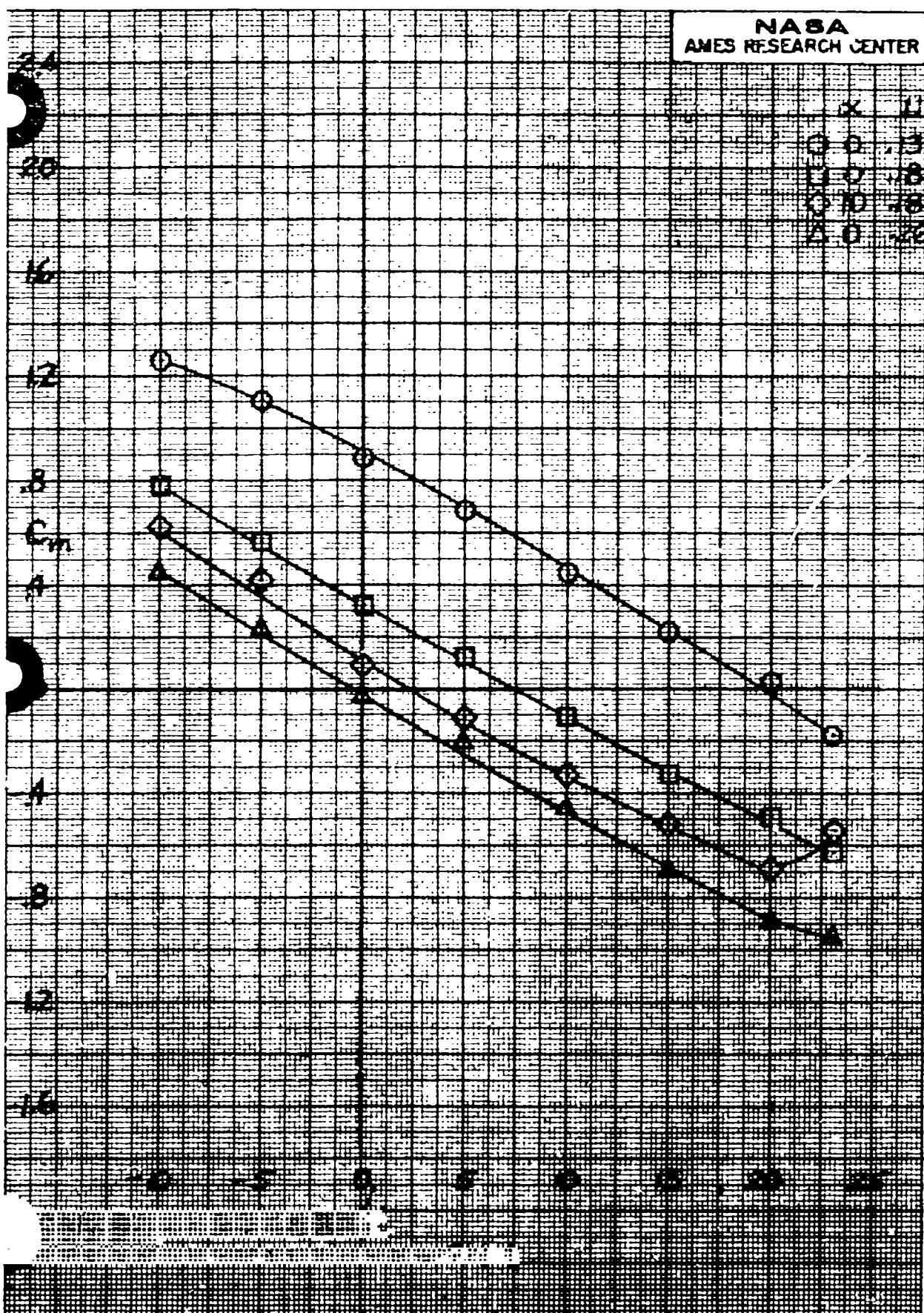
Figure 21.- Continued.



(d) $\beta_v = 0, \delta_{cn} = 56.$

Figure 21.- Continued.

NASA
AMES RESEARCH CENTER



(e) $\beta_v = 0, \sigma_v = 40, \delta_{cn} = 56.$

Figure 21.- Continued.

NASA
AMES RESEARCH CENTER

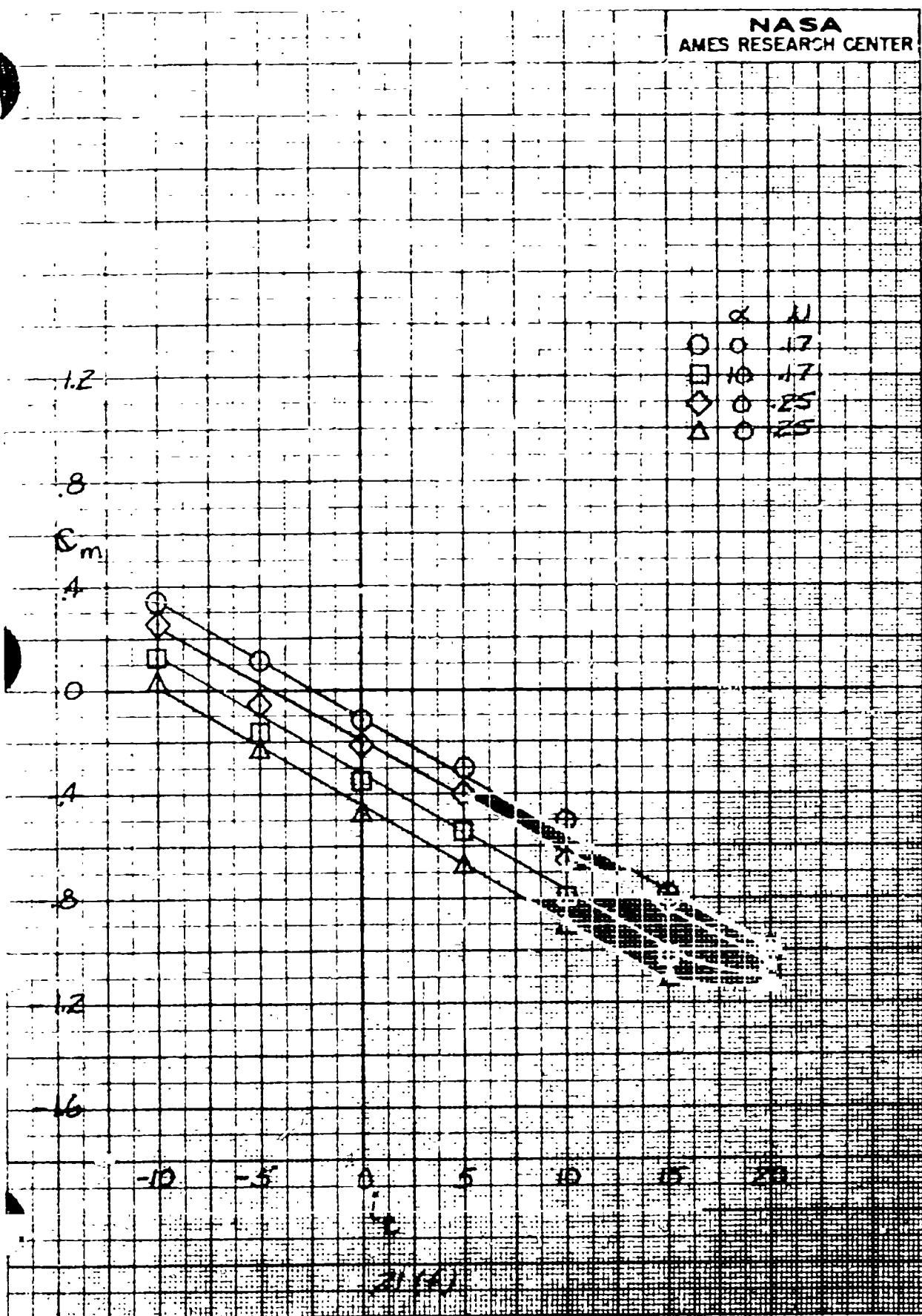


Figure 21.- Continued.

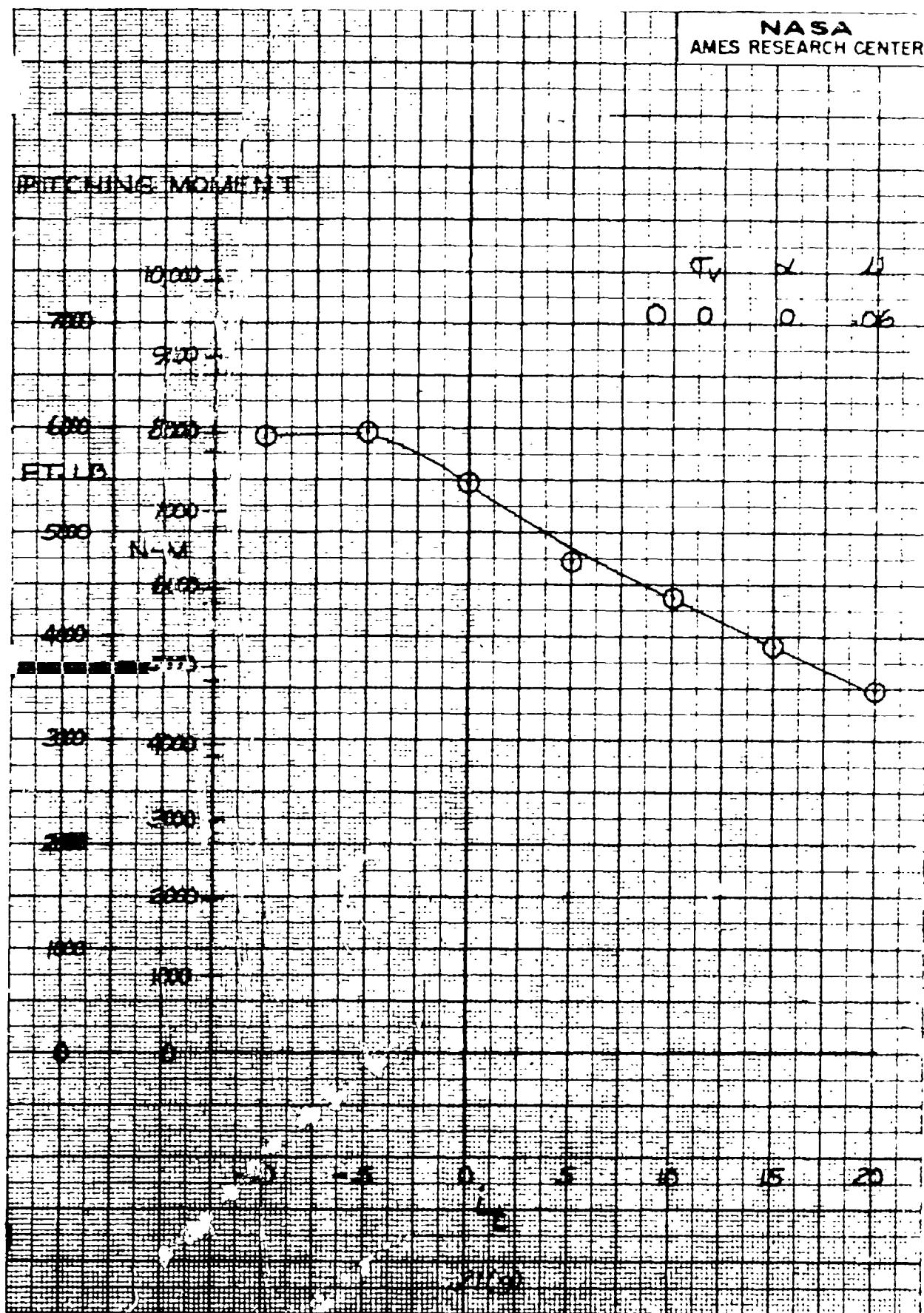
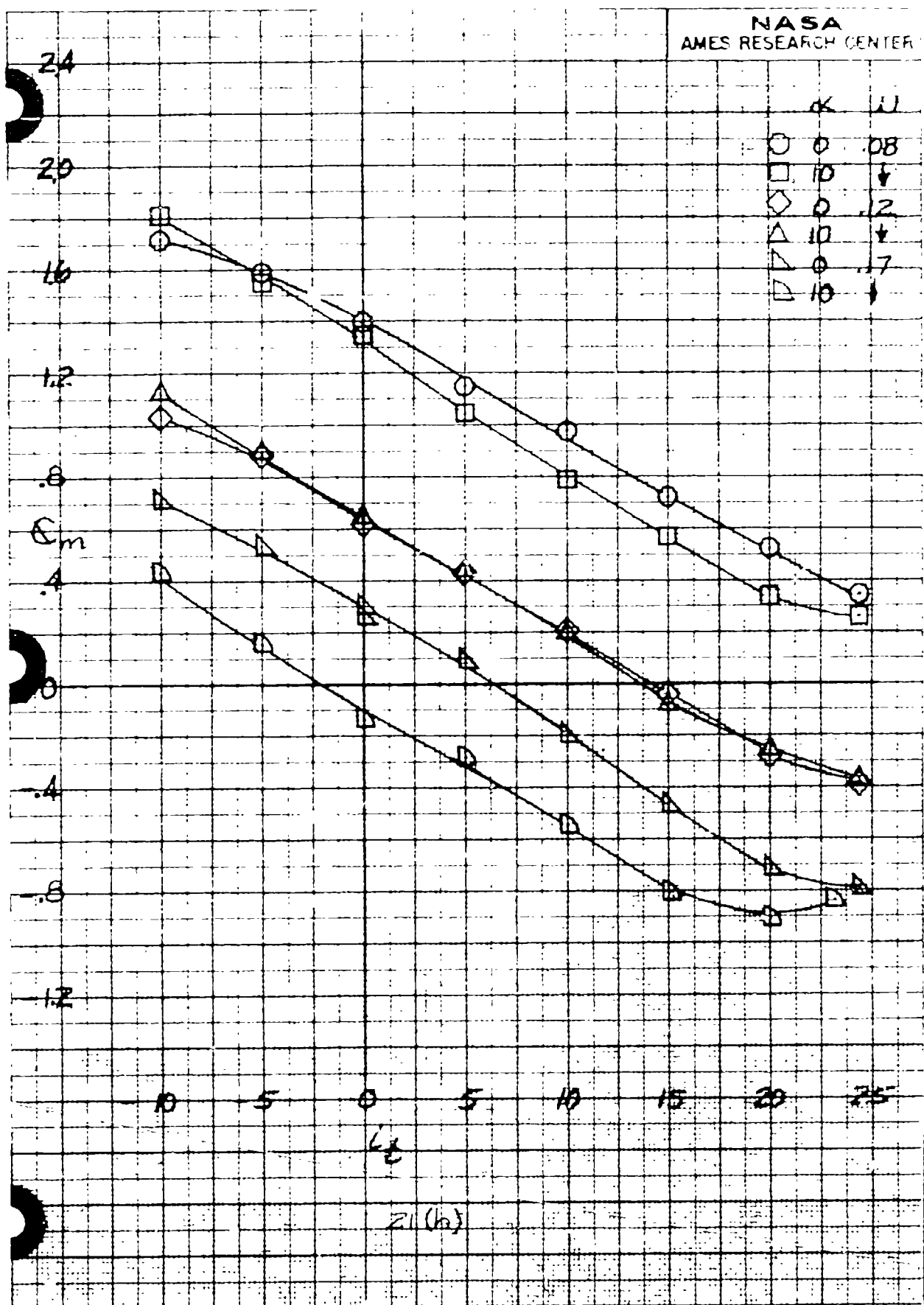


Figure 21.- Continued.



(h) $\alpha_v = 0$, $\beta_v = 40$, $\gamma_{cn} = 90$.

Figure 21.- Concluded.

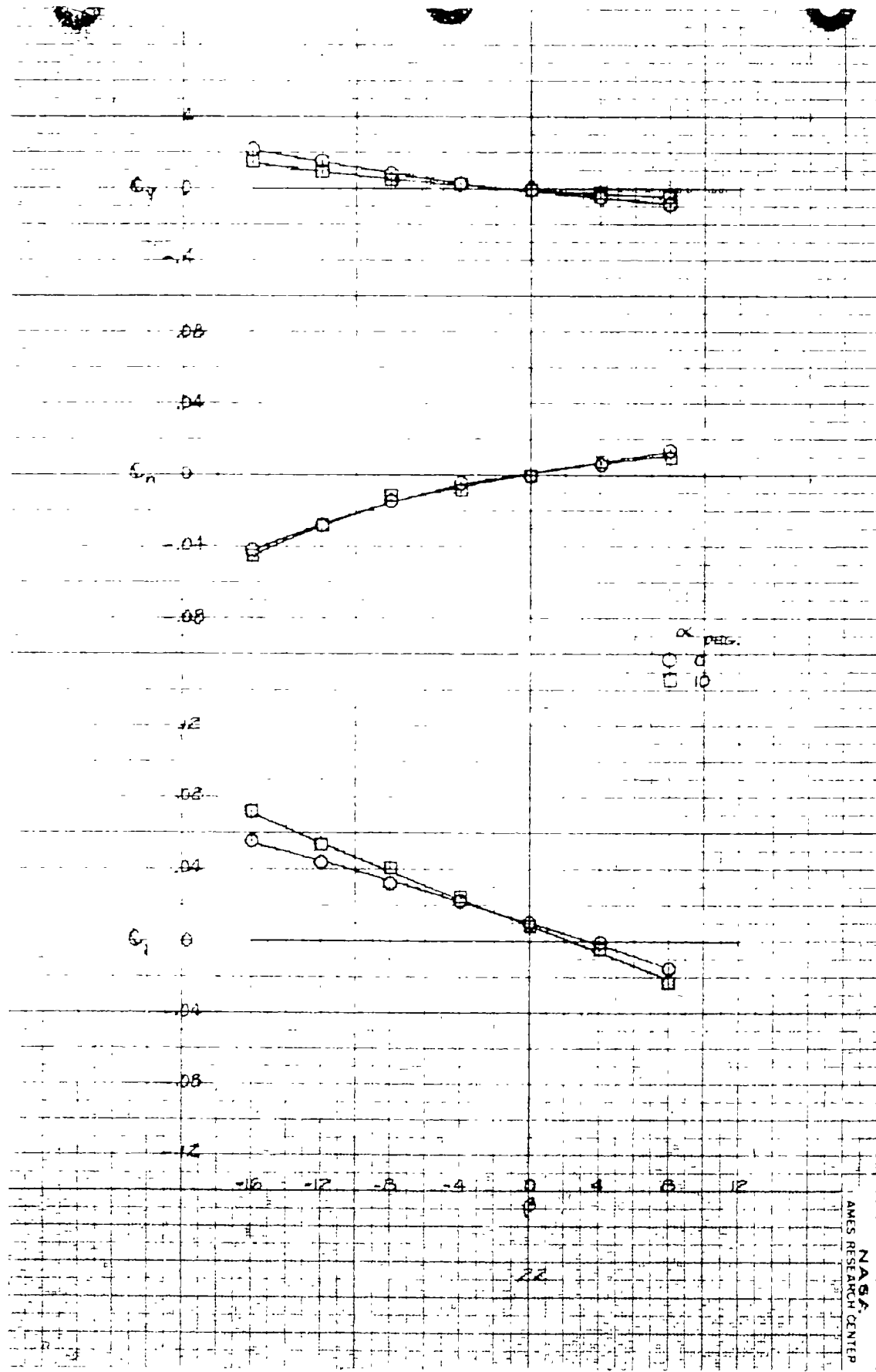


Figure 22.- The variation in lateral-directional characteristics with sideslip angle; power off, $\kappa_v = 90$, $\gamma = 90$, forward fan inlets sealed, $\kappa_n = 90$, tail on, $\gamma_f = 30$.

N.A.S.A.
AMES RESEARCH CENTER

REPRODUCIBILITY OF THE ORIGINAL PAGE IS POOR.

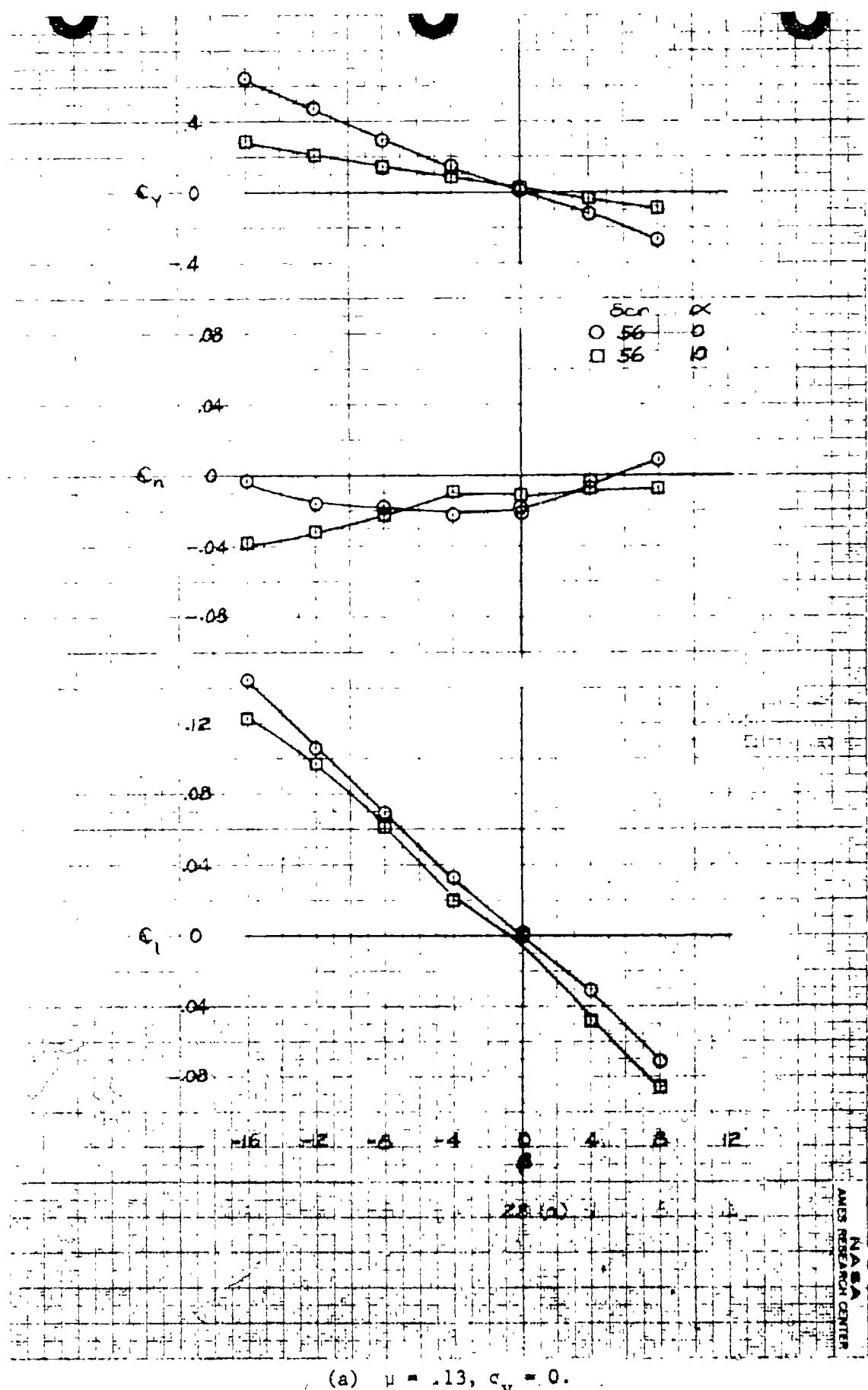
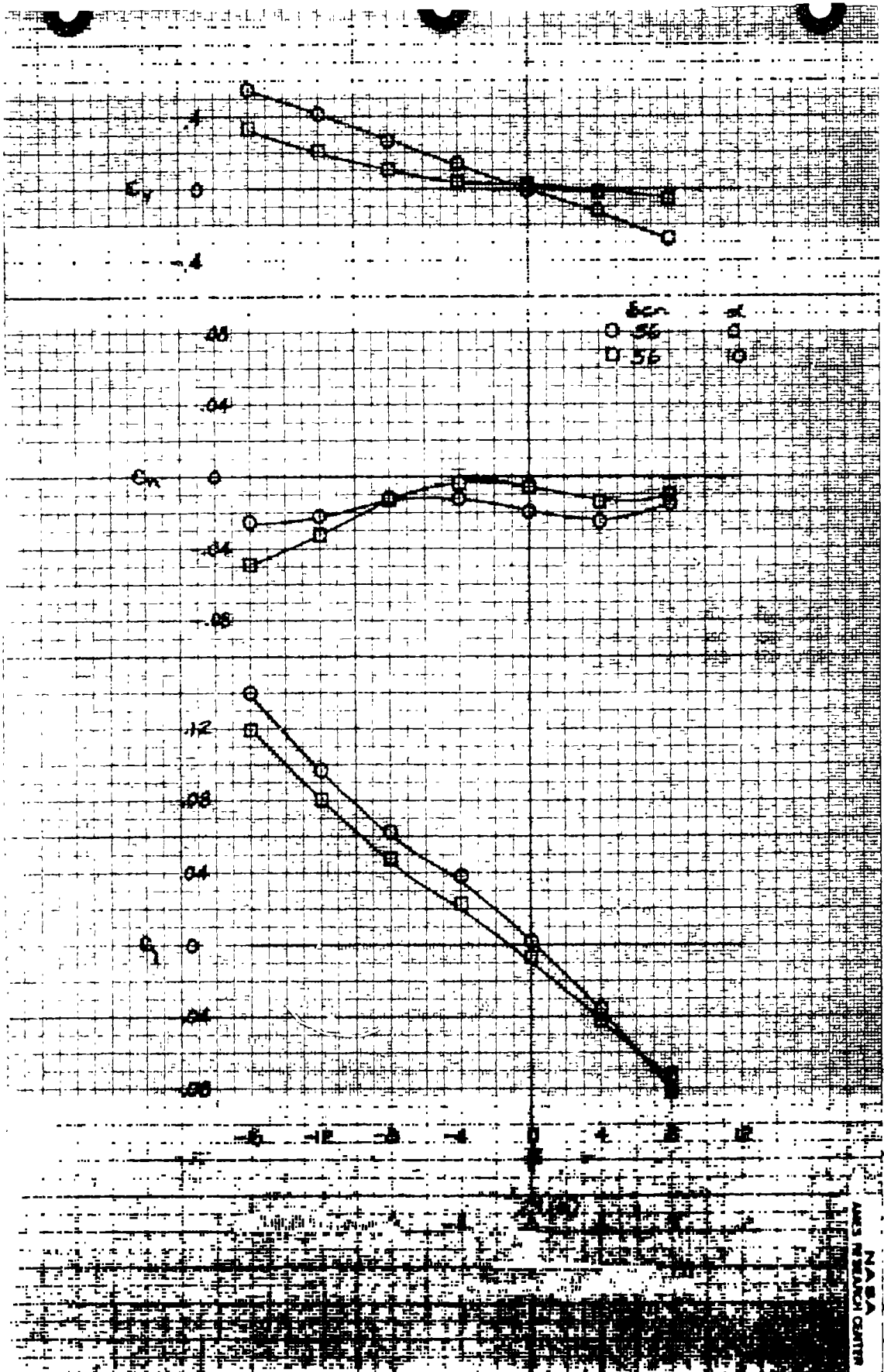
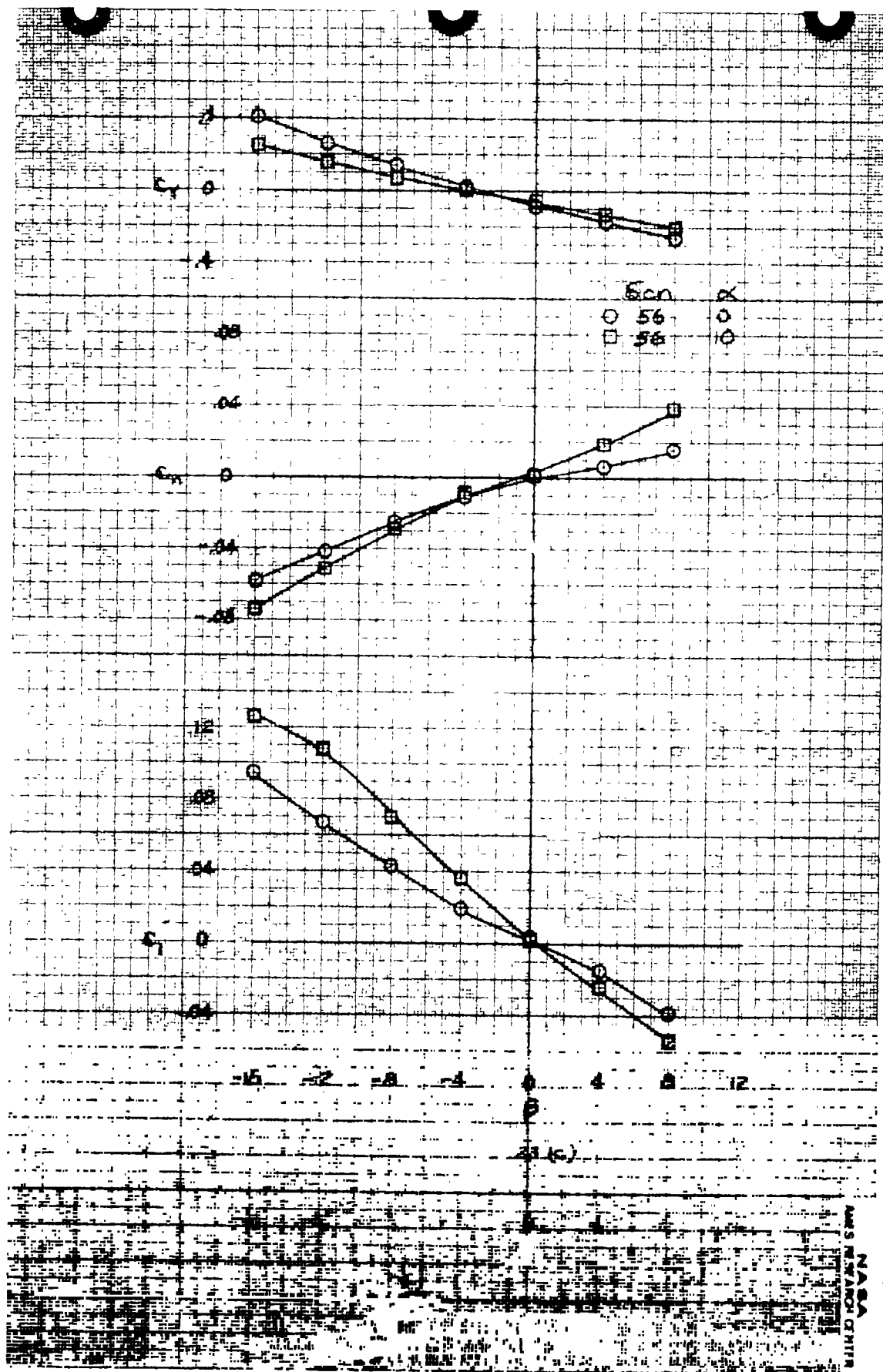


Figure 23.- The variation in lateral-directional characteristics with sideslip angle; $c_v = 0$, tail on, four fans, $\delta_f = 30^\circ$.



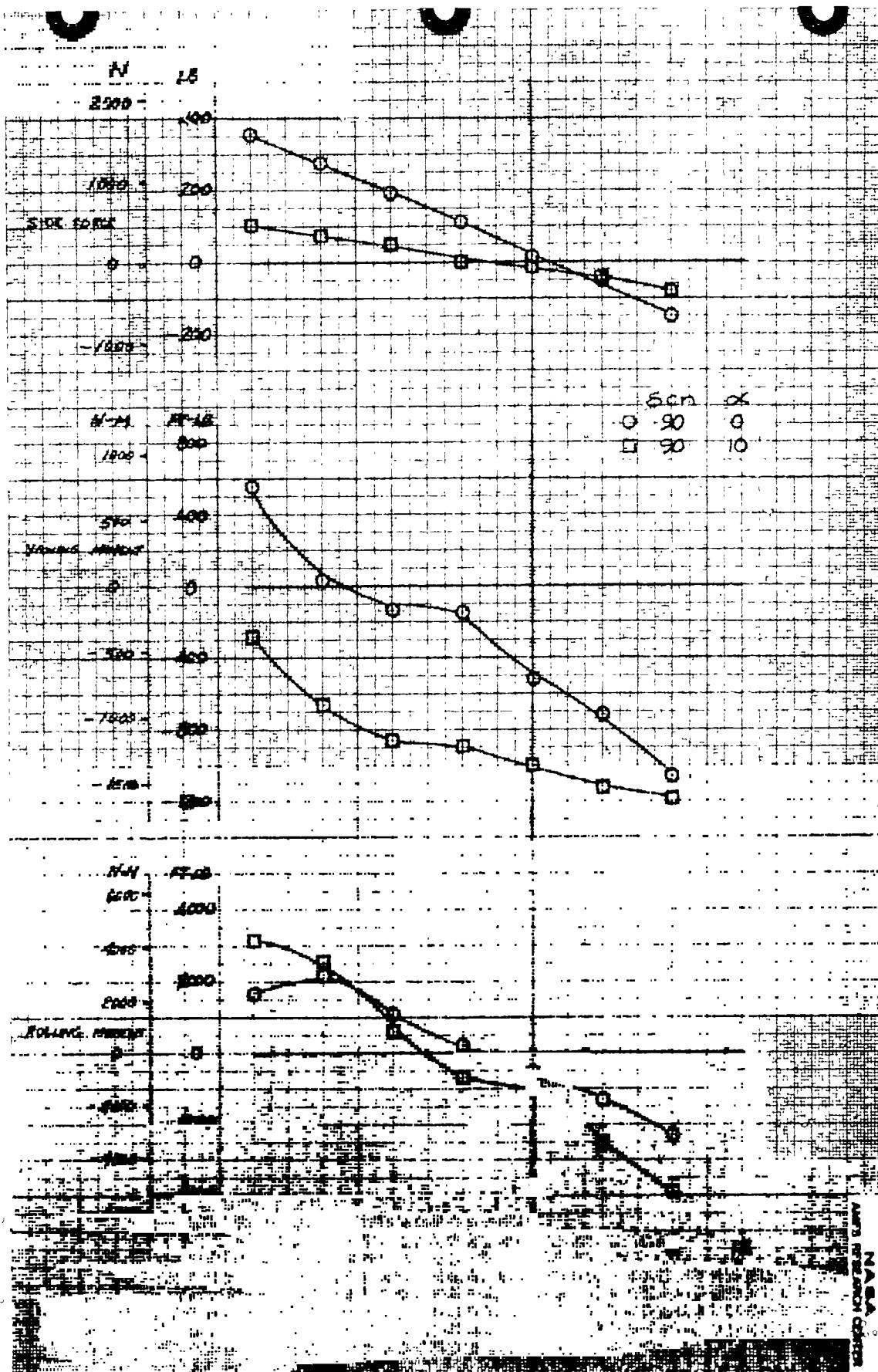
(b) $\mu = .18$, $\sigma_v = .40$.

Figure 23.- Continued.



(c) $\mu = .25$, $\sigma_y = 80$.

Figure 23.- Continued.



(d) $\mu = .06, \sigma_v = 40.$

Figure 23.- Continued.

REPRODUCIBILITY OF THE ORIGINAL PAGE IS POOR.

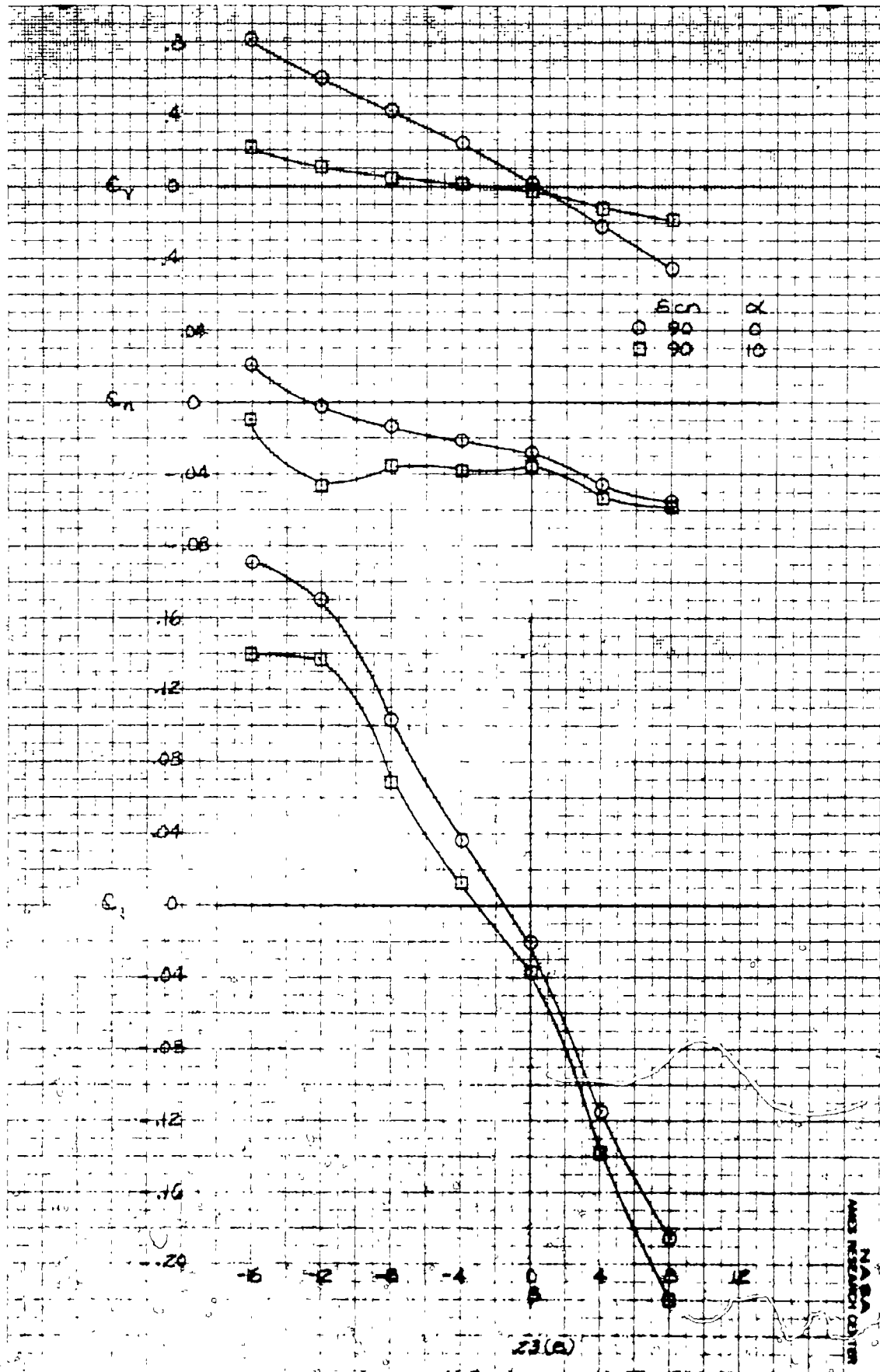
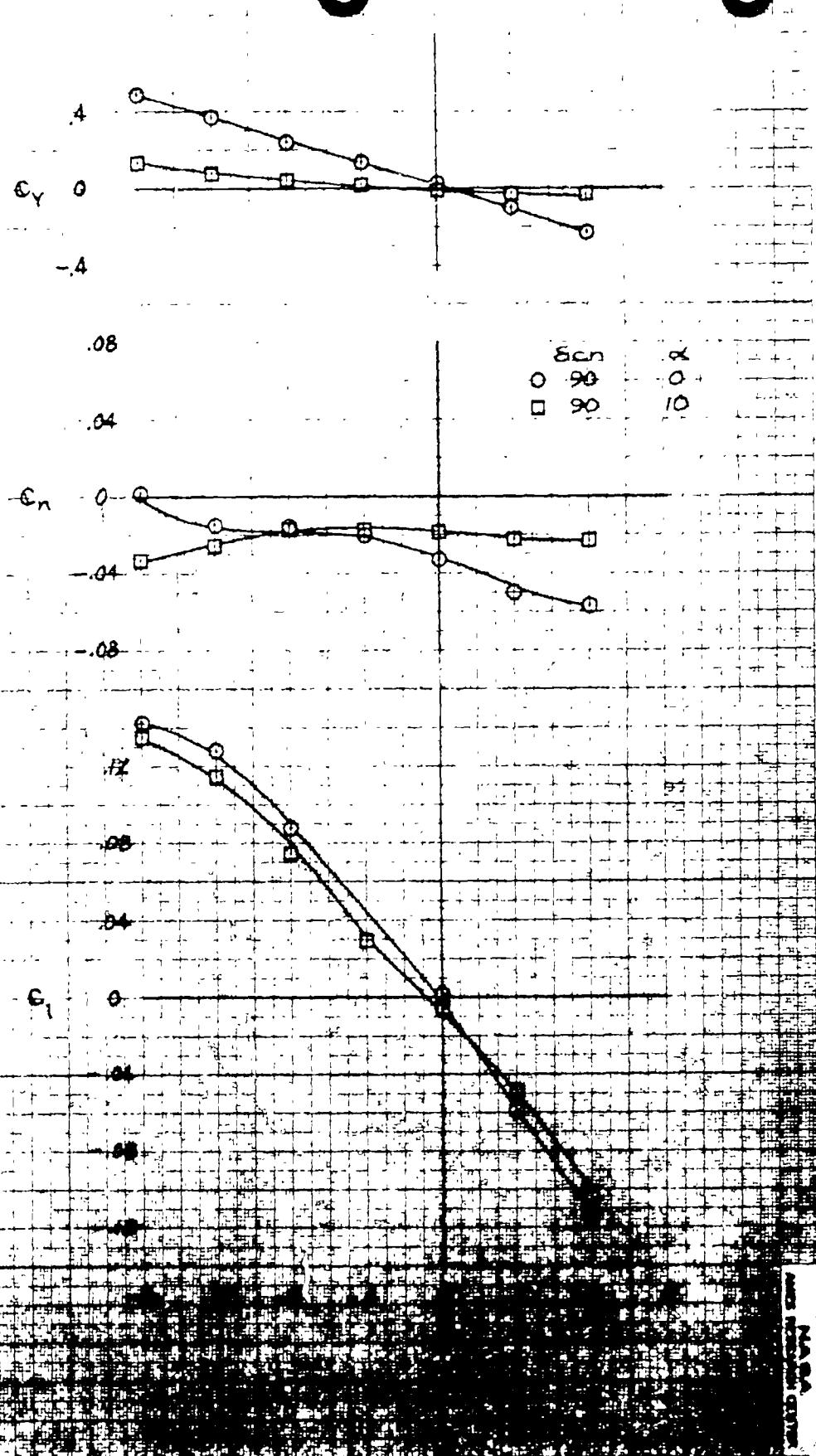


Figure 23.- Continued.

REPRODUCIBILITY OF THE ORIGINAL PAGE IS POOR.



(?) $\mu = .12, c_v = 40,$

Figure 23. Continued.